Nucleon Wave Function from Lattice QCD

DISSERTATION

zur Erlangung des Doktorgrades
der Naturwissenschaften (Dr. rer. nat)
der naturwissenschaftlichen Fakultät II - Physik
der Universität Regensburg

vorgelegt von

Nikolaus Warkentin

aus Regensburg

April 2008

Promotionsgesuch eingereicht am 22. April 2008
Promotionskolloquium am 28. Mai 2008

Die Arbeit wurde angeleitet von Prof. Dr. Andreas Schäfer

Prüfungsauschuß:

Vorsitzender:	Prof. Dr. Ch. Back
1. Gutachter:	Prof. Dr. A. Schäfer
2. Gutachter:	Prof. Dr. V. Braun
Weiterer Prüfer:	Prof. Dr. I. Morgenstern

ABSTRACT

In this work we develop a systematic approach to calculate moments of leading-twist and next-to-leading twist baryon distribution amplitudes within lattice QCD. Using two flavours of dynamical clover fermions we determine low moments of nucleon distribution amplitudes as well as constants relevant for proton decay calculations in grand unified theories. The deviations of the leading-twist nucleon distribution amplitude from its asymptotic form, which we obtain, are less pronounced than sometimes claimed in the literature. The results are applied within the light cone sum rule approach to calculate nucleon form factors that are compared with recent experimental data.

Contents

CHAPTER 1

The Global Frame

Quantum field theories are the state-of-the-art in modern physics. The development of quantum mechanics and the aim to include properties of fields in this framework resulted finally in the formulation of the first quantum field theory, the quantum electrodynamics. This theory demonstrates the successful unification of quantum mechanics and electrodynamics allowing highly precise calculations of matter properties at the atomic scale. Many effects, like anomalous magnetic moment of the electron, the Lamb shift of the energy levels of hydrogen, could be predicted and are tested to a precision, which can only rarely be reached within physics. Quantum electrodynamics was not only the first physical relevant quantum field theory, it served also as a prototype for other quantum field theories. Although it seems that quantum electrodynamics is driven to its limits, we are still detecting new properties and effects within this theory, like in the field of cavity-quantum electrodynamics.

From the theoretical point of view, the next step was to describe not only the electromagnetic force by a quantum field theory but also the other fundamental forces which act at nucleonic scale, namely the weak and the strong interaction. Up to now, only the gravitation resists to be formulated as a quantum field theory. The present knowledge of the interplay and some partial connections between the different quantum field theories is condensed in the standard model of particle physics. It is the essence of what is known by the physicists about the fundamental forces in the nature up to our day.

Therefore the aim of todays and tomorrows experiments is a better understanding of the **complete** standard model and, may be even more important, the search for new physics to answer the unresolved secrets of nature. Hence it is not only

important to understand each known force separately but also the interplay and the hidden connections of the different sectors of the standard model are of the key importance for the future. In quantum mechanics probably the most important breakthrough was achieved by calculating the different properties of the most simplest object, the hydrogen wave function. Within the standard model we have still not reached the point to be able to calculate the wave functions of the most simple objects, the hadrons like mesons and baryons. As the hadrons are built up from more elementary particles which interact through weak and strong forces, the calculation would involve obviously both of these forces. However, as the name may implicate, the weak force is less important in this cases and is not taken into account within this work .

The theory of the strong interaction is Quantum Chromodynamics (QCD) which will be the basis of the calculations in this work. However, as already pointed out, QCD cannot be studied isolated but the connections to other parts of the standard model are also of crucial importance. Any prediction and also any description of tomorrows and todays experiments involves all parts of the standard model. Thus, to approve or to falsify the standard model we need highly precise theoretical descriptions of all ingredients in standard model. The understanding of the nucleon properties is of particular importance for experiments. To inspect the nature at the femtometer scales we need microscopes with very high resolution. Thus we need very high energies which are at the moment only reachable if we use nucleons as probe. But as long as there is a lack of the true theoretical understanding of the nucleon properties, all experimental results and theoretical predictions are limited by our present knowledge. Thus in full analogy to the hydrogen wave function, we would like to have an analogous description of the nucleon. The knwoledge of the full nucleon wave function would be an enormous improvement, but the calculation of that seems to be almost impossible due to the intricacy of the quantum chromodynamics. However, as long as we can not access the full nucleon wave function we can reduce the complexity of the problem. In this work we calculate quantities which contain less information than the full nucleon wave function, but are already close to that. Although the information is slightly reduced, this quantities provide a lot of additional informations compared to others usually used to describe the nucleon structure. Thus, this additional information is of great importance to understand the experimental results now and in the future.

Of course we do not want to understand only the standard model but would also like to discover unknown physical phenomena beyond it. This also requires calculations using our present knowledge. In the next two section of this chapter we will give a short overview of the standard model and a connection to the physics beyond the standard model based on some recent publications in this field [1, 2, 3, 4] in order to establish a gross framework in which our results should

be set. For a more detailed introduction we refer the reader to the standard text-books e.g., [5], and for recent developments to the selected papers [1, 2, 3, 4] and references therein. In the second chapter we focus our attention on the theory underlying our calculation, the Quantum Chromodynamics where we introduce also the objects of our interest, the Nucleon Distribution Amplitudes (NDA) and proton decay constants, which are related to possible theories beyond the standard model. The following chapters contain then the details about our approach and overview of results, we have obtained.

1.1 Standard Model ...

The standard model of particle physics is the most successfull theory in physics. It describes three of the four known interactions and is still valid beyond the energies it was designed for. The wide applicability range of the standard model and the innumerable experimental confirmations are the key reasons for its success. From the theoretical point of view the standard model has a simple and elegant structure being at the same time as economical as possible. By requiring Lorentz invariance of the theory and few local symmetries we obtain almost full description of the phenomena like the strong and electroweak interactions, confinement and symmetry breaking, hadronic and leptonic flavour physics etc. The study of all these aspects has kept many physicists busy for the last three decades and we are still not at the point where we can claim to understand all ascpects of the standard model.

The success of the standard model is mostly based on few key features which are related to our current understanding of nature:

- The standard model brings together the relativity and quantum mechanics, therefore the elementary particles are described by quantum fields.
- Being an effective theory the predictions are based on the regularisation of divergent quantum corrections and the renormalisation procedure which introduces a scale dependence of the observed quantities.
- All interactions are related to local symmetries and are described by Abelian and non-Abelian gauge theories.
- The masses of all particles are generated dynamically by confinement (hadrons) and spontaneous symmetry breaking (fermions) induced by the Higgs field.

Now let us take a closer look on the ingredients of the standard model. The "ugly" fermionic sector of the standard model has three families or generations of

particles

Quarks	$\begin{pmatrix} u \\ d \end{pmatrix}$	$\begin{pmatrix} c \\ s \end{pmatrix}$	$\begin{pmatrix} t \\ b \end{pmatrix}$
Leptons	$\begin{pmatrix} e \\ \nu_e \end{pmatrix}$	$\begin{pmatrix} \mu \\ \nu_\mu \end{pmatrix}$	$\begin{pmatrix} \tau \\ \nu_\tau \end{pmatrix}$

Since 1989 it is believed that there are no more generation because the experiments carried out in SLAC and CERN strongly suggest that there are three and only three generations of fundamental particles within the standard model [6]. This is inferred by showing that the lifetime of the massive Z^0 gauge boson is consistent only with the existence of exactly three very light (or massless) neutrinos. Of course the existence of an additional very heavy neutrinos is not excluded.

In the gauge sector the spin 1 gauge bosons describe the fundamental interactions of the standard model,

$A^a_\mu, a = 1, \ldots, 8:$	the gluons of the strong interaction
$W^I_\mu, I = 1, 2, 3, B_\mu:$	W and B bosons of the electroweak interaction.

These gauge interactions have a beautiful geometric interpretation and are associated with the symmetry group of the standard model

$$G_{\text{SM}} = SU(3)_{\text{C}} \times SU(2)_{\text{W}} \times U(1)_{\text{Y}}$$

where the subscripts C, W and Y denote the colour, weak isospin and hypercharge, respectively. Since the leptons do not carry any colour charge, the only particles which interacts strongly are the quarks, which are confined in hadrons as colour singlets. We will come later to this part of the standard model and will discuss it more extensively, since it will be the basis of this work.

The electroweak part of the standard model $G_{\text{WE}} = SU(2)_{\text{W}} \times U(1)_{\text{Y}}$ is a chiral gauge theory, and this gauge symmetry is spontaneously broken. The building blocks of the chiral gauge theory are the massless left- and right-handed fermions with the possibility of different gauge quantum numbers. Having different representations for $SU(2)_{\text{W}}$ (a chargeless one-dimensional singlet representation and a charged two-dimensional doublet representation) and some experimental information about present couplings it is possible to figure out the grouping of the particles. The left-handed fermions are grouped to transform as $SU(2)_{\text{W}}$ doublets while the right handed fermions transform as $SU(2)_{\text{W}}$ singlets. Accordingly the left-handed fermions couple to W^I_μ and B_μ fields, whereas the right-handed couple to the B_μ field only.

The last and maybe the most interesting ingredient of the standard model is the complex scalar Higgs field Φ. It is the only particle of the standard model which is not yet confirmed experimentally. As a doublet under $SU(2)_{\mathrm{W}}$ transformations the Higgs field couples to W_μ^I and B_μ fields and in the Lagrangian it generates a mexican hat potential of the form

$$V(\Phi^\dagger\Phi) = -\mu_h^2\Phi^\dagger\Phi + \frac{1}{2}\lambda(\Phi^\dagger\Phi)^2, \quad \mu_h^2 > 0.$$

This potential has a minimum away from the origin at $\Phi^\dagger\Phi = \mu_h^2/\lambda$ which fixes the modulus of $\Phi^\dagger\Phi$, the other three degrees of freedom can be eliminated by a appropriate gauge transformation. Rewriting the theory in terms of the physical degrees of freedom the $SU(2)_{\mathrm{W}}$ symmetry becomes hidden and three of the four physical fields, which are combinations of the original W_μ^I and B_μ fields, acquire mass terms through the coupling to the Higgs field. The remaining massless neutral vector field is the photon and the three massive vector fields are the two charged $W^\pm$ bosons and one neutral Z boson.

Sometimes it ist stated that the Higgs mechanism leads to spontaneous symmetry breaking what in some way hides the true meaning. The gauge symmetry is not really broken but only hidden and is therefore not directly manifest in the physical fields. But what are the consequences of the spontaneous symmetry breaking for the fermions? Remember, the left- and right-handed fermions couple differently to the G_{WE} gauge bosons and there are additionally allowed Yukawa couplings to the Higgs doublet. After the spontaneous symmetry breaking the Higgs field has a non-zero vacuum expectation value $\langle\Phi\rangle = \mu_h/\sqrt{\lambda}$ and the Yukawa couplings of the fermions to the Higgs field become effectively masses. These mass CKM-matrix named after Cabibbo, Kobayashi and Maskawa is not diagonal what is reflected by the fact that the mass eigenstates are not the weak eigenstates leading to CP violation.

1.2 ... and a Glimpse Beyond

Despite all the beauty, the standard model has aesthetic deficiencies we cannot ignore. If someone studied the standard model for some time he would recognise that the standard model and so our present understanding of the nature has some obvious hints that there must be something which is more general. The awareness that there is more fundamental description of the nature comes from the already known structure of the standard model. However, the answer are beyond the standard model. On the other hand our present knowledge guides us on the right way towards a better understanding of nature.

The structure of the gauge sector in the standard model is extremely economical and precise at the same time. It describes three different forces only by three continuous parameters. These parameters are becoming approximately equal at very high energies and we are forced to ask ourselves, if there is one greater symmetry which we just do not see. The product structure $SU(3)_{\mathrm{C}} \times SU(2)_{\mathrm{W}} \times U(1)_{\mathrm{Y}}$, the reducibility of the fermion representation, the cancellation of quantum anomalies, the quantisation of the charges and the peculiar assignments of hypercharges encourage us only further to believe in a more fundamendal and beautiful symmetry. We expect that this symmetry would contain the three factors, unite the representations and explain the hypercharges.

The smallest group into which the three groups of the standard model will fit is the $SU(5)$. A larger symmetry group e.g., $SO(10)$ or some related alternative is even more welcome. The $SO(10)$ contains all the particles and one additional $SU(3)_{\mathrm{C}} \times SU(2)_{\mathrm{W}} \times U(1)_{\mathrm{Y}}$ singlet particle in a single spinor **16** representation. It has the quantum numbers of the right-handed neutrino and is especially attractive in the "seesaw" mechanism which can explain the smallness of the neutrino masses. A further appealing property is the natural explanation of the hypercharges. Because of the extended symmetry hypercharges are then related to colour and weak charges

$$Y = -\frac{1}{6}(R + W + B) + \frac{1}{4}(G + P)$$

where R, W, B are colour and G, P weak charges.

As we mentioned before the larger symmetry implies that the different couplings in the standard model should be equal, but due to symmetry breaking are different at low energy scale. Taking a definite hypothesis about the particle spectrum in the unified theory we get prediction for the distortion of the different couplings. Including the vacuum polarisation from the particles we know about in the minimal standard model we obtain only approximate unification of the couplings around 10^{16} GeV .

Since the unification is only approximate it seems that we failed in our attempt to unify the theory and to keep the theory as economical as possible. Of course there are some alternatives on the market e.g., technicolour models, large extra dimension scenarios and brane-world scenarios, which render the unification of couplings as an accident. But the idea of unification is so attractive, that it is even worth to give up the economy and to introduce a complete new world of extremely heavy particles. The reward is a further and much larger symmetry, the supersymmetry called SUSY. Within SUSY the gauge bosons and fermions do not stand anymore separately but fall into common multiplets. And every presently known particle has then a heavier superpartner with same quantum numbers but differing in spin by $1/2$ and mass. The gain of this new particle zoo is an accurate unifi-

cation of the couplings if one includes the vacuum polarisation of the additional particles.

At this point one can be disappointed since the 10^{16} GeV unification scale is far beyond our present possibilities and one may believe that nature is teasing us, allowing us to recognise that there is something else, but not giving us the possibility to figure it out. But there is no need for such high energies. Already at next generation experiment as the Large Hadron Collider (LHC) some of the particles may become accessible. Another possibility will be to look for decay processes, e.g., proton decay, which are not allowed within the standard model but other theories. This approach implies that we can predict observations within standard model sp precisely, that we are able to state that a certain observation contradicts the theoretical description. This requires obviously highly precise theoretical calculations in all parts of the standard model but also precise experimental results.

In summary we can state that the standard model is the foot in the door to understand the fundamental of nature better and it will surely be a working horse for a long time in future. All alternatives will have a hard time to compete with the beauty and accuracy of the standard model, but now we are also at the point where the standard model reached its limits, and we are encouraged to look for a new, maybe even more beautiful theory.

CHAPTER 2

Continuum QCD

In the last chapter we gave an overview of basic ideas of the standard model and stressed the importance and the interplay of all its parts. In future experiments the nucleon and its properties will be an important testing field for the standard model but also for the search for alternatives. As the nucleon is a composite object, and the interaction of its parts is described by the theory of strong interaction, the Quantum Chromodynamics, we will introduce now the basic concepts and some techniques of this theory. The aim is to describe the nucleonic properties using our present understanding of this theory. However, this can be decomposed in two partially independent problems.

On one hand we can calculate the properties of the nucleon using the quantum chromodynamics with the aim to make some predictions which can be used in future calculations and/or tested in experiments. In analogy to quantum mechanical wave function of the hydrogen we would also like to obtain analogous information on the internal structure of the nucleon. Obviously it is a more demanding task compared to the calculation of the hydrogen wave function.

On the other hand we can assume, that our present knowledge has to be modified by some unknown effects which allow e.g., in the standard model forbidden nucleon decay. Using a low energy effective theory it is also possible to obtain some predictions on such effects. Comparing those with the experiments will allow us to look for physics beyond the standard model. In our case as an approach we use a low energy effective theory, the chiral perturbation theory, which is based on the approximate chiral symmetry. Although the chiral symmetry is broken in the nature it plays a crucial role in the theory of the strong interaction. Thus, in the following sections, we will give some basic overview on the QCD and introduce

the objects which describe the nucleon. Due to the importance of chiral symmetry we also give some general introduction to the chiral perturbation theory and how we can gather informations relevant for nucleon decay from QCD.

2.1 Non-Abelian Gauge Theories

The construction of the non-Abelian theories is in some way similar to the Abelian case, but there are of course additional obstacles one has to fight. Before we start to consider the construction of non-Abelian theories we review shortly the basis, i.e., groups with non-commuting elements. Our focus is on the $SU(n)$ groups, groups of $n \times n$ unitary matrices with determinant 1 as these are the groups in the standard model.

The $n \times n$ complex matrix U has $2n^2$ real degrees of freedom. The unitary constraint $U^\dagger U = \mathbb{1}$ implies that $U^\dagger U$ is Hermitian and we have additional equality $(U^\dagger U)^\dagger = U^\dagger U$. Thus the diagonal entries are real and the lower triangle is the hermitian conjugate of the upper one yielding $n + n(n-1)$ real constraints. One further real constraint is $\det U = 1$ giving finally $2n^2 - n - n(n-1) - 1 = n^2 - 1$ real degree of freedom for the elements of the $SU(n)$. Hence the $SU(n)$ group members can be written in terms of $n^2 - 1$ real parameters α_i as exponentials

$$U = \exp\left\{i\alpha_i \lambda^i\right\}, \tag{2.1}$$

where $i = 1 \ldots (n^2-1)$ and λ^i are the generators of the group. Usually λ^i are chosen to be Hermitian and from the group product one can derive the commutation relation for the generators

$$\left[\lambda^a, \lambda^b\right] = i f^{abc} \lambda^c, \tag{2.2}$$

where f^{abc} is the antisymmetric structure constant depending on the choice of the generators.

As next step we consider complex fields which are $SU(n)$ multiplets. This means that we consider a n-component vector φ_i and the $SU(n)$ matrices acts on it multiplicatively:

$$\varphi = \begin{pmatrix} \varphi_1 \\ \vdots \\ \varphi_n \end{pmatrix} \rightarrow \varphi' = U\varphi, \qquad \varphi^\dagger = \left(\varphi_1^\dagger, \ldots, \varphi_n^\dagger\right) \rightarrow \left(\varphi^\dagger\right)' = \varphi^\dagger U^\dagger \tag{2.3}$$

Then a Lagrangian constructed in full analogy to classical mechanics as kinetic term minus potential

$$L = \left(\partial_\mu \varphi\right)^\dagger \left(\partial^\mu \varphi\right) - V\left(\varphi^\dagger \varphi\right) \tag{2.4}$$

is obviously invariant under unitary transformations since the product $\varphi^\dagger\varphi$ is an invariant quantity.

The generalisation from global to local symmetry $U = U(x)$ leads to the problem that the kinetic term is not invariant anymore, because the derivatives act then on $U(x)$ as well,

$$\partial_\mu\varphi \;\rightarrow\; \partial_\mu\varphi' = \partial_\mu\left(U\varphi\right) = U\partial_\mu\varphi + \left(\partial_\mu U\right)\varphi. \tag{2.5}$$

Thus to save the invariance the partial derivative must be replaced by a covariant derivative,

$$\partial_\mu \rightarrow \mathcal{D}_\mu = \partial_\mu + igA_\mu \tag{2.6}$$

where the gauge field $A_\mu = A^a_\mu\lambda^a$ is a matrix and λ^a are the generators of the group. The requirement for the invariance of the kinetic term

$$\begin{aligned}\left(\mathcal{D}_\mu\right)' &= \left[\left(\partial_\mu + igA_\mu\right)\varphi\right]' = \left(\partial_\mu + igA'_\mu\right)\left(U\varphi\right)\\ &= U\left(\partial_\mu + U^{-1}\left(\partial_\mu U\right) + igU^{-1}A'_\mu U\right)\varphi \stackrel{!}{=} U\mathcal{D}_\mu\varphi_i\end{aligned} \tag{2.7}$$

yield a transformation law for the field A_μ

$$A'_\mu = UA_\mu U^{-1} - \frac{i}{g}U\partial_\mu U^{-1}. \tag{2.8}$$

Up to now we do not have a kinetic term with A_μ in the Lagrangian, therefore no dynamics for the field A_μ is present. The desired kinetic term should be gauge invariant[1] and contain derivatives up to second order. The starting point therefore is in analogy to Abelian gauge theories the field strength tensor which is a commutator of two covariant derivatives

$$\begin{aligned}F_{\mu\nu} =& -\frac{i}{g}\left[D_\mu, D_\nu\right] = \partial_\mu A_\nu - \partial_\nu A_\mu + ig\left[A_\mu, A_\nu\right] = F^a_{\mu\nu}\lambda^a\\ F^a_{\mu\nu} =& \partial_\mu A^a_\nu - \partial_\nu A^a_\mu - gf^{abc}A^b_\mu A^c_\nu.\end{aligned} \tag{2.9}$$

The crucial point in the non-Abelian theories can be realised in the field strength tensor. It contains not only derivatives, like in the Abelian case, but also a quadratic term in the potentials. Thus the fields A_μ do not interact only with the fields φ_i but also directly with each other. Unlike in Abelian theory the field strength tensor is not invariant, but transforms as covariant quantity

$$F_{\mu\nu} \;\rightarrow\; F'_{\mu\nu} = UF_{\mu\nu}U^{-1}. \tag{2.10}$$

A kinetic term which should be quadratic in $F_{\mu\nu}$ and gauge invariant is then easily constructed by

$$L_{\text{kin}} = -\frac{1}{4}F^a_{\mu\nu}F^{a\,\mu\nu} = -\frac{1}{2}\text{tr}\left(F_{\mu\nu}F^{\mu\nu}\right). \tag{2.11}$$

[1] Otherwise we have to introduce a further gauge field

The gauge invariance follows from $\mathrm{tr}\,(UF^2U^{-1}) = \mathrm{tr}\,(U^{-1}UF^2) = \mathrm{tr}F^2$ where the normalisation convention

$$\mathrm{tr}\left(\lambda^a\lambda^b\right) = \frac{1}{2}\delta^{ab} \tag{2.12}$$

was used.

So far we considered the $SU(n)$ gauge theory at the classical level. Compared to Abelian gauge theory, the quantisation in the non-Abelian case is a more demanding task due to the self-interaction of the gauge field. As in the Abelian case the Green's function for the gauge field should be the inverse of the differential operator in the equations of motion. But due to gauge freedom the operator has zero eigenvalues and hence is not invertible. This problem can be solved pragmatically by fixing the gauge. However this causes lot of additional difficulties during the calculations due to loss of the gauge invariance.

A more clever and elegant way is the Faddeev and Popov trick [7], where one inserts a gauge-fixing term in the gauge action. This new gauge-fixing term is not gauge invariant, but represents a certain gauge condition which can be chosen freely. In Abelian theories the trick does not cause any serious problems, but in non-Abelian theories we have then one more non-trivial ingredient. Due to self-interaction of the gauge field the Faddeev Popov trick introduces a new set of anticommuting fields that are scalars under the Lorentz transformations. Thus the quantum excitations of these fields have wrong relation between spin and statistics and therefore are not physical. These fields, called Faddeev-Popov ghosts due to their strange properties, cancel exactly the contributions from non physical degree of freedom of the gauge bosons and hence can be interpreted as negative degree of freedom. But what is about the lost gauge invariance? It turns out that the gauge invariance is not really lost but rather traded for another symmetry. Independently discovered by C. Becchi, A. Rouet, R. Stora [8] and I. Tyutin [9, 10]. This new BRST-symmetry ensures that we still get physically sensible results.

2.2 The Theory of Strong Interaction

After the preparatory work for non-Abelian gauge theories we turn now to Quantum Chromodynamics, the theory of strong interaction within the standard model. At the end of the first half of the last century there was a crisis in particle physics. The discovery of many new particles led to an inflation of particle numbers. With the growth of this particle 'zoo' also the confusion of the physicist grew leading to the conviction that these particles are not fundamental. In 1964 it is was found independently by M. Gell-Mann [11] and G. Zweig [12, 13] that the different particles can be explained if the hadrons are built from more fundamental particles,

the quarks[2] which must be spin $1/2$ fermions.

The quarks allow to construct baryons as compositions of three quarks and mesons are then pairs of quarks and anti-quarks. Using three different types of quarks the different hadrons were then fitted into roughly mass degenerate multiplets of a global flavour group $SU(3)_f$. Nowadays the total number of quarks found increased to six and pairs of quarks are grouped then to form families or generations (Table 2.1).

Family	q	Name	e_q	Weak Isospin	Flavour	Mass (MeV^2)
1	u	*up*	$+\frac{2}{3}$	$+\frac{1}{2}$	$I_z = +\frac{1}{2}$	$\approx 1.5 \ldots 4$
1	d	*down*	$-\frac{1}{3}$	$-\frac{1}{2}$	$I_z = -\frac{1}{2}$	$\approx 4 \ldots 8$
2	s	*strange*	$-\frac{1}{3}$	$-\frac{1}{2}$	$S = -1$	$\approx 80 \ldots 130$
2	c	*charm*	$+\frac{2}{3}$	$+\frac{1}{2}$	$C = 1$	$\approx 1150 \ldots 1350$
3	b	*bottom (beauty)*	$-\frac{1}{3}$	$-\frac{1}{2}$	$B = -1$	$\approx 4100 \ldots 4400$
3	t	*top (truth)*	$+\frac{2}{3}$	$+\frac{1}{2}$	$T = 1$	≈ 174300

Table 2.1: Overview of quarks, grouped in families with the corresponding masses and charges in terms of the elementary electric charge e_q.

The different generations have similar pattern of quantum numbers, but with succeeding generation the quarks become heavier. The *up, down* and *strange* quark are usually termed the light quarks with masses below $\Lambda_{QCD} \approx 200$MeV, while the *charm, bottom* and *top* are the heavy quarks. As in many other applications we can ignore here safely the heavy quarks and should concern from now on only the light quarks with the effective flavour group $SU(3)_f$.

Taking the quarks to transform under fundamental $\mathbf{3}$ representation and anti-quarks to transform under the $\overline{\mathbf{3}}$ representation the nine possible $q\overline{q}'$ combinations containing the light *up, down* and *strange* quarks are grouped into an octet and a singlet of light quark mesons (Figure 2.1)

$$\mathbf{3} \otimes \overline{\mathbf{3}} = \mathbf{8} \oplus \mathbf{1} \tag{2.13}$$

The approximate $SU(3)_f$ flavour symmetry for "ordinary" baryons implies that baryons which are made up from three quarks qqq fall into one of the multiplets on the right hand side of

$$\mathbf{3} \otimes \mathbf{3} \otimes \mathbf{3} = \mathbf{10}_S \oplus \mathbf{8}_M \oplus \mathbf{8}_M \oplus \mathbf{1}_A, \tag{2.14}$$

where the subscript indicate the symmetry, mixed symmetry or antisymmetry under interchange of any two quarks in the three quark state (Figure 2.2).

[2]The name quarks introduced for this particles by M. Gell-Mann is based on the book Finnigan's Wake by James Joyce [14] ("Three quarks for Muster Mark").

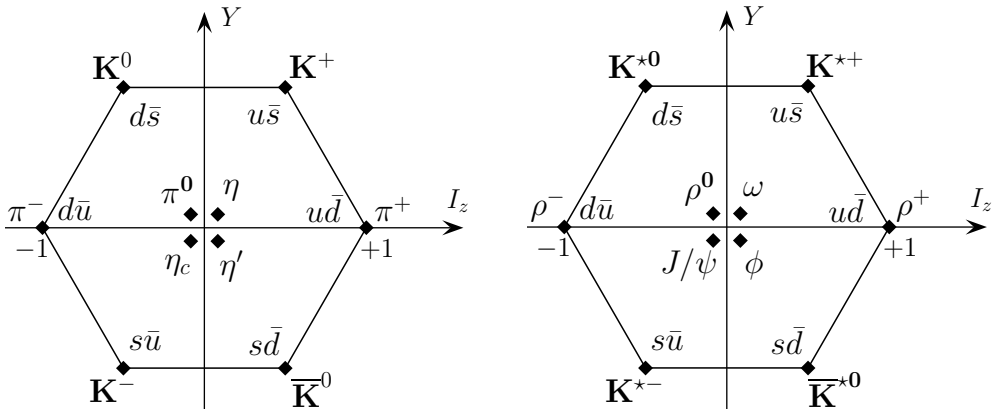

Figure 2.1: The Octet multiplets for spin 0 (pseudoscalar) and spin 1 (vector) mesons.

The quark model was the first step in the understanding of the particle 'zoo', but it lacked any dynamics. Furthermore it violated also the Pauli principle, e.g. the Δ^{++} state would be composed of three *up*-quarks each carrying spin $+1/2$, necessary to obtain the observed angular momentum $(J, J_z) = (3/2, 3/2)$. The way out was suggested a short time later by O. Greenberg [15] and by M.Y. Han and Yoichiro Nambu [16] introducing a new quantum number 'colour' for the quarks. As this quantum number was never observed the hadrons must be colour singlets. Although already 1969 the analysis of Standford Linear Accelerator data by J. Bjorken [17] gave evidence that the proton is composed from quarks[3], it was still believed that the quarks are purely mathematical objects, since they were never observed. The possible explanation therefor and the dynamics were introduced then 1973 by H. Fritzsch and M. Gell-Mann [18, 19], the quantum field theory of strong interaction was formulated. This theory of quarks and gluons is similar in structure to quantum electrodynamics (QED) but with colour charged particles and therefore is called quantum chromodynamics (QCD). Based on $SU(3)_{\mathrm{C}}$ local colour gauge symmetry and reusing our preparatory work from the last section we take for the QCD as action

$$\boxed{\mathcal{L} = -\frac{1}{4} F^a_{\mu\nu} F^{a\,\mu\nu} + \sum_{f=1}^{n_f} \bar{q}^f \left(i\gamma^\mu D_\mu - m_f\right) q^f} \tag{2.15}$$

with

$$\begin{aligned} F_{\mu\nu} =& \partial_\mu A_\nu - \partial_\nu A_\mu - ig\,[A_\mu, A_\nu] \\ D_\mu =& \partial_\mu - ig\lambda^a A^a_\mu. \end{aligned} \tag{2.16}$$

[3]They do not used the name "quarks", but called the constituents "partons".

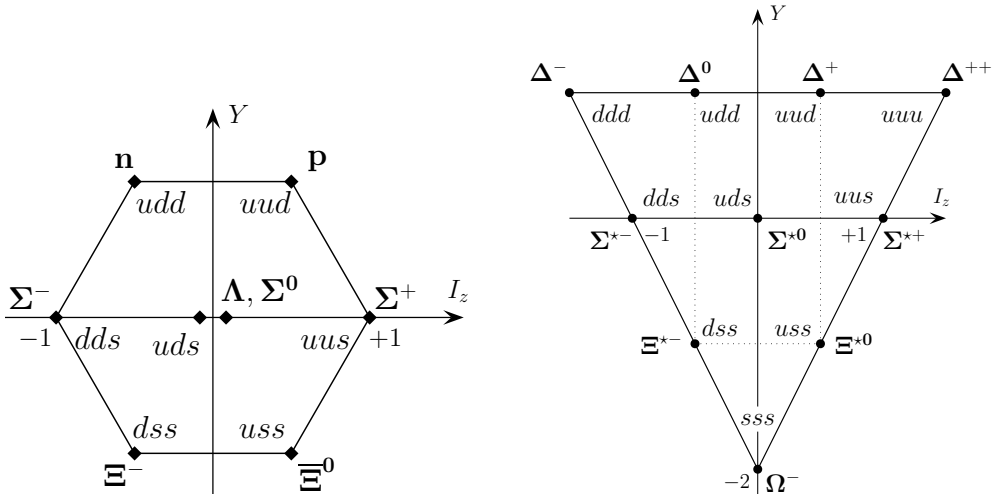

Figure 2.2: The Octet and Decuplet for spin half and three half baryons.

The index f denotes the different quark flavours and n_f is the number of the used flavours, γ_μ are the Dirac matrices.

Without losing a local gauge $SU(3)_\mathrm{C}$ invariance we can add a topological term proportional to $\theta \tilde{F} F$ with another parameter θ where $\tilde{F}_{\mu\nu} = \epsilon_{\mu\nu\omega\rho} F^{\omega\rho}$ is the dual of F. The physical quantity connected to this term is the topological charge defined as

$$Q = -\frac{1}{32\pi^2} \int \mathrm{d}^4x \ \mathrm{tr} \left(\tilde{F}_{\mu\nu} F^{\mu\nu} \right) \tag{2.17}$$

which takes integer values in the third homotopy group of the gauge group. For $\theta \neq 0$ or π this term explicitly breaks parity as well as CP invariance. From the measurements of the electric dipole moment of the neutron we have at the moment an upper bound of $|\theta| < 10^{-9}$ suggesting $\theta = 0$. Hence this term should not bother us here. However the smallness of θ is puzzling since the CP invariance is already explicitly broken in the electroweak sector of the Standard Model by the complex phase of the Cabbibo-Kobayashi-Maskawa matrix. This puzzle is commonly known as the strong CP problem and is also intimately connected to the axial anomaly which we discuss in section 2.6.1.

2.3 QCD Phenomenology

2.3.1 Asymptotic Freedom & Confinement

After we have introduced the basics of the quantum chromodynamics we take now a closer look on the properties of this theory. As already mentioned QCD

is a non-Abelian gauge theory and the gauge bosons interact directly with each other. This introduces a new level of complication in theoretical calculations and of course changes also the properties of this theory compared to QED. Maybe the most important consequence is the behaviour of the strong coupling constant as a function of the scale μ. This dependence is described by the β-function

$$\frac{\mathrm{d}\,\alpha_s(\mu)}{\mathrm{d}\ln\mu^2} = \beta(\alpha_s) \quad \text{with} \quad \beta(\alpha_s) = -\frac{\alpha_s^2}{\pi}(\beta_0 + \beta_1\frac{\alpha_s}{\pi} + \dots) \tag{2.18}$$

which assumes that α_s is small so that the perturbative expansion is justified. For the QCD, the $SU(3)_\mathrm{C}$ gauge theory with $N_c = 3$ colours one has

$$\beta_0 = \frac{11}{12}N_c - \frac{n_f}{6} \tag{2.19}$$

which is positive for $n_f \leq 33/2$. Then eq. (2.18) implies that with increasing energy the coupling becomes smaller, so in the limit of high energies the particles in QCD are only weakly coupled and the perturbative approach should be possible. This phenomenon, also known as *asymptotic freedom*, was discovered already in 1973 by D. Politzer, F. Wilczek and D. Gross [20, 21] and was awarded with a Nobel Prize in Physics 2004. Contrary, this behaviour also implies that at low energies the coupling should become strong and the perturbative approach would break down. QCD in this strong coupled region is much less understood since it requires nonperturbative calculations.

Due to the strong coupling at low energies the quarks are *confined* within hadrons and therefore can not be observed as free particles. Thus, also colour charges can not be observed freely and particles built up from quarks like mesons (quark and anti-quarks) or baryons (three quarks) must be colour neutral. As one tries to separate two quarks from each other they form a colour flux tube out of gluon fields. Therefore the force between the quarks stays constant and the total energy of the system is rising linearly with increasing distance. Thus, at some distance it is energetically favourable for the system to generate a quark and anti-quark pair out of the vacuum producing independent but still bound colourless states. Although this picture of string breaking is confirmed by lattice calculations [22] we are still lacking a true understanding of confinement. Thus to understand nature we need also to understand the mechanism of the *confinement* and how the different hadrons are built up from quarks. Lattice QCD provides a nonperturbative approach allowing us to examine the strongly coupled region and to obtain results that are not reachable within perturbative calculations. In particular, using Lattice QCD a proof of *confinement* seems also to be within reach [23, 24], putting us further in the understanding of the standard model.

2.3.2 QCD Scale and the Origin of Hadron Masses.

The notion of scale in a quantum field theory is not restricted to QCD. However, the QCD scale is of particular interest as it is connected through confinement to hadron masses. Naively one can assume that hadron masses should be of the order of involved quark masses which is, of course, immediately falsified just by measuring the proton mass. Even in the chiral limit of vanishing quark masses hadrons would be not massless which can be traced back to the trace anomaly.

At classical level the QCD Lagrangian in the limit of vanishing quark masses does not have any intrinsic scale and therefore the rescaling of the involved fields will leave the action unchanged. This means that after rescaling the fields by

$$\phi(x) \rightarrow e^{-d_\phi \tau}\phi(xe^{-\tau}), \tag{2.20}$$

where d_ϕ is the canonical mass dimension of the field, the theory remains unchanged. The associated dilatation current which is conserved due to Noether theorem is

$$J_d^\mu = \Theta^{\mu\nu}x_\nu, \quad \partial_\mu J_d^\mu = \Theta^\mu{}_\mu = 0 \tag{2.21}$$

with the energy-momentum tensor $\Theta^{\mu\nu}$. In a quantum field theory which is coupled to gravitation the energy-momentum tensor can be obtained by varying the Lagrangian $\mathcal{L}$ with respect to space-time metric $g_{\mu\nu}$

$$\Theta^{\mu\nu} = 2\frac{\delta}{\delta g_{\mu\nu}(x)}\int \mathrm{d}^4x\mathcal{L} \tag{2.22}$$

and therefore the scale transformation as a change in spacetime metric

$$g_{\mu\nu}(x) \rightarrow e^{2\tau}g_{\mu\nu}(x) \tag{2.23}$$

will change the Lagrangian just by the trace of $\Theta^{\mu\nu}$.

In a quantum field theory the couplings of fields are not constant but changes with the scale as

$$g \rightarrow g + \tau\beta(g) \tag{2.24}$$

where $\beta(g)$ describes the theory dependent coupling scaling. The corresponding change in the Lagrangian is then

$$\tau\beta(g)\frac{\partial}{\partial g}\mathcal{L} \tag{2.25}$$

inducing in most cases breaking of scale invariance. Therefore the trace of the energy-momentum tensor is then

$$\partial_\mu J_d^\mu = \Theta^\mu{}_\mu = \beta(g)\frac{\partial}{\partial g}\mathcal{L}. \tag{2.26}$$

This is also known as the *trace anomaly*. Rewriting the last formula in terms of QCD fields yields for the trace of energy-momentum tensor in QCD

$$\Theta^{\mu}{}_{\mu} = \frac{\beta(g)}{2g^3} F^a_{\lambda\sigma} F^{a\,\lambda\sigma}. \tag{2.27}$$

Therefore the mass expectation value in QCD for any hadronic state $|p\rangle$ with momentum p

$$\langle p|\Theta^{\mu}{}_{\mu}|p\rangle = 2p^{\mu}p_{\mu} = 2m_H^2 \neq 0 \tag{2.28}$$

will not vanish, the sizes and masses of the hadrons therefore are determined by the QCD scale which is experimentally $\Lambda_{\mathrm{QCD}} \approx 200\,\mathrm{MeV}$.

However at this point one may ask why the proton masses are so far below the Planck scale M_{P} constructed from the Newton's constant G

$$M_{\mathrm{P}} = \frac{1}{\sqrt{G}} \approx 10^{19}\mathrm{GeV}, \tag{2.29}$$

which is the grand unification scale of gravitation and other interactions. As Wilczek has explained [25], the nucleon mass is much smaller than the Planck scale partly due to the asymptotic freedom of QCD. It seems that also chiral symmetry, which we consider at the end of this chapter, plays a crucial role as discussed e.g., in [26].

2.3.3 Nucleon Form Factors

Many of the known results in QCD were obtained over years from electron-nucleon scattering experiments (Figure 2.3) where an electron scatters elastically with the nucleon at momentum transfer $-q^2 = Q^2 \approx 1\,\mathrm{GeV}^2$. Since the QED coupling constant is small one can consider the limit of one photon exchange so that the scattering amplitude can be written as a product

$$T_{fi} = (-ie)^2 \bar{v}_e(k')\gamma_\mu v_e(k) \times \frac{i}{Q^2}\langle p'|J^\mu(q)|p\rangle \tag{2.30}$$

with vector current

$$J^\mu = \frac{2}{3}\bar{u}\gamma^\mu u - \frac{1}{3}\bar{d}\gamma^\mu d + \ldots \tag{2.31}$$

acting on pronto state $|p\rangle$ and v_e the electron spinors. The informations about the nucleon structure are then obtained from the formfactors. Those are defined from general Lorentz decomposition of the matrix element in eq. (2.30). Being a compound particle the Dirac and Pauli form factors F_1 and F_2 respectively describe the deviation from pointlike structure of the general decomposition

$$\langle p'|J^\mu(q)|p\rangle = \bar{N}(p')\left[\gamma_\mu F_1(q^2) + i\sigma^{\mu\nu}\frac{q_\nu}{2m_N}F_2(q^2)\right]N(p) \tag{2.32}$$

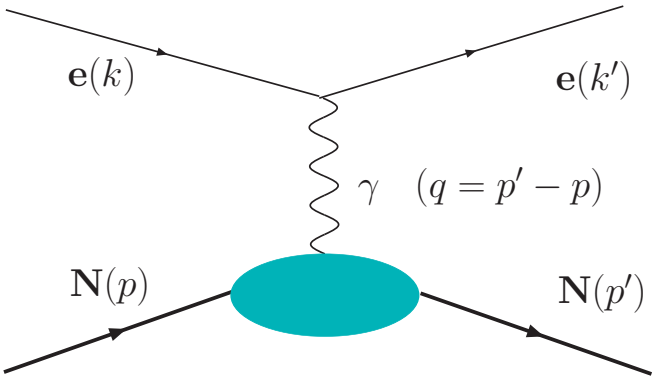

Figure 2.3: Electron-nucleon scattering for the case of one photon exchange. The green ellipse denotes the nonperturbative QCD part, which is described by the nucleon form factors (eqs. (2.30) and (2.32)).

where m_N is the mass of the nucleon and $N(p)$ ($N(p')$) the nucleon spinor before (after) the scattering process and $\sigma_{\mu\nu} = i(\gamma_\mu - \gamma_\nu)/2$. The values of the Dirac and Pauli form factors at $Q^2 = 0$ define the electric charge and the anomalous magnetic moment of the nucleon:

$$F_1^p(0) = 1, \quad F_1^n(0) = 0, \quad F_2^p(0) = \kappa_p = 1.79, \quad F_2^n = \kappa_n = -1.91, \quad (2.33)$$

where the index p and n stands for proton and neutron respectively. From experimental point of view the more convenient combination are the electric and magnetic Sachs form factors

$$\begin{aligned} G_e(q^2) =& F_1(q^2) + \frac{q^2}{(2m_N)^2} F_2(q^2) \\ G_m(q^2) =& F_1(q^2) + F_2(q^2) \end{aligned} \quad (2.34)$$

which are preferable, since the cross section can be written as the sum of squares of these form factors, i.e. there is no interference term. In the special frame of reference, the Breit-frame ($q = (0, 0, 0, -Q)$ and $p = (E, 0, 0, p_3)$), $G_e(q^2)$ describe the distribution of the electric charge and $G_m(q^2)$ the magnetic current distribution. Both form factors, G_m and G_e correspond also in the same frame of reference to helicity conserving and helicity-flip amplitude respectively.

The experimental values of G_m below $5\,\mathrm{GeV}^2$ are described very well by the famous dipole ansatz:

$$\frac{1}{\mu_p} G_m^p(Q^2) \approx \frac{1}{\mu_n} G_m^n(Q^2) \approx \frac{1}{(1 + Q^2/\mu_0^2)^2}; \qquad \mu_0 \approx 0.71\mathrm{GeV}^2 \quad (2.35)$$

with

$$G_m^p(0) = \mu_p = 2.79 \qquad G_m^n(0) = \mu_n = -1.91. \quad (2.36)$$

Also for the electric form factor one observes dipole behaviour below 1 GeV^2 for Q^2. For larger values of momentum transfer the status was unclear until end of the last century since the later SLAC data [27] contradicted the older DESY results [28]. These measurements were based on the Rosenbluth separation of the cross section and only recently the Jefferson Lab Hall 1 Collaboration extracted the ratio $G_e^p(Q^2)/G_m^p(Q^2)$ from the simultaneous measurement of longitudinal and perpendicular polarisation components of the recoil nucleon [29, 30]. In this experiment the systematic deviation from the dipole behaviour was observed confirming the tendencies seen earlier at DESY.

There are two possibilities to generalise these form factors. One can not only consider the longitudinal distribution but also the transverse distribution of the quarks within the nucleon. Those will lead to Generalised Parton Distributions which describe the three dimensional structure of the nucleon and the forward limit will be the form factors. Here we want to consider another direction of the generalisation, the Nucleon Distribution Amplitudes. But before we can start we have to review shortly the Operator Product Expansion.

2.4 Operator Product Expansion

All deep inelastic scattering calculations involving distribution amplitudes rely so far on the operator product expansion or OPE. Introduced 1969 by Wilson [31] into particle physics to face various problems in strong interaction calculations and proven few years later by W. Zimmermann [32] in perturbative quantum field theory, it became the most important tool in quantum field theorical calculations. Given the importance of this tool, it was proven also for conformal field theories [33, 34, 35], while the formal mathematical proofs based on different axiomatic settings on Minkowski space-time were found in [36, 37, 38, 39]. Recently OPE was also extended to general Lorentzian curved space-time [40].

The operator product expansion states that a product of operators at different space-time points which is usually singular in quantum field theories can be written as an asymptotic series of coefficient functions times a local operator at a nearby point y

$$\mathcal{O}_1(x_1)\dots\mathcal{O}_n(x_n) = \sum_k E_{1\dots n,k}(x_1,\dots,x_n)\mathcal{O}_{1\dots n,k}(y). \tag{2.37}$$

For small distances the Wilson coefficients E can be calculated perturbatively, while the local operators on the right-hand-side encodes the nonperturbative content. Therefore, the operator product expansion is used in a small distance region, where the smallness is usually ensured by an “internal reason” like the W-boson

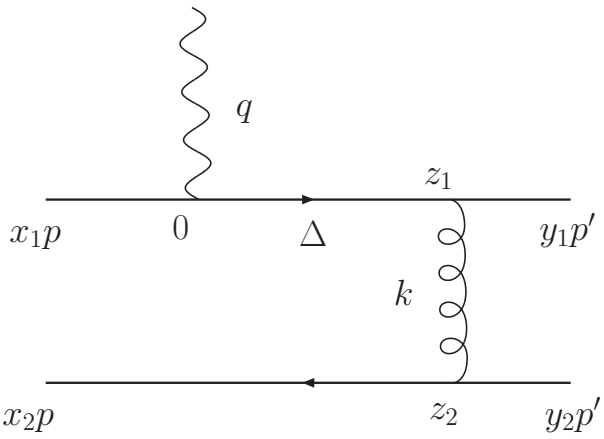

Figure 2.4: Lowest order Feynman diagram with the gluon exchange between two valence quarks of the meson. $\Delta = p' - x_2 p$, $\Delta^2 \approx x_2 q^2$, $k = y_2 p' - x_1 p$ $k^2 \approx x_1 y_2 q^2$

mass or the heavy c and b-quark masses. In this case the leading terms in the operator product expansion are operators with minimal dimensionality. In our case of exclusive processes in deep inelastic scattering the smallness of the relative distance is ensured by an "external reason", the large momentum transfer. Then the parameter which determines the importance of the operators in the expansion is the twist which is defined as the dimension of the operator minus its spin.

As the method for obtaining operator expansion for exclusive processes does not follow directly from the Wilson expansion of local operator products we demonstrate it here for a "simple" case, the meson form factor which is defined as matrix element

$$\langle p'|J_\mu|p\rangle \tag{2.38}$$

where the quark current $J_\mu = \bar{q}\gamma_\mu q$ is sandwiched between mesonic states with different momenta p and p'. The main idea for the approach we illustrate below was proposed in [41] and applied e.g., in [42].

Mesons are built of a quark and antiquark, therefore the lowest order Feynman diagrams describing the coupling of the photon to these quarks have the form given in Figure 2.4. The virtuality of the quark and gluon propagators, $\langle 0|\bar{q}(z_1)q(0)|0\rangle$ and $\langle 0|\bar{G}_\nu(z_1)G_\rho(z_2)|0\rangle$, is of order $\Delta^2 \sim k^2 \sim q^2$, i.e. $(z_1-0)^2 \sim (z_2-0)^2 \sim (z_2-z_1)^2 \sim 1/q^2$, so the use of perturbation theory for this parts is justified due to the asymptotic freedom of the QCD. On the other hand quarks which are produced close to each other at the distance of order $(z_2 - z_1) \sim 1/q$ and stay a long time collinear to each other will interact strongly. Therefore we should not calculate the external quark lines explicitly but should remain with the Heisenberg operator acting in the small virtuality and small momentum transfer

subspace. Then, we can write the meson formfactor as

$$\langle p'|J_\mu|p\rangle \to \oint \mathrm{d}z_1\mathrm{d}z_2\langle p'|\left\{\bar{q}_\alpha(z_1)\exp\left(ig\int\limits_{z_2}^{z_1}\mathrm{d}\sigma_\mu G_\mu(\sigma)\right)q_\beta(z_2)\right\}_{ij}|0\rangle$$
$$\times C^{ijkl}_{\mu,\alpha\beta\gamma\delta}\langle 0|\left\{\bar{q}_\gamma(z_2)\exp\left(ig\int\limits_{0}^{z_2}\mathrm{d}\sigma_\nu G_\nu(\sigma)\right)q_\delta(0)\right\}_{kl}|p\rangle \tag{2.39}$$

where $\oint$ means a integration over the small space-time volume $\sim 1/q^4$ around 0, i,j,k,l are the colour indices and $\alpha,\beta,\gamma,\delta$ the spinor indices. $C^{ijkl}_{\mu,\alpha\beta\gamma\delta}$ dentotes the hard scattering part of the process. The meaning of this expression becomes more clearly as we look at the operator expansion of the current at short distances

$$J(0) \to [\bar{q}(0)q(0)] + g^2\oint \mathrm{d}z_1\mathrm{d}z_2\,[\bar{q}q]\,|0\rangle C_1\langle 0|\,[\bar{q}q]$$
$$+ g^3\oint \mathrm{d}z_1\mathrm{d}z_2\mathrm{d}z_3\,[\bar{q}qF]\,|0\rangle C_2\langle 0|\,[\bar{q}q] + \ldots, \tag{2.40}$$

where we have suppressed for simplicity the different indices and F is the field strength tensor. The eq. (2.40) can be understood as follows. Due to quantum fluctuations in the small vicinity of 0 the photon transforms into two independent systems of quarks and gluons which move then in opposite directions. The amplitude C_i for this transition can be calculated perturbatively. After taking the matrix element between the mesonic states the matrix elements of the moving quarks and gluons describe then the transition of the partonic systems to mesons. Due to the increasing dimension of the operators on the right hand side of eq. (2.40) the contributions becomes suppressed by additional powers of $1/q$ implying that the minimal Fock state with two quarks is the leading one.

However also the leading Fock state operator is still a nonlocal operator but should be seen as a generating functional for local operators required by the OPE which are then obtained by Taylor expansion of the nonlocal operators. Let us exemplify that on the leading bilocal quark-antiquark operator. The leading twist contribution to the bilocal matrix element can be then written as

$$\langle 0|\bar{q}(z)q(0)|p\rangle = \sum_{n=0}^{\infty}\frac{i^n}{n!}z_{\mu_1}\ldots z_{\mu_n}\langle 0|\bar{q}\overleftrightarrow{D}^{\{\mu_1}\ldots\overleftrightarrow{D}^{\mu_n\}}q(0)|p\rangle + \textit{higher twist} \tag{2.41}$$

where $\overleftrightarrow{D} = (\overrightarrow{D} - \overleftarrow{D})$ and the curly brackets $\{\ldots\}$ denotes total symmetrisation in Lorentz indices and the substraction of traces. Hence at large Q^2 only the leading twist of the leading Fock state will contribute to the meson formfactor.

At the end we should stress that we described here only roughly the scheme to obtain the operator expansion for the mesons in the asymptotic case. However, for baryons and for not so large Q^2, the analysis will be obviously more involved because of increased number of valence quarks and contributions from higher twists which are not negligible in this energy region. Additionally, we want to point out that later we will use operator expansion within the framework of the Light Cone sum rules (LCSR), which allow calculation at intermediate values of Q^2. Therefore, we will use a version of the operator expansion, which is adapted to the Light Cone sum rules, but the ideas and the line of arguments are basically the same as displayed in this section. Unfortunately the discussion of the different sum rule methods is far beyond the scope of this work and therefore we will restrict ourselves in further discussion of Light Cone sum rule approach only to some basic parts required in our calculations.

2.5 Distribution Amplitudes

The knowledge of the wave function of any system in quantum mechanics gives us the possibility to predict and calculate many properties of this system. As in quantum mechanics also in QCD we would like to know the wave functions of the bound systems like mesons or baryons. However, the complexity of these systems is much higher, requiring a more sophisticated approach. To reduce the complexity of the problem we consider the Distribution Amplitudes which are defined in terms of the Bethe-Salpeter type wave function

$$\Psi_{\text{BS}}(x) = \langle 0|T\left[q(x_1, k_{1,\perp})q(x_2, k_{2,\perp})q(x_3, k_{3,\perp})\right]|p\rangle \tag{2.42}$$

with x_i being the logitudinal momentum fractions carried by partons and $k_{i,\perp}$ their transverse momenta and $|p\rangle$ the proton state with momentum p. The leading twist distribution amplitudes are then obtained by integrating out the transverse momenta

$$\Phi(x_i, \mu) = Z(\mu)\int^{|k_\perp|\leq\mu} \mathrm{d}^3 k_{i,\perp}\Psi_{\text{BS}}(x, k_\perp) \tag{2.43}$$

where Z is the renormalisation factor for the quark field operator and x_i are the remaining logitudinal quark momenta fractions. Higher-twist distribution amplitudes are more numerous and describe either the contribution of the "bad" components in the wave function, or contributions of transverse momenta or higher Fock states with additional gluons and/or quark-antiquark pairs.

There are different possibilities to establish the connection between the Distribution Amplitudes and the observable physical quantities. As we are going to present later some results obtained in Light Cone sum rule approach, we also introduce the Nucleon Distribution Amplitudes within this context.

2.5.1 In a Nutshell

In the past the main results about the nucleon structure were obtained within the frame of inclusive processes where one measures only the scattered electron. Nevertheless the aim of the future experiments is to go to higher luminosity and to more and more exclusive channels measuring as much as possible of the produced particles. One of the main reasons to deal with increased experimental and theoretical difficulties is the growing understanding in the recent time how much can be learned about the internal hadronic structure and especially the spin structure from these processes. The increased experimental possibilities require also larger efforts from the theoretical side to make fully quantitative predictions of hard exclusive processes.

In QCD, the theory of strong interaction, many powerful results are obtained from perturbative calculations applicable to a large variety of scattering processes. The success of this approach is based mainly on the factorisation properties of the investigated reactions. In this framework the scattering process is factorised in perturbative and non-perturbative parts. Since the non-perturbative parts are universal for different scattering processes it is possible to relate them to each other order by order in the coupling constant of the strong interaction using perturbation theory for the non-universal part. In the case of the inclusive processes the non-perturbative parts are described by the distribution and fragmentation functions for quarks and gluons. These functions have to be either calculated in a framework beyond the scope of perturbation theory or have to be extracted from a subset of experimental data and then to be used for other. In the case of the hard exclusive processes the measured quantities are various form factors.

In this work we focus on the calculation of the quark distribution amplitudes of the nucleon. Although being equally important and complementary to the conventional distribution functions the distribution amplitudes are much less studied. These unsatisfying situation is mainly based on the more challenging situation one has to deal with during the experimental and theoretical studies of the distribution amplitudes. Thus, for facilitating fully quantitative predictions for processes involving these objects the knowledge of the nonperturbative quark distribution amplitudes within a hadron is essential.

Distribution amplitudes were introduced in [41, 43, 44, 45, 46, 47] and describe the hadron structure in terms of valence quark Fock states at small transverse separation and, unlike distribution functions in inclusive processes, can not be accessed "directly" in experiments. Only some indirect insight can be obtained by measuring physical quantities like the magnetic form factor of the nucleon $G_M(Q^2)$. At very large values of Q^2 the electromagnetic form factors of the nucleon can be expressed as a convolution of a hard scattering kernel $h(x_i, y_i, Q^2)$

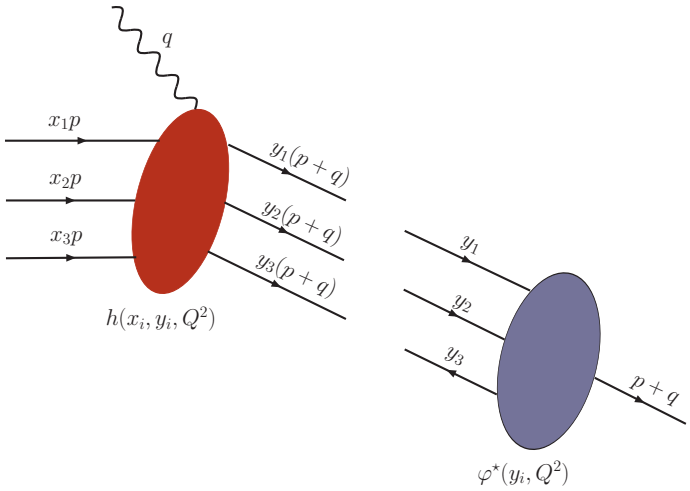

Figure 2.5: The factorisation of the subprocess relevant in the calculations involving the quark distribution amplitudes of the nucleon. The hard scattering kernel $h(x_i, y_i, Q^2)$ calculable within the perturbative QCD is denoted by the red ellipses, while the blue one stands for the nucleon distribution amplitude describing the transition of three collinear valence quarks to the nucleon.

and the quark distribution amplitude in the nucleon $\varphi(x_i, Q^2)$ [44]:

$$G_M(Q^2) = \int_0^1 [\mathrm{d}x] \int_0^1 [\mathrm{d}y] \varphi^\star(y_i, Q^2) h(x_i, y_i, Q^2) \varphi(x_i, Q^2) + O(m^2/Q^2), \tag{2.44}$$

where $[\mathrm{d}x] = \mathrm{d}x_1 \mathrm{d}x_2 \mathrm{d}x_3 \delta(1 - \sum_{i=1}^3 x_i)$, and $-Q^2$ equals the squared momentum transfer in the hard scattering process (cf., Figure 2.5). In this case only the leading twist nucleon distribution amplitude contributes. The variables x_i (y_i) can be interpreted in a appropriate gauge as the momentum fractions carried by the valence quarks before (after) the hard scattering.

The theoretical study of non-perturbative quantities, like distribution amplitudes, is a demanding task in QCD. The sum rule approach used for the calculation of moments of distribution amplitudes has large systematic uncertainties making it difficult to obtain reliable results. Apart from QCD sum rule determinations, an analytical approach to the distribution amplitude is feasible only for sufficiently large values of Q^2, where the asymptotic form $\varphi(Q^2 \to \infty) = 120 x_1 x_2 x_3$ [45, 48] is obtained. Loosely speaking, the nucleon distribution amplitude looses at high energies any information about the original form and the final asymptotic form is a universal one. However, given the logarithmic evolution in Q^2 this knowledge is not really usefull at reasonable energy scales.

At intermediate values ($1\mathrm{GeV}^2 \leq Q^2 \leq 10\,\mathrm{GeV}^2$) of the momentum transfer

Q^2 electromagnetic form factors can be calculated from nucleon distribution amplitudes using Light Cone sum rules. In contrast to the relatively simple picture at large Q^2 the factorisation does not hold anymore since the non-factorisable terms contribute also significantly [49]. Furthermore, also higher twist terms of nucleon distribution amplitudes [49, 50, 51, 52] became important and give a large contributions. Experimentally, this kinematic region gained also a lot of interest in recent years, because new data from JLAB [29, 30, 53, 54] for the well-known electromagnetic form factors of the nucleon contradict common textbook knowledge, for details see [55] and references therein.

To close the gap in the understanding and to put the calculations on a solid basis, a better and more quantitative understanding of the distribution amplitudes is desirable. Lattice QCD, as a nonperturbative approach, allows to calculate matrix elements of local operators which can be related to moments of the distribution amplitudes. These moments are non-perturbative parameters which can be used then as input in sum rule calculations of the physical quantities of interest. However, the advantages of lattice calculations have to be paid by the reduced symmetry due to the discretisation of the space-time. Thus on the lattice a straight-forward calculation will be distorted by additional unwanted operator mixings. Therefore, careful choice of used operators is an essential step in lattice calculations and can greatly improve or completely destroy the predictive power of the obtained results.

In the following we present the theoretical framework needed to sensibly set up such a calculation on the lattice and use it to calculate the moments of the nucleon distribution amplitudes up to second order. Similar analysis were done earlier to calculate moments of structure functions [56, 57, 58], generalised parton distributions [59, 60] and meson distribution amplitudes [61] based on the irreducibly transforming two quark operators [62]. However the analysis for the baryons is more demanding due to the presence of three quarks. Furthermore, our approach allows us additionally to calculate matrix elements which are relevant for the proton decay in grand unified theories.

2.5.2 Leading-Twist Nucleon Distribution Amplitudes

After a short phenomenological introduction of the distribution amplitudes as nonperturbative objects of interest in QCD we turn now our attention to a more technical and quantitative description. The nucleon distribution amplitudes were introduced within the classical framework of hard exclusive processes in [41, 63, 43, 44, 48, 45, 46, 47]. Since we are going to present later some results obtained using LCSR approach it is natural to introduce also the Nucleon Distribution Amplitudes within the context of the LCSR to establish the connection between those parts as it was done e.g in [49, 64, 52]. However we want to stress

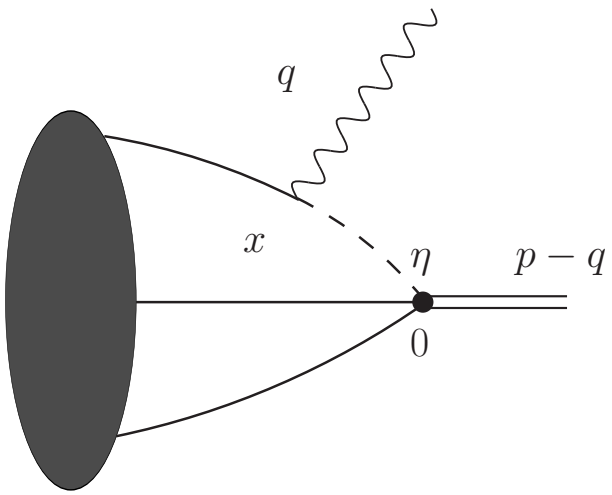

Figure 2.6: LO contribution to the correlation function in eq. (2.45)

once more that the concept of the distribution amplitudes is not restricted to light cone sum rules calculations, the distribution amplitudes are more general objects and can be used also in other not related approaches.

The starting point for LCSR calculations is the correlator

$$C_\nu(p,q) = i \int \mathrm{d}^4x \; e^{iq\cdot x} \langle 0|T\left\{\eta(0) J_\nu(x)\right\}|p\rangle \tag{2.45}$$

where J_ν is some current which couples to the proton state $|p\rangle$ and η some interpolating nucleon field. For definiteness we will use for J_ν an electromagnetic current and for η the Chernyak-Zhitnitsky interpolator [46, 65, 66]

$$J_\nu = J_\nu^{em} = \frac{2}{3}\bar{u}\gamma_\nu u + \frac{1}{3}\bar{d}\gamma_\nu d, \tag{2.46}$$

$$\eta_{\text{CZ}}(0) = \epsilon^{abc}\left[u^a(0) C \not{z} u^b(0)\right] \gamma_5 \not{z} d^c(0), \tag{2.47}$$

where the coupling of the interpolator to the nucleon is given by

$$\langle 0|\eta_{\text{CZ}}|P\rangle = f_N (p\cdot z) \not{z} N(p) \tag{2.48}$$

Here z is a light-cone vector, $z^2 = 0$, and the coupling determines the normalisation of the leading twist nucleon distribution amplitude [44, 67] we are interested in. Inserting a nucleon intermediate state in the eq. (2.45) and using the definition in eq. (2.30) for nucleon form factors it readily follows

$$\begin{aligned} z^\nu C_\nu(p,q) =& \frac{f_N}{m_N^2 - p'^2}(p'\cdot z)\left\{\left[2F_1(Q^2)(p'\cdot z) - F_2(Q^2)(q\cdot z)\right]\not{z}\right. \\ &\left. + F_2(Q^2)\left[(p'\cdot z) + \frac{1}{2}(q\cdot z)\right]\frac{\not{z}\not{q}}{m_N}\right\} N(p) + \ldots, \end{aligned} \tag{2.49}$$

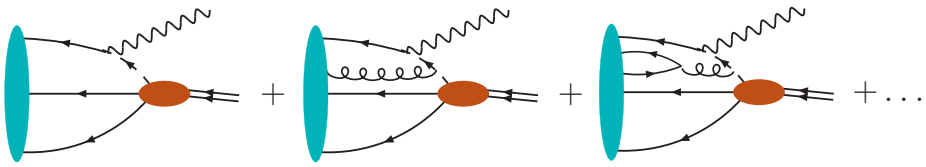

Figure 2.7: The leading fock state plus higher fock states contributions (see text for more details) to the correlation function in eq. (2.45) .

where

$$p' = p - q, \tag{2.50}$$

and the dots stand for higher resonances and the continuum.

On the other hand, at large Euclidean momenta p'^2 and $q^2 = -Q^2$ the correlation function can be calculated in perturbation theory using operator product expansion. The leading order contribution is shown in Figure 2.6 and has the form [49]

$$\begin{aligned} z_\nu C^\nu(p,q) =& \frac{1}{2\pi^2}\int \mathrm{d}^4x\, \frac{e^{iqx}}{x^4}\,(C\not{x})\,(\gamma_5\not{x})_\gamma \\ &\times \left[\frac{2}{3}\langle 0|\epsilon^{abc}u^a_\alpha(0)u^b_\beta(0)d^c_\gamma(x)|P\rangle + \frac{8}{3}\langle 0|\epsilon^{abc}u^a_\alpha(0)u^b_\beta(x)d^c_\gamma(0)|P\rangle\right], \end{aligned} \tag{2.51}$$

where we have performed operator product expansion similarly to those in eq. (2.40) to leading order in Fock states. Therefore the hard part (dashed line in Figure 2.6) can be calculated perturbatively, while the soft parts are expressed as matrix elements. To be precise one should also take into account higher Fock states. The reason is the hard quark propagator $\not{x}/x^4$ in eq. (2.51), which receives corrections in the background colour field [68] giving finally rise also to higher Fock states (Figure 2.7). However, although not strictly shown it is believed that such corrections do not play a significant role as for example seen in [69]. Therefore from now on we will consider only operators with three valence quarks like it was done to obtain eq. (2.51) which should give us a good enough description of the non-perturbative contributions for the correlator in eq. (2.45).

The common idea of sum rules is to match the dispersion relations in eq. (2.49) with the QCD calculations of eq. (2.51) at certain "not so large" Euclidean values of momentum p'^2 flowing through the nucleon interpolating current η. The problem thereby are the remaining nonperturbative matrix elements on the right-hand side of eq. (2.51), which describe a transition from a certain three-quark state to the nucleon.

Obviously the three-quark operator used in the remaining matrix elements of eq. (2.51) are not the most general one but can be seen as a special case of a more

general trilocal quark operator:

$$\begin{aligned}\epsilon^{abc}\langle 0|\left[\exp\left(ig\int_{z_1}^{z_3}A_\mu(\sigma)\mathrm{d}\sigma^\mu\right)u_\alpha(z_1)\right]^a \\ \times\left[\exp\left(ig\int_{z_2}^{z_3}A_\nu(\tau)\mathrm{d}\tau^\nu\right)u_\beta(z_2)\right]^b d^c_\gamma(z_3)\;|p\rangle,\end{aligned} \tag{2.52}$$

where path ordering is implied for the exponentials, a, b, c are the colour indices and $|p\rangle$ denotes the nucleon state with momentum p.

Considering the quarks in the matrix element of eq. (2.52) on the light cone and using the transformation properties of the fields under Lorentz symmetry and parity it is possible to rewrite the leading twist contribution in terms of three invariant functions V, A and T [70]

$$\begin{aligned}(2.52) = \frac{1}{4}\{&(p\cdot\gamma C)_{\alpha\beta}(\gamma_5 N)_\gamma V(z_i\cdot p) + (p\cdot\gamma\gamma_5 C)_{\alpha\beta}N_\gamma A(z_i\cdot p) \\ &+(i\sigma_{\mu\nu}p^\nu C)_{\alpha\beta}(\gamma^\mu\gamma_5 N)_\gamma T(z_i\cdot p)\} + \text{higher twist},\end{aligned} \tag{2.53}$$

where C is the charge conjugation matrix, N the nucleon spinor and f_N the nucleon decay constant. Then in the light-cone limit $x^2 \to 0$ the remaining matrix elements in eq. (2.51) can be quite easily related to the nucleon distribution amplitudes on the right-hand side of eq. (2.53).

Beyond the large Q^2 limit at intermediate energies of $Q^2 = 1\ldots 10\,\mathrm{GeV}^2$ the contributions of the higher twist distribution amplitudes [50] are similarly important. In this part our main focus is on leading twist and we will consider higher twist later.

In momentum space

$$V(x_i) \equiv \int V(z_i\cdot p)\prod_{i=1}^{3}\exp\left(ix_i(z_i\cdot p)\right)\frac{\mathrm{d}(z_i\cdot p)}{2\pi}, \qquad V(x_i)\equiv V(x_1,x_2,x_3) \tag{2.54}$$

the distribution amplitudes $V(x_i)$, $A(x_i)$ and $T(x_i)$ describe the quark distribution inside the nucleon as a function of the longitudinal momentum fractions x_i carried by the valence quarks in the nucleon, $0 \le x_i \le 1$ and $\sum x_i = 1$. The leading-twist expansion in eq. (2.53) is equivalent to the following form of the proton state [46, 65, 66]

$$\begin{aligned}|p,\uparrow\rangle = \int_0^1[\mathrm{d}x]\,\frac{V(x_i)-A(x_i)}{2\sqrt{24x_1x_2x_3}}\big[&|u^\uparrow(x_1)u^\downarrow(x_2)d^\uparrow(x_3)\rangle \\ &-|u^\uparrow(x_1)d^\downarrow(x_2)u^\uparrow(x_3)\rangle\big]\end{aligned} \tag{2.55}$$

with the integration measure

$$[\mathrm{d}x] = \mathrm{d}x_1\mathrm{d}x_2\mathrm{d}x_3\delta(1-x_1-x_2-x_3). \tag{2.56}$$

To be precise we want to note, that the distribution amplitudes also depend on the renormalisation scale μ, which we will suppress as long as not explicitly required.

2.5.3 Moments of Leading-Twist Distribution Amplitudes

Since it is so far not possible to access the quark distribution amplitudes directly we consider their moments, which are defined as

$$V^{lmn} = \frac{1}{f_N} \int_0^1 [\mathrm{d}x]\; x_1^l x_2^m x_3^n \; V(x_1, x_2, x_3) \tag{2.57}$$

with the normalisation constant f_N and equivalent definitions for other leading twist distribution amplitudes. Using eq. (2.53) and (2.54) one can relate the moments of the quark distribution amplitudes to matrix elements of the following local operators

$$\begin{aligned}
\mathcal{V}_\tau^{\rho\bar{l}\bar{m}\bar{n}}(0) &= \epsilon^{abc}[i^l D^{\lambda_1} \dots D^{\lambda_l} u_\alpha^a(0)](C\gamma^\rho)_{\alpha\beta}[i^m D^{\mu_1} \dots D^{\mu_m} u_\beta^b(0)] \\
&\quad \times [i^n D^{\nu_1} \dots D^{\nu_n} (\gamma_5 d^c(0))_\tau] \qquad (2.58)\\
\mathcal{A}_\tau^{\rho\bar{l}\bar{m}\bar{n}}(0) &= \epsilon^{abc}[(i^l D^{\lambda_1} \dots D^{\lambda_l} u_\alpha^a(0)](C\gamma^\rho\gamma_5)_{\alpha\beta}[i^m D^{\mu_1} \dots D^{\mu_m} u_\beta^b(0)] \\
&\quad \times [i^n D^{\nu_1} \dots D^{\nu_n} d_\tau^c(0)] \qquad (2.59)\\
\mathcal{T}_\tau^{\rho\bar{l}\bar{m}\bar{n}}(0) &= \epsilon^{abc}[i^l D^{\lambda_1} \dots D^{\lambda_l} u_\alpha^a(0)] \left(C(\sigma^{\xi\rho})\right)_{\alpha\beta} [i^m D^{\mu_1} \dots D^{\mu_m} u_\beta^b(0)] \\
&\quad \times [i^n D^{\nu_1} \dots D^{\nu_n} (\gamma_\xi\gamma_5 d^c(0))_\tau] \qquad (2.60)
\end{aligned}$$

by

$$\begin{aligned}
\langle 0|\mathcal{V}_\tau^{\rho\bar{l}\bar{m}\bar{n}}(0)|p\rangle &= -f_N V^{lmn} p^\rho p^{\bar{l}} p^{\bar{m}} p^{\bar{n}} N_\tau(p) \qquad (2.61)\\
\langle 0|\mathcal{A}_\tau^{\rho\bar{l}\bar{m}\bar{n}}(0)|p\rangle &= -f_N A^{lmn} p^\rho p^{\bar{l}} p^{\bar{m}} p^{\bar{n}} N_\tau(p) \qquad (2.62)\\
\langle 0|\mathcal{T}_\tau^{\rho\bar{l}\bar{m}\bar{n}}(0)|p\rangle &= 2f_N T^{lmn} p^\rho p^{\bar{l}} p^{\bar{m}} p^{\bar{n}} N_\tau(p), \qquad (2.63)
\end{aligned}$$

where $\bar{l}\bar{m}\bar{n}$ with $\bar{l} = \lambda_1 \dots \lambda_l$ etc. denotes the Lorentz structure given by the covariant derivatives $D_\mu = \partial_\mu - igA_\mu$, the index ρ reflects the gamma matrice present in the operators and f_N is the nucleon decay constant.

Due to the presence of two u-quarks in the nucleon we have for the moments of the nucleon distribution amplitude additional relations

$$V^{lmn} = V^{mln}, \quad A^{lmn} = -A^{mln}, \quad T^{lmn} = T^{mln}. \tag{2.64}$$

If we define

$$\phi^{lmn} = \frac{1}{3}(V^{lmn} - A^{lmn} + 2T^{lnm}), \tag{2.65}$$

which is a natural combination in our analysis, then we have due to isospin 1/2 symmetry

$$T^{lmn} = \frac{1}{2}(\phi^{lnm} + \phi^{mnl}). \tag{2.66}$$

Due to the analogous identities for V and A, we can express the moments of V, A and T in terms of only one independent distribution amplitude ϕ^{lmn}:

$$V^{lmn} = \frac{1}{2}\left(2\phi^{lmn} + 2\phi^{mln} - \phi^{nlm} - \phi^{nml}\right), \tag{2.67}$$

$$A^{lmn} = \frac{1}{2}\left(-2\phi^{lmn} + 2\phi^{mln} - \phi^{nlm} + \phi^{nml}\right). \tag{2.68}$$

Then the normalisation of the nucleon decay constant f_N is defined by the choice $T^{000} = V^{000} = \phi^{000} = 1$. The combination $\varphi^{lmn} = V^{lmn} - A^{lmn}$, often used in QCD sum rule calculations, can be easily related ϕ^{lmn} according to

$$\varphi^{lmn} = 2\phi^{lmn} - \phi^{nml}, \tag{2.69}$$

$$\phi^{lmn} = \frac{1}{3}\left(2\varphi^{lmn} + \varphi^{nml}\right). \tag{2.70}$$

Because of momentum conservation ($\sum_i x_i = 1$) we have additional relations between lower and higher moments of the distribution amplitude:

$$\phi^{lmn} = \phi^{(l+1)mn} + \phi^{l(m+1)n} + \phi^{lm(n+1)}, \tag{2.71}$$

which in particular imply

$$\begin{aligned} 1 =& \phi^{000} = \phi^{100} + \phi^{010} + \phi^{001} \\ =& \phi^{200} + \phi^{020} + \phi^{002} + 2(\phi^{011} + \phi^{101} + \phi^{110}) = \dots. \end{aligned} \tag{2.72}$$

2.5.4 Modelling the Leading-Twist Nucleon Distribution Amplitude

Although the moments of the nucleon distribution amplitude are the quantities we calculate, we would also like to have some functional form of the leading twist distribution amplitude. However, as there may be very different functional forms associated with the few accessible moments we need some additional information to constrain the possible form. This additional information can be provided by the renormalisation group equation of the distribution amplitudes. Expanding the leading-twist nucleon distribution amplitude in terms of polynomials P_n to order N

$$\varphi(x_i, \mu^2) = 120 x_1 x_2 x_3 \sum_{n=0}^{N} c_n P_n(x_i) \left(\frac{\alpha_s(\mu)}{\alpha_s(\mu_0)} \right)^{\gamma_n / b_0} \tag{2.73}$$

such that the mixing matrix is diagonal [71, 72] and calculating the coefficients c_n from an independent subset of ϕ^{lmn} we can obtain a model function for the distribution amplitude φ.

As initial expansion in (2.73) we use a conformal expansion (see [71, 50] and references therein for details)

$$\varphi(x_i) = \varphi^{\text{as}}(x_i) \sum_{k=0}^{N} \sum_{n=0}^{k} c_{k,n}(\mu) \Psi_{k,n}^{(12)3}(x_i) \tag{2.74}$$

with

$$\Psi_{k,n}^{(12)3}(x_i) = (x_1 + x_2)^n P_{k-n}^{(2n+3,1)}(x_3 - x_1 - x_2) C_n^{3/2} \left(\frac{x_1 - x_2}{x_1 + x_2} \right) \tag{2.75}$$

where the constraint $\sum_{i=1}^{3} x_i = 1$ is implied and $C_n^{2/3}$ and $P_n^{(\alpha,\beta)}$ are Gegenbauer and Jacobi polynomials, respectively. The superscript $(12)3$ stands for the order in which the conformal spins of the valence quarks are summed to form the total spin $k + 3$. First the spins of the two *up*-quarks summed to spin $n + 2$, and then the *down*-quark is added.

This conformal expansion of distribution amplitude can be seen as a field-theoretic analogon to the partial wave expansion in quantum mechanics. In both cases one utilises the symmetry of the problem to introduce a set of separated coordinates. Here the conformal symmetry [73] is the analogon to e.g., radial symmetry in quantum mechanics, and allows to separate longitudinal and transverse degrees of freedom [74, 71, 75, 76]. As the explicit dependence on the transverse coordinates (c.f., (2.43)) is integrated out it is described by the renormalisation group, while the dependence on the longitudinal momentum fractions

is described by a set of orthogonal polynomials $\Psi_{k,n}^{(12)3}$ that form an irreducible representation of the collinear subgroup $SL(2,R)$ of the conformal group.

Since the renormalisation group equations to leading logarithmic accuracy do not break the conformal symmetry the components in the distribution amplitude with different conformal spin k do not mix under renormalisation to this accuracy. Thus the task to diagonalise expansion (2.75) is greatly simplified. The renormalisation group equation for distribution amplitude operators $\mathcal{B}$ can be written as [77, 68]

$$\left(\mu\frac{\partial}{\partial\mu}+\beta(g)\frac{\partial}{\partial g}\right)\mathcal{B}=\mathcal{H}\cdot\mathcal{B} \tag{2.76}$$

where $\mathcal{H}$ is some integral operator, which can be rewritten in the form

$$\mathcal{H}=\left(\frac{N_c+1}{N_c}\right)\left[\mathcal{H}_{12}^{v}+\mathcal{H}_{23}^{v}+\mathcal{H}_{31}^{v}+\frac{3C_F}{2}-\mathcal{H}_{12}^{e}-\mathcal{H}_{23}^{e}\right]. \tag{2.77}$$

A further advantage of the expansion in (2.75) is that the diagonalisation procedure is now reduced to the diagonalisation of a simple algebraic equation [71]

$$\left[\frac{N_c}{N_c+1}\mathcal{H}-\frac{3C_F}{2}\right]\Psi_{k,n}^{(12)3}=\mathcal{E}_{k,n}\Psi_{k,n}^{(12)3} \tag{2.78}$$

with fixed $0<k<N$. The action of the operators $\mathcal{H}_{ab}$ on $\Psi^{(ab)c}$ can be written as

$$\mathcal{H}_{ab}^{v}\Psi_{k,n}^{(ab)c}=2\left[\psi(n+2)-\psi(2)\right]\Psi_{k,n}^{(ab)c}, \tag{2.79}$$

$$\mathcal{H}_{ab}^{e}\Psi_{k,n}^{(ab)c}=\frac{1}{(n+2)(n+1)}\Psi_{k,n}^{(ab)c}, \tag{2.80}$$

with the digamma function $\psi(n)$. In order to evaluate the action of $\mathcal{H}$ on our initial expansion basis polynomials $\Psi_{k,n}^{(12)3}$ they can be easily reexpressed in terms of the basis polynomials $\Psi_{k,n}^{(23)1}$ and $\Psi_{k,n}^{(13)2}$ which are given by

$$\Psi_{k,n}^{(23)1}(x_1,x_2,x_3)=\Psi_{k,n}^{(12)3}(x_2,x_3,x_1), \tag{2.81}$$

$$\Psi_{k,n}^{(13)2}(x_1,x_2,x_3)=\Psi_{k,n}^{(12)3}(x_1,x_3,x_2). \tag{2.82}$$

Using the obtained anomalous dimensions

$$\gamma_{k,n}\equiv\left(\frac{N_c+1}{N_c}\right)\mathcal{E}_{k,n}+\frac{3}{2}C_F \tag{2.83}$$

and calculating finally the moments of the diagonalised expansion, comparing these results with ϕ^{lmn} we are able to obtain a model function in terms of moments, which is explicitly given for $N = 2$ as

$$\begin{aligned}
\varphi(x_1,x_2,x_3,\mu) &= 120x_1x_2x_3f_N(\mu_0)\Big[L^{\frac{2}{3b_0}} \\
&- \frac{63}{8}(\phi^{100}-\phi^{001})(1-5x_1-x_2+3x_3)L^{\frac{26}{9b_0}} \\
&+ \frac{7}{8}(1-3\phi^{010})(1+3(x_1-3x_2+x_3))L^{\frac{10}{3b_0}} \\
&- \frac{63}{200}(5-7\phi^{010}-4\phi^{101}-8(\phi^{200}+\phi^{002}))\left(94x_1^2+54x_2^2+21x_3(1+2x_3)\right. \\
&\left.+x_2(11+64x_3)-x_1(31+12x_2+104x_3)-3\right)L^{\frac{38}{9b_0}} \\
&+ \frac{189}{40}(4(\phi^{200}-\phi^{002})-3(\phi^{100}-\phi^{001}))\left(1+22x_1^2-18x_2^2-7x_3(1+2x_3)\right. \\
&\left.+x_1(8x_3-76x_2-3)+x_2(17+48x_3)\right)L^{\frac{46}{9b_0}} \\
&+ \frac{9}{100}(15-21\phi^{010}-14(\phi^{200}+\phi^{002})-42\phi^{101})\left(98x_1^2-182x_2^2\right. \\
&\left.+7x_1(28x_2-24x_3-11)+7x_3(1+2x_3)+7x_2(9+16x_3)-1\right)L^{\frac{16}{3b_0}}\Big].
\end{aligned} \tag{2.84}$$

with $b_0 = \frac{11}{3}N_c - \frac{2}{3}n_f$ and

$$L \equiv \frac{\alpha_s(\mu)}{\alpha_s(\mu_0)}. \tag{2.85}$$

This form is of course not unique as we already pointed out before. Furthermore, as the convergence of the polynomial expansion is in the sense of L^2 norm, the restriction to the leading few moments may be a very strong simplification. On the other hand, based on additional information provided by the renormalisation group this model allows us to study at least some interesting aspects of the distribution amplitude.

2.5.5 Moments of Next-to-Leading Twist Nucleon Distribution Amplitudes

In the case of higher twist distribution amplitudes we restrict ourselves to operators without any derivatives. Thus the problem is simplified greatly since the Lorentz decomposition of a local three quark matrix element involves only four

structures [50]:

$$\begin{aligned} &4\langle 0|\epsilon^{abc}u^a_\alpha(0)u^b_\beta(0)d^c_\gamma(0)|p\rangle = \\ &\quad V_1^0(\not{p}C)_{\alpha\beta}(\gamma_5 N)_\gamma + V_3^0 m_N(\gamma_\mu C)_{\alpha\beta}(\gamma^\mu\gamma_5 N)_\gamma \\ &\quad + T_1^0(p^\nu i\sigma_{\mu\nu}C)_{\alpha\beta}(\gamma^\mu\gamma_5 N)_\gamma + T_3^0 m_N(\sigma_{\mu\nu}C)_{\alpha\beta}(\sigma^{\mu\nu}\gamma_5 N)_\gamma. \end{aligned} \tag{2.86}$$

where we have used for convenience the same notation as in [50], the leading twist constants V_1^0 and T_1^0 corresponds to $f_N V^{000}$ and $f_N T^{000}$ in our notation respectively and as already pointed out they are equal. The two new constants determine the normalisation of the twist four distribution amplitudes. Alltogether we have only three independent nonperturbative constants. The combinations $\lambda_1 = (V_1^0 - 4V_3^0)$ and $\lambda_2 = 6(V_1^0 - 4T_3^0)$ are also known in the literature. They describe the coupling to nucleon of two possible independent nucleon interpolating fields that are used in calculations of dynamical nucleon properties in the QCD sum rule approach. One of the operators $\mathcal{L}_\tau$ was introduced in [78] and the another $\mathcal{M}_\tau$ in [79]

$$\mathcal{L}_\tau(0) = \epsilon^{abc}\left[u^a(0)C\gamma^\rho u^b(0)\right] \times (\gamma_5 d^c(0))_\tau \tag{2.87}$$

$$\mathcal{M}_\tau(0) = \epsilon^{abc}\left[u^a(0)C\sigma^{\mu\nu} u^b(0)\right] \times (\gamma_5\sigma_{\mu\nu} d^c(0))_\tau \tag{2.88}$$

with the matrix elements given by

$$\langle 0|\mathcal{L}_\tau(0)|p\rangle = \lambda_1 m_N N_\tau \tag{2.89}$$

$$\langle 0|\mathcal{M}_\tau(0)|p\rangle = \lambda_2 m_N N_\tau. \tag{2.90}$$

2.6 Detour to Chiral Symmetry

From the previous discussion in this work it should become clear that chiral symmetry plays an crucial role in QCD. In lattice QCD calculations chiral symmetry is even more important but much more difficult to preserve. Chiral symmetry in QCD is only exact in the limit of zero quark masses, however the masses of *up*- and *down*- quarks are far smaller than the QCD scale. Therefore it should be a good low energy approximation to assume zero quark masses. In this limit the fermionic part of the QCD Lagrangian simplifies to

$$\mathcal{L}_F = \sum_f^{n_f} \bar{q}^f i\gamma^\mu \mathcal{D}_\mu q^f. \tag{2.91}$$

As next we decompose the quark fields q into left- and right-handed components

$$\begin{aligned} q_L &= \gamma_L q, \quad q_R = \gamma_R q, \quad q = q_L + q_R \\ \bar{q}_L &= \bar{q}\gamma_R, \quad \bar{q}_R = \bar{q}\gamma_L, \quad \bar{q} = \bar{q}_L + \bar{q}_R \end{aligned} \tag{2.92}$$

with

$$\gamma_R = \frac{\mathbb{1} + \gamma_5}{2}, \qquad \gamma_L = \frac{\mathbb{1} - \gamma_5}{2}. \tag{2.93}$$

After inserting the decomposed spinors into the Lagrangian we obtain

$$\mathcal{L} = \sum_f^{n_f} \left(\bar{q}_L^f i\gamma^\mu \mathcal{D}_\mu q_L^f + \bar{q}_R^f i\gamma^\mu \mathcal{D}_\mu q_R^f \right), \tag{2.94}$$

i.e., the Lagrangian decouples into two parts for left- and right-handed quarks resulting in $U(n_f)_L \otimes U(n_f)_R$ chiral symmetry.

Due to the quantum anomaly in the axial $U(1)_A$ symmetry the symmetry of the quantum field theory is then reduced to $SU(n_f)_L \otimes SU(n_f)_R \otimes U(1)_B$ where the $U(1)_B = U(1)_{L=R}$ symmetry represents baryon number conservation.

2.6.1 The Axial Anomaly and the Atiyah-Singer Index Theorem

As a consequence of the $U(1)_A$ quantum anomaly the flavour-singlet axial current

$$j_\mu^5(x) = \bar{q}\gamma_\mu\gamma_5 q, \tag{2.95}$$

which is classically conserved has a non-zero divergence in the quantum field theory

$$\partial^\mu j_\mu^5 = -\frac{n_f}{32\pi^2}\epsilon_{\mu\nu\omega\rho}\mathrm{tr}\left[F^{\mu\nu}(x)F^{\omega\rho}(x)\right] \tag{2.96}$$

due to topological effects in the theory. In particular the axial charge $Q^5(t) = \int \mathrm{d}^3x j_0^5(\vec{x}, t)$ is related to the topological charge from eq. (2.17) by

$$Q^5(t=\infty) - Q^5(t=-\infty) = n_f Q. \tag{2.97}$$

Furthermore the axial anomaly is also deeply connected with the Atiyah-Singer index theorem, which relates the zero-modes of the massless Dirac operator to the topological charge. Since the eigenvalues of the massless Dirac operator $\gamma^\mu\mathcal{D}_\mu$ are purely imaginary and come in complex conjugate pairs the zero eigenvalues are the only ones which are not paired. The eigenvectors of the zero modes have a definite handiness because the massless Dirac operator anti-commutes with γ_5. The Atiyah-Singer theorem states that

$$\mathrm{index}\left(\gamma^\mu\mathcal{D}_\mu\right) = n_L - n_R = n_f Q \tag{2.98}$$

i.e., the difference between the number of the left- and right-handed zero-modes is proportional to the topological charge.

2.6.2 Spontaneous Chiral Symmetry Breaking

Although chiral symmetry is only approximate in QCD, we can still expect almost degenerate states in the spectrum of strongly interacting particles. Since the masses of *up* and *down* quarks are far below the QCD scale, such an approximate symmetry is observed in nature and hadrons can be classified as isospin multiplets. Adding the *strange* quark, the symmetry becomes more approximate but is still visible in the spectrum. Furthermore one observes very light pseudo-scalar particles, the three pions $\pi^{\pm}, \pi^0$, and somewhat heavier pseudo-scalar particles, the four kaons $K^{\pm}$, K^0, $\bar{K}^0$ and the η-meson. Thus, it leads us to the indication that chiral symmetry must be spontaneously broken and the observed pseudo-scalar particles must be the corresponding Goldstone bosons.

According to the Goldstone theorem the number of the massless particles is given by the number of the generators of the full symmetry group minus the number in the unbroken subgroup. Here the full chiral symmetry group is

$$G_\chi = SU(n_f)_L \otimes SU(n_f)_R \otimes U(1)_B, \tag{2.99}$$

which is broken down to

$$H_\chi = SU(n_f)_{L=R} \otimes U(1)_B. \tag{2.100}$$

Hence we expect $n_f^2 - 1$ massless Goldstone bosons. Assuming only approximate symmetry for *up* and *down* quarks we have then three massless Goldstone bosons which can be identified with the three light pions. For $n_f = 3$ we have then additionally the kaons and the η-meson, alltogether eight massless Goldstone bosons. Of course the pions, kaons and η-meson are not really massless since the chiral symmetry is explicitly broken by the quark masses. But the breaking is relatively small so that we can still identify the Goldston bosons.

In contrast to the electro-weak spontaneous symmetry breaking due to the Higgs field the chiral symmetry breaking has not been derived analytically yet from QCD Lagrangian and its origin remains mysterious. However, in lattice QCD, which is a nonperturbative formulation of QCD, it was shown[4] that the chiral symmetry is indeed spontaneously broken [80, 81] in the strong coupling limit. The numerical simulations in lattice QCD confirm this result even in the weakly coupled regime by observing the chiral condensate

$$\chi = \langle \bar{q} q \rangle, \tag{2.101}$$

which is an order parameter of the chiral symmetry breaking. If the chiral symmetry is restored the chiral condensate is invariant under chiral rotations and would vanish, otherwise in the chiral broken sector the chiral condensate has a non-zero expectation value.

[4] In the proof the authors used staggered fermions for the fermionic part of the action, which is controversial due to not yet completely understood properties.

2.6.3 Low-Energy Effective Theory

Since the pions are the lightest particles in QCD they dominate the dynamics of the strong interaction at low energy. A low-energy effective description of QCD is provided by the Chiral Perturbation Theory (χPT). Therein the pion dynamics is predicted by a systematic expansion in powers of external momenta and quark masses. Since pions are Goldstone bosons they are described by fields in the coset space $U(x) \in G_\chi/H_\chi = SU(n_f)$.

The extension of the theory to non-zero baryon numbers is a non-trivial task. An overview on this topic can be found in [82, 83], while here we give only a sketch how this can be done. Extending the chiral perturbation theory to sectors with non-zero baryon number one includes the baryons in the form of a Dirac spinor field $N(x)$ and $\bar{N}(x)$ that transforms as an $SU(2)_I$ isospin doublet. Global chiral rotations $L \otimes R \in SU(2)_L \otimes SU(2)_R$ can be realised then nonlinearly on this field. In order to realise a chirally invariant action one introduces an $SU(2)$ flavour "gauge" field

$$v_\mu(x) = \frac{1}{2}\left[u^\dagger(x), \partial_\mu u(x)\right] \tag{2.102}$$

with

$$u(x) = U^2(x), \quad \text{and} \quad u_\mu = iu^\dagger \partial_\mu U u^\dagger \tag{2.103}$$

In leading order one can then write a low-energy Lagrangian for nucleons and pions of the form

$$\mathcal{L}_\chi = \mathcal{L}_\pi + \mathcal{L}_N \tag{2.104}$$

with

$$\begin{aligned} \mathcal{L}_\pi =& \frac{F_\pi^2}{4}\mathrm{tr}\left(\partial_\mu U^\dagger \partial^\mu U\right) + \frac{\langle\bar{q}q\rangle}{2n_f}\mathrm{tr}\left(MU^\dagger + UM^\dagger\right) \\ \mathcal{L}_N =& \bar{N}(i\gamma^\mu D_\mu - m_N)N + \frac{1}{2}g_A \bar{N}\gamma^\mu u_\mu \gamma_5 N \end{aligned} \tag{2.105}$$

where F_π is the pion decay constant, $\langle\bar{q}q\rangle$ is the chiral condensate, which must be calculated non-perturbatively or extracted from experiment, and M is the mass matrix. The covariant derivative in the nucleon Lagrangian $\mathcal{L}_N$ is given by $D_\mu = \partial_\mu + v_\mu$.

2.7 GUT Decay Constants

Now we consider the processes relevant for nucleon decays in great unified theories. One of the three requirements for the baryogenesis in the early universe by Sakharov [84] is the violation of the baryon number conservation. In 1976 it

Figure 2.8: Diagrams contributing to the nucleon decay amplitude $p \longrightarrow \pi^0 + e^+$.

was recognised by 't Hooft [85] that within the standard model the electro-weak anomaly violates baryon number conservation by a nonperturbative effect and hence could not be seen in the perturbative calculations. The divergence of the left-handed baryon plus lepton currents is given by

$$\partial_\mu J_{B_L+L_L} = \frac{3g^2}{32\pi^2}\epsilon_{\alpha\beta\gamma\delta}W_a^{\alpha\beta}W_a^{\gamma\delta} \tag{2.106}$$

where $W_a^{\alpha\beta}$ is the $SU(2)_W$ field strength. It can be shown that the right hand side has a topological nature and the anomaly is related to tunnelling between topologically different n-vacua through the instanton field configurations. However the tunnelling amplitude A being of order

$$A \sim e^{-8\pi^2/g^2} \sim 10^{-137} \tag{2.107}$$

is too small to generate a reasonable number of baryons during the whole life time of the universe and the related process was not considered to be relevant for baryogenesis. Nine years later, 1985, it was recognised [86] that at temperatures $T \gtrsim 100$ GeV the energy will be large enough to hop over the barrier and the process will become unsuppressed. Thus if the remaining two Sakharov conditions can be fullfilled within the standard model it can in principle describe the baryogenesis. However it is a hard task to find e.g., strong enough source for CP violation in the standard model and it is believed that this problem should still be addressed within the extensions of the standard model or grand unified theories. Beyond these, there are of course other strong reasons we already discussed in the introduction to look for physics beyond the standard model.

Nucleon decay at low energies is the most dramatic prediction of these theories and the detection of such decay will put us forward in the understanding of nature. Already our existence proves, that the lifetime of the proton must be very large and the present lower bound for the proton lifetime obtained from experimental results [87, 88, 89] excludes already e.g., some modifications of the minimal SUSY $SU(5)$ [89]. and the $\mathcal{N} = 1$ SUSY [90].

Nucleon decay calculations involve GUT dynamics modified by the short distance corrections calculated within the standard model and hadronic matrix elements encoding the much less understood long distance behaviour of QCD. The

proton decay itself is a short distance process in the sense that at least two quarks are within the distance of order $O(1/M_{\rm GUT})$ with $M_{\rm GUT}$ the scale of grand unification. Using nucleon chiral Lagrangian approach discussed before and extending it by matrix elements which allow baryon number violation [91, 92, 93, 94, 95] it is possible to relate the nucleon lifetime in leading order to matrix elements of the local three quark operators

$$\mathcal{U}_\tau(0) = \epsilon^{abc}\left[\gamma_R u^a(0) C\gamma_R d^b(0)\right](\gamma_L u^c(0))_\tau \tag{2.108}$$

$$\mathcal{W}_\tau(0) = \epsilon^{abc}\left[\gamma_L u^a(0) C\gamma_L d^b(0)\right](\gamma_L u^c(0))_\tau \tag{2.109}$$

with the left- and right-handed projectors $\gamma_L = (1-\gamma_5)/2$, $\gamma_R = (1+\gamma_5)/2$. The matrix elements of this operators are involved in the calculation of the proton decays in Figure 2.8

$$\langle 0|\mathcal{U}_\tau(0)|p\rangle = \alpha(\gamma_L N)_\tau \tag{2.110}$$

$$\langle 0|\mathcal{W}_\tau(0)|p\rangle = \beta(\gamma_L N)_\tau. \tag{2.111}$$

There are only two low energy constants α and β to lowest order in momenta in the effective Lagrangian of the nucleon decay which extend the usual three-flavour baryon chiral Lagrangian. The knowledge of these two constants in combination with other parameters allows to calculate nucleon decay matrix elements, e.g. the form factors relevant for the proton to π^0 decay read

$$W_0^{RL}(p\to\pi^0) = \alpha(1+D+F)/\sqrt{2}f \tag{2.112}$$

$$W_0^{LL}(p\to\pi^0) = \beta(1+D+F)/\sqrt{2}f \tag{2.113}$$

with f the tree level pion decay constant normalised such that the experimental value $f_\pi \simeq 131$ MeV. D and F are the baryon couplings to the axial current, whereby the axial charge is the sum of both $g_A = D+F$.

CHAPTER 3

Lattice QCD

As we have displayed in the previous chapter the perturbative approach in QCD is a good tool to study physics at high energy scales and many phenomena observed in experiments can be described in this approach very well. However, our interest is the nucleon wave function, or more exactly the moments of the associated nucleon distribution amplitudes. And at this point the perturbation theory must fail, since the distribution amplitudes are low energy objects in QCD. Thus the calculation of low energy parameters calls for an alternative approach. One of the possibilities is to use an effective low energy theory, the Chiral Perturbation theory we discussed before. Another possibility is to use Lattice QCD where one regularise QCD nonperturbatively through discretisation of the space time. Being in someway complementary approaches, both have certain advantages and disadvantages which can be reduced if both methods are combined. In our case the method of choice is Lattice QCD which we introduce now in greater detail.

The discretised Euclidean version of QCD was first introduced by Wilson [96] and does not require model assumptions. Therefore, the calculations within lattice QCD are from first principles. Apart from simulation specific parameters this formulation does not involve additional parameters compared to the continuum formulation. Like in the continuum the parameters of the lattice QCD Lagrangian, like masses and couplings, must be determined by comparison with nature. In order to extrapolate to the physical point these parameters have to be tuned. This freedom can be seen as an advantage which allows us to simulate how nature would look like at different quark masses. On the other hand the unphysical regimes of todays simulations introduce additional problem making it difficult to comapre with the physical reality. Further limitations are caused by the finite vol-

ume and discretisation effects. Thus, in order to estimate the possible influences the simulations should span a large enough parameter space.

In the following we focus on the relevant basics of the lattice approach to QCD and introduce the required techniques. We start in the continuum and formulate in the first three section the QCD in a form, which is best suited for discretisation. Then, we will introduce the discretised form of the QCD action used in our calculations and explain the relevant basic numerical techniques, needed to simulate this. The most important general tools, like operator overlap improvement, are explained in Sections 3.6 - 3.9. In the last three sections 3.10 - 3.12 we explain details of the main tools and techniques which are essential for the calculation of the moments of the distribution amplitudes.

3.1 Path Integral and Correlation Functions

Because we know the QCD Lagrangian the quantum field theory formalism should n principle allow us to calculate any quantity we want. But due to nonlinearity of QCD we failed until today to obtain analytical results. However modern high performance computers allow precision calculations from first principles using numerical approach. The best starting point to "solve" QCD on computer is the Feynman path integral formalism in Euclidean space time which is obtained by means of the Wick rotation $t \to -it$.

At first the quantity we want to calculate must be expressed as a vacuum matrix element of some operator $\mathcal{O}$. In QCD this operator is constructed as a product of gluon fields A_μ and quark fields Ψ. Then the vacuum expectation value of $\mathcal{O}$ can be calculated as

$$\langle \mathcal{O} \rangle = \frac{1}{Z} \int [\mathrm{d}\psi] \left[\mathrm{d}\bar{\psi}\right] [\mathrm{d}G]\, \mathcal{O}\left[\psi, \bar{\psi}, A\right] e^{-S_{\mathrm{QCD}}\left[\psi,\bar{\psi},A\right]}, \tag{3.1}$$

with the partition function

$$Z = \int [\mathrm{d}\psi] \left[\mathrm{d}\bar{\psi}\right] [\mathrm{d}A]\, e^{-S_{\mathrm{QCD}}\left[\psi,\bar{\psi},A\right]}. \tag{3.2}$$

The vacuum expectation value is obtained by evaluating the operator $\mathcal{O}$ for one field configuration and then to integrate over all possible field configurations whereby each configuration is weighted with the exponential of the QCD action S_{QCD}. The expression is then normalised by the prescription that the expectation value of the unity operator is one.

As we are going to calculate the nucleon distribution amplitudes the operator $\mathcal{O}$ in eq. (3.1) will obviously involve fermionic fields namely the quarks. The

noncommuting nature of fermions requires a special care and therefore we define the generating functional

$$W\left[\eta,\bar{\eta}\right]=\int\left[\mathrm{d}\psi\right]\left[\mathrm{d}\bar{\psi}\right]\left[\mathrm{d}A\right]e^{-S_{\mathrm{QCD}}\left[\psi,\bar{\psi},A\right]}e^{\bar{\eta}\psi}e^{\eta\bar{\psi}}, \tag{3.3}$$

where we have additional source terms $\bar{\eta}\psi$ and $\eta\bar{\psi}$ with currents η and $\bar{\eta}$. The expectation value of a quark operator can then be written as a functional derivative of the generating functional

$$\left\langle\psi_{i_1}\dots\psi_{i_n}\bar{\psi}_{j_1}\dots\bar{\psi}_{j_n}\right\rangle=\frac{1}{Z}\frac{\delta}{\delta\bar{\eta}_{i_1}}\dots\frac{\delta}{\delta\bar{\eta}_{i_n}}\frac{\delta}{\delta\eta_{j_1}}\dots\frac{\delta}{\delta\eta_{j_n}}W\left[\eta,\bar{\eta}\right]\Big|_{\eta,\bar{\eta}=0}. \tag{3.4}$$

The propagator of a quark or equally the Green function is then given as

$$\mathcal{D}^{-1}_{i,j}(x_i,x_j)=\left\langle\psi_i(x_i)\bar{\psi}_j(x_j)\right\rangle=\frac{1}{Z}\frac{\delta}{\delta\bar{\eta}_i}\frac{\delta}{\delta\eta_j}W\left[\eta,\bar{\eta}\right] \tag{3.5}$$

Applying the usual trick by completing the square in the fermion fields and change the variables, the fermionic part of the generating functional can be written as a Gaussian integral which can be integrated analytically resulting in

$$W\left[\eta,\bar{\eta}\right]=\int\left[\mathrm{d}G\right]\det\mathcal{D}e^{-S_G}e^{\bar{\eta}_i(x_i)\mathcal{D}^{-1}_{i,j}\eta_j}. \tag{3.6}$$

Thus the problem is now reduced to evaluating only the gauge action while the fermionic contribution is now encoded in the determinant of the Dirac operator and its exponential disappears in the evaluation of a matrix element due to eq. (3.4) as the currents η and $\bar{\eta}$ are set to zero.

3.2 Two-Point Correlation Functions

Hadron masses and matrix amplitudes are measured on the lattice from two-point correlation functions. In the following we describe the general procedure necessary to obtain these quantities as discussed e.g. in [97]. Let us consider therefore two operators $\mathcal{O}_1$ and $\mathcal{O}_2$ which are functions of quark and anti-quark fields. Then the correlation function is either obtained from the partition function eq. (3.1) as

$$C(t;\vec{p})=\left\langle\mathcal{O}_1(t;\vec{p})\mathcal{O}_2^\dagger(0;\vec{p})\right\rangle \tag{3.7}$$

or alternatively we can define it using an operator formalism with operators living in a suitable Fock space propagating in time via a transfer matrix, $\mathcal{S}\equiv\exp(-\mathcal{H})$ with $\mathcal{H}$ the Hamiltonian. Thus, we can write the correlator also as

$$C(t;\vec{p})=\left\langle\mathcal{O}_1(t;\vec{p})\mathcal{O}_2^\dagger(0;\vec{p})\right\rangle\equiv\mathrm{tr}\left[\mathcal{S}^{T-t}\mathcal{O}_1(0;\vec{p})\mathcal{S}^t\mathcal{O}_2^\dagger(0;\vec{p})\right] \tag{3.8}$$

with T the time extension of the lattice. The operator $O_2^\dagger(0;\vec{p})$ acts as a source for a particle moving with momentum p while $\mathcal{O}_1(t;\vec{p}) \equiv \mathcal{S}^{-t}\mathcal{O}_1(0;\vec{p})\mathcal{S}^t$ acts as the sink. The equivalence of these two formulations allows to relate the correlation functions, which are calculated using the path integral formalism, to physical quantities. For a more extensive discussion of this relation we refer to e.g., [98] and proceed now with the nucleon correlators.

3.3 Euclidisation

As already proposed, Lattice QCD is based on a nonperturbative regularisation scheme of a quantum gauge theory introduced by Wilson [96] in 1974 by discretising the spacetime. If one performs this discretisation in a finite spacetime volume it is obvious that the number of degrees of freedom in eq. (3.1) becomes finite. However, for a physically reasonable volume it excess any controllable number. The second problem is that the integrand in eq. (3.1) is oscillatory as the action is imaginary in Minkowski space-time. However, both problems can be accessed by performing an analytic continuation from Minkowski to Euclidean space-time. Therefore the real time axes is Wick rotated onto the imaginary axes:

$$x_0 \rightarrow -ix_4. \tag{3.9}$$

Thus the action becomes real in Euclidean space-time and the oscillating integration weight acquire now the form of the Boltzmann factor in statistical physics. The achieved probabilistic interpretation of eq. (3.1) in Euclidean space-time calls for Monte Carlo simulations to face the large number of degrees of freedom and so to calculate the path .

As during the euclidisation procedure also the metric changes from the $g_{\mu\nu}$ to $\delta_{\mu\nu}$ we also have to transform the Dirac gamma matrices in order to preserve the associated Clifford algebra. The relevant set of Dirac gamma matrices as used in our calculation is given in Appendix A.1. Obviously there is some freedom which representation can be used for the Clifford algebra. The motivation for our choice, the Weyl representation, should become clear later in section 3.11.

3.4 Lattice QCD Action

The next obvious task to formulate QCD on a lattice is to rewrite the QCD Lagrangian in discretised form such that the gauge and other symmetries of QCD are preserved. This can be divided in two separate problems, the discretisation of the gauge action S_G and the fermionic action S_F. In order to discretise those a four

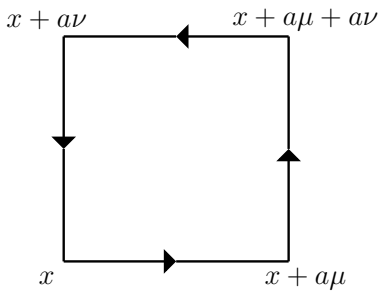

Figure 3.1: The plaquette term $U_{\mu\nu}$ of the Wilson gauge action

dimensional grid of space-time points is introduced. The introduction of a hypercubic lattice breaks Lorentz invariance which should be restored in the continuum limit. However the remaining hypercubic symmetry is still present in the theory [99, 100]. To translate the QCD Lagrangian to the lattice we need some clever finite difference techniques, in particular for the Dirac operator. The discretisation of the gauge part is quite straight forward and therefore we will start with it. As second we will address the fermionic part which is more demanding and is still problematic in ourdays lattice calculations.

3.4.1 Gauge Action

In the continuum gauge transformations involve space time derivatives of group-valued functions. On the lattice we do not have infinitesimally close points and replace the derivative by finite differences. However, we need to be more carefully as we want to keep the gauge invariance in the discretised theory. Therefore we need the concept of so called parallel transporter introduced independently by Wegner and Wilson, as well as Smit. On discretised spacetime the parallel transporter U from point x to the neighbour point in μ direction $x + a\hat{\mu}$ is defined as

$$U(x, x + a\hat{\mu}) \equiv U_{x,\mu} = \mathcal{P} \exp \left\{ iag_0 \int_0^1 \mathrm{d}\xi \, G_\mu(x + (1 - \xi)a\hat{\mu}) \right\}, \qquad (3.10)$$

a straight line path between x and $x + a\hat{\mu}$ with $\hat{\mu}$ the unit vector in μ direction. The local gauge transformation of the parallel transporter has then the form:

$$U(x, x + a\hat{\mu}) \rightarrow \Omega(x) U(x, x + a\hat{\mu}) \Omega(x + a\hat{\mu})^\dagger \qquad (3.11)$$

where Ω are elements of $SU(3)_\mathrm{C}$, the colour group. Connecting two separated space-time points the parallel transporters naturally lives on the links of the lattice

(Figure 3.1). These link variables are used to construct the gauge part of the action. The colour trace of any closed loop ('Wilson loop') of link variables is gauge invariant. The smallest possible loop, the plaquette, one can obtain on the lattice is the usual building block of the gauge action

$$U_P(x;\mu\nu) = U_{x,\mu}U_{x+\hat{\mu},\nu}U^{\dagger}_{x+\hat{\nu},\mu}U^{\dagger}_{x,\nu}. \tag{3.12}$$

Then the standard Wilson action for the gauge sector is the sum over all plaquettes

$$S_G = -\beta\left(\sum_P \frac{1}{N_c}\mathrm{tr}\left(U_P + U_P^{\dagger}\right) - 1\right) \tag{3.13}$$

with β the lattice coupling constant. In the limit of vanishing lattice spacing $a \to 0$ it reduces to the usual continuum Yang-Mills action

$$S_G = \frac{\beta}{4N_c}\int \mathrm{d}x\,\mathrm{tr}\,(F_{\mu\nu}F^{\mu\nu}) + O(a^2). \tag{3.14}$$

3.4.2 Fermion Action

The discretisation of the fermion action is much more troublesome. Naively discretising the fermionic part of the QCD action leads in the continuum to the famous 'fermion doubling' problem [101, 102]. The fermion action can be generically written as

$$S_F = \sum \bar{\psi}\mathcal{M}\psi \tag{3.15}$$

where $\mathcal{M}$ is the fermion operator, a lattice approximation to the Dirac operator. In this work we use the so called Wilson-Clover action which avoid the fermion doublers by adding the Wilson term to the naive discretised fermion action. Thus on the lattice we will use in our calculations the lattice fermion action of the form

$$\begin{aligned} S_F = \sum \Big(& \bar{\psi}\overleftrightarrow{\not{D}}\psi + am_0\bar{\psi}\psi && \text{Naive term} \\ & -\frac{1}{2}a\bar{\psi}\nabla^2\psi && \text{Wilson term} \\ & +\frac{1}{4}iac_{sw}g^2\bar{\psi}\sigma_{\mu\nu}F_{\mu\nu}\psi\Big) && \text{Clover Term} \end{aligned} \tag{3.16}$$

where in the first line we have a simple discretisation of the fermion action. The covariant derivative $\overleftrightarrow{D}$ is constructed from forward and backward derivatives as

$$\vec{D}_\mu\psi(x) = \left(\frac{1}{2}\left(U(x,x+a\hat{\mu})\delta_{x+a\hat{\mu},y} - U^{\dagger}(x,x-a\hat{\mu})\delta_{x-a\hat{\mu},y}\right)\right)\psi(y) \tag{3.17}$$

$$\left(\bar{\psi}(x)\right)\overleftarrow{D}_\mu = \bar{\psi}(y)\left(\frac{1}{2}\left(\delta_{y,x+a\hat{\mu}}U(x+a\hat{\mu},x) - \delta_{y,x-a\hat{\mu}}U^{\dagger}(x-a\hat{\mu},x)\right)\right) \tag{3.18}$$

and setting

$$\overleftrightarrow{D} = \frac{1}{2}\left(\overrightarrow{D} - \overleftarrow{D}\right). \tag{3.19}$$

Higher order derivatives can be obtained by appropriately combining the forward and backward derivative operators.

Taking the limit of the (free) naive fermion propagator however gives poles in the massless fermion propagator not only at $ap = (0,0,0,0)$ but also whenever $ap_\mu = \pi$ causing the already mentioned fermion doubling. Therefore the Wilson term is introduced in the second line of eq. (3.16) to avoid this problem. This term gives a contribution $\propto \sum_\mu = (1 - \cos(ap_\mu))/a$ to the propagator and so the doubler masses are $\propto 1/a$ and vanish as the continuum limit $a \to 0$ is taken. But we have to pay a three-fold price:

1. Even for massless fermions we loose completely the chiral symmetry, which is present in the continuum (at least approximately).

2. Without chiral symmetry the fermion mass is not prevented anymore from running up to the lattice scale $1/a$. For about two decades lattice QCD suffered from this hierarchy problem in the fermion sector. Recovering chiral symmetry in the continuum limit then requires additive mass renormalisation, involving a delicate fine-tuning of the bare fermion mass

$$am = am_0 - am_0^{cont} \tag{3.20}$$

   where one has to determine am_0^{cont}.

3. In the continuum limit the fermion part is now worse than the gauge part as we have now $O(a)$ discretisation errors.

Point 1 and 2 are a fundamental problem in lattice QCD calculations. The solutions are provided by more sophisticated actions like overlap [103, 104] or domain wall [105, 106]. These actions are numerically more expensive and will become available with reasonably high statistics only in the near future. However for point three we can achieve some progress by adding a further term and so restore the $O(a^2)$ behaviour. Adding further irrelevant operators (i.e. higher dimensional) to the action [107] and tuning them to remove the discretisation errors we can restore the $O(a^2)$ behaviour. At the lowest order, i.e. $O(a)$ improvement (for review cf. [108, 109]), there are 5 possible gauge invariant irrelevant operators [110] (including the Wilson term). Restricting ourselves to the improvement of on-shell quantities, when the correlation functions are evaluated at non-zero physical distances and no contact terms between operators appear, the equations

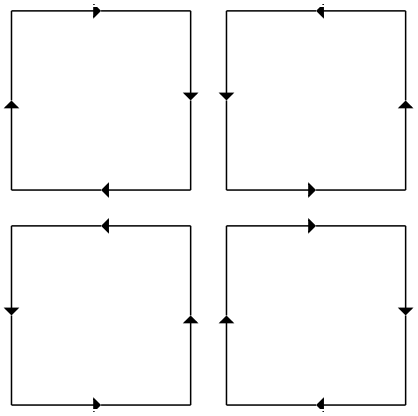

Figure 3.2: The clover-leaf of the discretised field strength tensor.

of motions can be used and we are left with only one remaining operator, the "clover" term. This is the last term in eq. (3.16) with

$$F_{\mu\nu}(x) = \frac{1}{8ig} \sum_{\pm\mu,\pm\nu} \left(U^P_{\mu\nu}(x) - U^P_{\mu\nu}(x)^\dagger \right), \tag{3.21}$$

where we have extended the definition of the plaquette to the Clover leave (Figure (3.2))

Now if we can achieve that one physical quantity (e.g. physical mass ratio) does not have a $O(a)$ term then

- this fixes $c_{sw}(g)$
- all other physical quantities are automatically improved to $O(a^2)$.

However the practical realisation is difficult and numerically demanding as one has to perform simulations at different $c_{sw}(g)$ values for one β. The ALPHA Collaboration were able to find [111] numerically $c_{sw}(g)$

$$c_{sw} = \frac{1 - 0.454g^2 - 0.175g^4 + 0.012g^6 + 0.045g^8}{1 - 0.720g^2} \tag{3.22}$$

and using this values it is possible to estimate $c_{sw}(g)$ for the β values used in our simulations.

3.5 Numerical Techniques

3.5.1 Monte Carlo Method

As already proposed the path integral in eq. (3.1) is calculated using Monte Carlo simulations. Here we shall now make some very brief comments on numerical al-

gorithms. The probabilistic interpretation implicates that we wish to find averages over some high dimensional probability distribution

$$\langle \mathcal{O} \rangle = \int [\mathrm{d}U]\, \mathcal{O}(U) P(U), \qquad P(U) = \frac{1}{Z} e^{-S(U)}. \tag{3.23}$$

The fermion part of the action does not appear at this point, being quadratic in the Grassmann fields it can always be integrated out to give a determinant in the gauge fields as seen in eq. (3.6). Statistical physics offers methods to deal with such problems, in particular we can simulate a Markov chain to obtain an approximate value for the wanted average. Let Q be the *transition matrix* then for a sequence we wish

$$P_{n+1}(U') = \int [\mathrm{d}U]\, P_n(U) Q(U, U'), \quad \int [\mathrm{d}U']\, Q(U, U') = 1 \tag{3.24}$$

In 'equilibrium', $P_n \to P$, and the Markov chain is solved by $P(U)Q(U,U') = P(U')Q(U',U)$, a sufficient but not necessary condition known as "detailed balance". The transition matrix Q can be considered as

$$\begin{aligned} Q(U, U') = &\begin{array}{c}\text{prob. of choosing a} \\ \text{candidate config.}\end{array} \times \begin{array}{c}\text{prob. of accepting} \\ \text{new config.}\end{array} \\ &= P_c(U \to U') \times P_a(U \to U') \end{aligned} \tag{3.25}$$

Many choices are possible, depending on what one is simulating. For example for *quenched* QCD where one drops the fermion determinant[1] we may sweep through the lattice defining for each link variable U_l a new one U_l' by the prescription

- $U_l' = U_0 U_l^{-1} U_0$ (over-relaxation, [112]) with

$$U_0 = \left(Proj \sum_{\text{staples}} U_{\text{staples}} \right)^{-1}$$

- $P_a = \min(1, e^{-\Delta S})$ (Metropolis Algorithm)

where the *staples* are build from the link variables that would complete the plaquettes of the link U_l. When one keeps the fermion determinant (*dynamical QCD*), the standard procedure is to use the Hybrid Monte Carlo algorithm [113].

To estimate the average a large number of independent configurations is generated and

$$\bar{\mathcal{O}} = \frac{1}{N_{\text{conf}}} \sum_{\text{conf}}^{N_{\text{conf}}} \mathcal{O}_n \tag{3.26}$$

[1] This approximation is uncontrolled but nevertheless is often done due to lack of computer power.

is calculated. Monte Carlo is very similar to performing an experiment and requires a careful analysis of errors. For N_{conf} configurations we expect

$$\text{Error} \propto \frac{1}{\sqrt{N_{\text{conf}}}}, \tag{3.27}$$

so the errors only decrease slowly; this is one of the main reasons why Monte Carlo calculations are so expensive in computer time.

3.5.2 The Green's Function

One important step within calculations is the computation of fermion propagators needed for the calculation of correlators. This involves inversion of a very large, sparse matrix. Here we sketch some of the details necessary to perform this inversion. We have already discussed the Dirac operator which is used in our simulations in subsection 3.4.2. For numerical purposes, it is conventional at first to introduce the 'hopping parameter' κ, lying between $1/6$ and $1/8$ re-scaling the quark fields

$$q \to \sqrt{2\kappa} q, \tag{3.28}$$

so that the bare quark mass is related to the hopping parameter by

$$am_0 = \frac{1}{2\kappa} - \frac{1}{16} \tag{3.29}$$

and to define then the critical value $\kappa_c(g_0^2)$ as the point where the bare quark mass vanishes,

$$am_q(g_0) = am_0 - am_{0c}(g_0) \equiv \frac{1}{2}\left(\frac{1}{\kappa} - \frac{1}{\kappa_c(g_0)}\right) \tag{3.30}$$

This allows to rewrite the Wilson-Dirac matrix in our case as

$$\begin{aligned} M_{xy} &= \equiv [D_W + C + am_0]_{xy} \\ &\to \left[1 + \frac{1}{2} i\kappa g c_{sw}(g_0) \sum_{\mu\nu} \sigma_{\mu\nu} F_{\mu\nu}\right] \delta_{xy} + \\ &\quad \kappa \sum_{\mu} \left[(\gamma_\mu - \mathbb{1})\, U_\mu(x) \delta_{x+\hat{\mu},y} - (\gamma_\mu + \mathbb{1})\, U_\mu^\dagger(x-\hat{\mu}) \delta_{x-\hat{\mu},y}\right]. \end{aligned} \tag{3.31}$$

In order to define the transfer matrix consistently periodic boundary conditions are taken in spatial while antiperiodic boundary condition is taken in the time direction. As the calculation of the Greens functions from all points x to all points y is numerically not possible, one in general wishes to find the Greens function from some given source s_α^a, so we have a matrix equation

$$Mv = s \tag{3.32}$$

to solve for v. For each Dirac and colour component we must invert the matrix, i.e. we have $4 \times 3 = 12$ inversions to perform to obtain the full Greens function. However using the staggered symmetry, $x_1 + x_2 + x_3 + x_4 = even/odd$, allows to re-write the Wilson-Dirac matrix in block form and to reduce in this way the number of needed inversions saving lot of the required computational time.

Some possible inverters that can be used are the Conjugate Gradient (CG) [114] (multiplying M first by γ_5 obtaining a hermitian matrix), Minimal Residual (MR) [115] or BiCGstab [116]. CG, while being reliable is slower than MR or BiCGstab. In our calculations we used mainly BiCGstab, except for the heavy quark masses on the smaller lattices where we used the MR algorithm.

At the end of this subsection we want to point out that the matrix inversion in lattice QCD is the most CPU intensive part of the calculation, because going for $am_q \rightarrow 0$ (the chiral limit) we approach the limit of vanishing pion mass. Not only we need then a larger lattice size to avoid finite size effects, but also the inversion becomes slower as the number of iterations required for the convergence increases as $\propto 1/am_q$.

3.5.3 The APEmille Machine

In the last section we have seen that the *even/odd* decomposition allows to reduce computation costs. While the implementation of this does not cause serious problems on vector computers, the implementation on parallel machine can cause some difficulties. Parallel machines consists of a number of processors, which are wired with certain topology which can lead to conflicts during the computation if two processors try to operate in the same time on the same data. As the largest part of our results was obtained on the APEmille machine, we would like to illuminate some numerical and technical details relevant for the calculation on a parallel machine and in particular the APEmille machine. The processors on the APE machines are arranged in three dimensional periodic arrays which can have different dimensions. In our calculations we have mainly used the $2 \times 8 \times 8$ layout of processors, which was sufficient for the calculations of the $24^3 \times 48$ lattices.

The architecture of the APE is *SIMD* (Single Instruction Multiply Data). On each node (i.e., processors) sits a sub-lattice of the total lattice. Thus for a given four-dimensional lattice, one of the dimension is placed completely on each processor, while the remaining three dimensions are distributed over all nodes. The nodes process the float numbers and are globally controlled by the Z controller where the integers are stored. Each node thus consists of a specially designed FPU (Floating Point Unit), called MAD processor for Multiply Adder Device capable to perform the complex operation $a \times b + c$ in one cycle. As the integers are processed by the $Z - CPU$, it controlls e.g., the global DO-loops. This "simple" architecture has the advantage that we do not have synchronisation problems.

On the other hand we have the disadvantage that the local control is difficult. A $WHERE$-statement allows some local control, but is inefficient, as large parts of the machine may be idle during the execution. However, in the present Lattice QCD calculations this disadvantage is of minor importance, as only occasionally at the boundary one needs local control. Communication on this machine is to the next nearest processors only - again sufficient for most Lattice QCD applications. However, some times it is necessary to communicate to the next to nearest node, i.e., during the calculation of the second order derivatives. Thus, it has to be done in two steps slowing down the computation. However, this communication very often can be hidden behind the calculation as in our case, and therefore does not affect the performance for our calculation.

The second problem of the architecture is that certain lattice sizes can cause problems with certain machine geometries. Let u exemplify this on a low dimensional example for a two dimensional 16×32 lattice on an one dimensional processor array with 32 nodes. If the lattice would be divided up in the simplest possible way, as illustrated in Figure 3.3(a), then there would be a conflict when updating space-like links, since different processors would be making simultaneous updates within the same plaquette leading to wrong results. A solution to this problem is illustrated in Figure 3.3(b), where we have used a new *slanted* coordinate system for dividing the lattice between the different processors. Thus we set

$$\begin{aligned} s_x =& (x + t) \bmod 16 \\ s_t =& t \end{aligned} \tag{3.33}$$

and use during the computation always the slanted coordinates (s_x, s_t). Now there are no conflicts during the gauge update.

An additional advantage of the slanted coordinate system is that it obviously allows algorithms that involve *even/odd* decomposition. As discussed previously the *even/odd* decomposition is important when we invert the fermion matrix to find the propagator. Without this decomposition the inversion would be slower, while in the slanted coordinate system the computation is accelerated as nearest neighbors are always on the neighboring processors.

3.6 Two-Point Correlators on the Lattice

The calculation of the nucleon distribution amplitudes will obviously involve the nucleon operator. As the nucleons are built up from three valence quarks the operator to create the nucleon on the lattice contains three quark fields. Additionally it should carry the correct quantum numbers to have an overlap with the nucleon state. However, the discussion here does not apply only to the nucleon, but to all

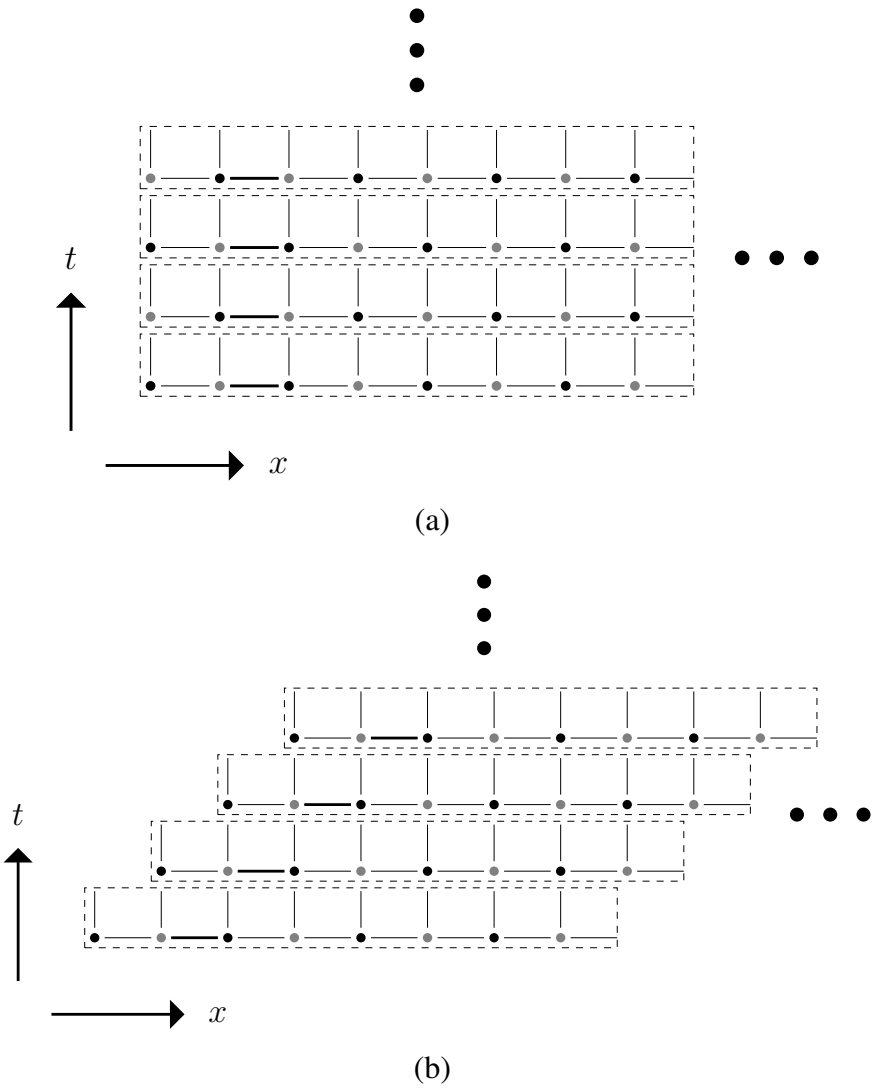

Figure 3.3: A t(vertical) - x (horizontal) part of the 4-dimensional lattice distributed onto the machine nodes. Each dashed rectangle represents one node coresponding to one t value. Lattice links are shown as lines. Every node operates simultaneously on one link (e.g., the bold lines). Even/odd lattice points corresponds to black/gray filled points. The Figure (a) illustrate the simplest possible distribution of the lattice on the machine nodes, while Figure (b) display the slanted distribution.

hadrons with three quarks and therefore can be easily extended to other baryons. In fact the operator for the nucleon can be also chosen in different ways and we will use here a certain choice, which should have a good overlap [117] with the nucleon state.

As a suitable interpolator for the proton [2] on the lattice we use

$$\mathcal{N}_\alpha(t;\vec{p}) = \frac{1}{\sqrt{V_3}} \sum_{\vec{x}} e^{-i\vec{p}\cdot\vec{x}} \epsilon^{abc} u^a_\alpha(t,\vec{x}) \left[u^b(t,\vec{x}) C\gamma_5 d^c(t,\vec{x})\right] \tag{3.34}$$

where C is the charge conjugation matrix. The last two quark fields form a diquark system, while the first quark field carries the spinor index.

During our calculations we have to evaluate the two-point correlator of the nucleon and another three quark operator

$$C_\Gamma(t;\vec{p}) = \langle \mathcal{O}(t;\vec{p}) \Gamma \mathcal{N}^\dagger(0;\vec{p}) \rangle \tag{3.35}$$

with

$$\mathcal{O}_\alpha(t;\vec{p}) = \frac{1}{\sqrt{V_3}} \sum_{\vec{y}} e^{-i\vec{p}\cdot\vec{y}} \epsilon^{abc} \left[u^a(t;\vec{y}) \Gamma_1 u^b(t;\vec{y})\right] (\Gamma_2 d^c)_\alpha(t;\vec{y}) \tag{3.36}$$

where Γ, Γ_1 and Γ_2 are some combinations of the Dirac gamma matrices. Additionally we can have also some covariant derivatives acting on the quark fields. However for the general discussion here we can restrict ourselves to the case without derivatives. Then by Wick contracting the fermion fields in the correlator the problem reduces to the calculation of the fermion propagator

$$G^{ab}_{\alpha\beta}(\vec{x},\vec{y}) = \langle q^a_\alpha(x) \bar{q}^b_\beta(y) \rangle \tag{3.37}$$

which in principle depends on the quark masses. However the *up*- and *down*-quarks are almost mass degenerate, so for both we can use the same propagator.

As we are averaging over the background gauge fields we can further simplify the calculation by employing translation invariance. We can move every source at $(\vec{y},0)$ to $(\vec{0},0)$ reducing the summation to the x sites only. Furthermore as the Green's functions are calculated on gauge configurations which may have strong correlations. In order to reduce this problem we place the sources on different sites for gauge configurations which are close to each other.

3.7 The Transfer Matrix on the Lattice

Rewriting the correlator from eq. (3.35) using the transfer matrix formalism on the lattice gives the Euclidean propagation of an operator from time slice 0 to

[2] By a simple isospin rotation $u \leftrightarrow d$ we can obtain directly also the relations for the neutron

time slice t. Hence we can rewrite the correlation function as

$$C_\Gamma(t;\vec{p}) = \frac{1}{V_3}\sum_{\vec{x},\vec{y}} e^{-i\vec{p}\cdot(\vec{x}-\vec{y})}\mathrm{tr}\left[\mathcal{S}^{T-t}O(\vec{x})\Gamma\mathcal{S}^t\mathcal{N}^\dagger(\vec{y})\right]. \tag{3.38}$$

Inserting the complete set of energy eigenstates and shifting the operators in the spatial plane to the origin by using the translation operator only the lowest nucleon mass states will dominate for large enough t

$$\begin{aligned} C(t;\vec{p}) =& \frac{\sqrt{Z_O(\vec{p})Z_N(\vec{p})}}{2E(\vec{p})}A_0 \\ & \sum_{\vec{s}}\left[\bar{v}(\vec{p},\vec{s})\Gamma v(\vec{p},\vec{s})e^{-E(\vec{p})t} + \bar{w}(\vec{p},\vec{s})\Gamma w(\vec{p},\vec{s})e^{-E(\vec{p})(T-t)}\right] \\ & + \frac{\sqrt{Z'_O(\vec{p})Z'_N(\vec{p})}}{2E'(\vec{p})}A_1 \\ & \sum_{\vec{s}}\left[\bar{v}'(\vec{p},\vec{s})\Gamma v'(\vec{p},\vec{s})e^{-E(\vec{p})t} + \bar{w}'(\vec{p},\vec{s})\Gamma w'(\vec{p},\vec{s})e^{-E'(\vec{p})(T-t)}\right]. \end{aligned} \tag{3.39}$$

where v, w are nucleon spinors in forward and backward time direction respectively. In the (3.39) we kept not only the lowest nucleon states with energy E but also the state of the nucleon parity partner with the energy E' and the spinor v', w'. The reason is that the energy of these states are relatively close and the time needed to suppress the second unwanted state is reasonably large on finite lattices. A partial cure can be achieved by projecting out this unwanted states. For the unpolarised stationary nucleon this can be done by applying the positive parity projection operator $\gamma_+ = (1+\gamma_4)/2$. Unfortunately for the moving nucleon required in some of our correlators we do not expect the complete suppression of the unwanted state. In order to construct a projection operator for moving nucleons we need information about the mass of the parity partner. However, in our case the suppression will be good enough also for moving nucleons and the uncertainty in the calculation is mostly dominated by other sources of error.

3.8 Operator Overlap Improvement

During the calculation of the correlators on the lattice we have to interpolate the hadrons by operators with the correct quantum numbers. Clearly as hadrons are not point-like objects the used interpolator should also have some extension; ideally to achieve a good signal we would like to have a very good overlap with the nucleon wave function. However, the perfect overlap is not possible as we do not know the nucleon wave function. Therefore to create a nucleon on the lattice we

use an interpolator which involves the three valence quarks of the nucleon plus some gamma matrices and has the right quantum numbers.

As the Green's function for the quarks, the constituents of the nucleon, is calculated using one point source, also the interpolating field for the nucleon will be a point-like object and we run into the risk that the amplitude for a nucleon, or equivalently the overlap of the used interpolator with a nucleon, in the correlation function might be very small. To help this situation we shall employ a type of improvement called smearing, where the source for the nucleon in the $(\vec{x}, 0)$ plane is smeared. Thus the nucleon amplitude in the correlator will not only depend on the renormalisation factor for the three quarks but also on the smearing parameters. We merge both constants in the factor $Z_N(\vec{p})$, which also depends on the nucleon momentum $\vec{p}$. Although we are not interested in the value of this factor, the determination of it will affect our calculation. We postpone the discussion how it is done technically to the relevant section.

The basic idea of smearing is to create an extended source which has approximately the same size as the real nucleon so that the overlap should be considerably enlarged compared to the point source. The most general smeared nucleon interpolator is given by

$$\begin{aligned}\mathcal{N}_\alpha = \frac{1}{\sqrt{V_3}} \frac{1}{V_3^{3/2}} \sum_{\vec{x}_1,\vec{x}_2,\vec{x}_3} & F(\vec{x}_1,\vec{x}_2,\vec{x}_3) e^{-i\vec{p}\cdot(\vec{x}_1+\vec{x}_2+\vec{x}_3)/3} \\ & \epsilon^{abc} u^a_\alpha(t;\vec{x}_1) \left[u^b(t;\vec{x}_2) C\gamma_5 d^c(t;\vec{x}_3)\right],\end{aligned} \tag{3.40}$$

where F, if known exactly, describes the true nucleon wave function. However the correlation function calculated from such a source would require the knowledge of the Green's functions from source positions $(0;\vec{x}_1)$, $(0;\vec{x}_2)$ and $(0;\vec{x}_3)$ for all $\vec{x}_1, \vec{x}_2$ and $\vec{x}_3$. While translation invariance allows to set one of the sources to $(0;\vec{0})$ it is not possible for all three sources simultaneously. Thus this general approach would require an enormous amount of computer power. To avoid this we a simpler smearing where F factorises into a product of function of $\vec{x}_1, \vec{x}_2$ and $\vec{x}_3$ (cf., [118]).

Factorising F is equivalently to smearing each quark individually. Denoting the smearing with label S we have then

$${}^S q^a_\alpha(t;\vec{x}) = \sum_{\vec{y},b} {}^S H^{ab}(t,\{U\};\vec{x},\vec{y}) q^b_\alpha(t;\vec{y}) \tag{3.41}$$

where the kernel H is diagonal in spin space and is chosen to have the correct gauge transformation properties, i.e., $H(t,\{U\};\vec{x},\vec{y})$ must be the parallel transporter from $(t;\vec{y})$ to $(t;\vec{x})$ so that under a gauge transformation

$$\bar{q}(t;\vec{x}) H(t,\{U\};\vec{x},\vec{y}) q(t;\vec{y}) \tag{3.42}$$

remains gauge invariant. ${}^{S}H$ is also taken as hermitian[3] ${}^{S}H^{\dagger} = {}^{S}H$. Then the smeared anti-quark is defined as

$$ {}^{S}\bar{q}^{a}_{\alpha}(t;\vec{x}) = \sum_{\vec{x},b} \bar{q}^{b}_{\alpha}(t;\vec{y}) {}^{S}H^{b}_{a}(t,\{U\};\vec{y},\vec{x}). \tag{3.43} $$

Note that it is possible to choose smearing for the quark and anti-quark fields as well as for source and sink separately. This is part of the so called cross correlation technique [119, 120, 121]. However, in our case we are only interested in ground states where the improvement from the cross correlation technique is relatively small. Therefore we will smear all sources (and sinks if required) in the same way. Thus, the local nucleon interpolator from (3.34) has a quite simple generalisation of the form

$$ {}^{\mathcal{S}}\mathcal{N}_{\alpha}(t;\vec{p}) = \frac{1}{\sqrt{V_3}} \sum_{\vec{x}} e^{-i\vec{p}\cdot\vec{x}} \epsilon^{abc} \, {}^{S}u^{a}_{\alpha}(t,\vec{x}) \left[{}^{S}u^{b}(t,\vec{x}) C\gamma_5 {}^{S}d^{c}(t,\vec{x}) \right]. \tag{3.44} $$

Analogously the smeared Green's function is defined by

$$ {}^{S'S}G^{ab}_{\alpha\beta}(\{U\};x,y) = \langle {}^{S'}q^{a}_{\alpha}(x) {}^{S}\bar{q}^{b}_{\beta}(y) \rangle \tag{3.45} $$

where ${}^{ll}G$ will be the original unsmeared Green's function and ${}^{ls}G$ one with smeared source and local sink. So in correlation functions we can simply replace the unsmeared Green's function by one which has the desired smearings on the source and sink.

The smeared Green's functions are then determined sequentially

- Generate a smeared source from a point source s_0 at $(t_0;\vec{x}_0)$ with $s^{a}_{0\alpha} = \delta_{\vec{x}\vec{x}_0}\delta_{tt_0}\delta^{aa_0}\delta_{\alpha\alpha_0}$:

$$ {}^{s}s^{aa_0}_{\alpha\alpha_0}(t,t_0;\vec{x},\vec{x}_0) = {}^{s}H^{aa_0}(t,\{U\};\vec{x},\vec{x}_0)\delta_{tt_0}\delta_{\alpha\alpha_0} \tag{3.46} $$

- Find the Green's function with smeared source ${}^{ls}G$ by inverting $M {}^{l}sG = {}^{s}s$, with M being the Dirac matrix. So we have

$$ {}^{ls}G^{ab}_{\alpha\beta}(t,t_0;\vec{x},\vec{x}_0) \equiv \sum_{\vec{y}b'} G^{ab'}_{\alpha\beta}(t,t_0;\vec{x},\vec{y}) {}^{s}H^{b'b}(t_0,\{U\};\vec{y},\vec{x}_0) \tag{3.47} $$

- From ${}^{ls}G$ we can generate the smeared-smeared propagator ${}^{ss}G$ by applying ${}^{s}H$ to the sink

$$ {}^{ss}G^{ab}_{\alpha\beta}(t,t_0;\vec{x},\vec{x}_0) = \sum_{\vec{y},a'} {}^{s'}H^{aa'}(t,\{U\};\vec{x},\vec{y}) {}^{ls}G^{a'b}_{\alpha\beta}(t,t_0;\vec{y},\vec{x}_0). \tag{3.48} $$

[3] More exactly ${}^{S}H^{\dagger ab}(t,\{U\};\vec{x},\vec{y}) = {}^{S}H^{ba}(t,\{U\};\vec{y},\vec{x})^{\star} = {}^{S}H^{ab}(t,\{U\};\vec{x},\vec{y})$

In practice there exist several roughly similar smearing prescriptions [118]. Here we shall use the Jacobi smearing technique [122, 123] which is gauge covariant. It is defined as

$$\sum_{\vec{x}'} K(t;\vec{x},\vec{x}')^s s(t;\vec{x}') = s_0(t;\vec{x}) \tag{3.49}$$

where s_0 is the original point source and D_s is a covariant derivative in the $x_4 = t$ plane. Writing K in the form

$$K = 1 - \kappa_s D_s \tag{3.50}$$

we need then $H = K^{-1}$. Instead to perform the complete inversion (cf., [124]), the smeared source is obtained by N_s Jacobi iterations

$${}^s s^{(n)}(t;\vec{x}) = s_0(t;\vec{x}) + \kappa_s D_s {}^s s^{(n-1)}(t;\vec{x}) \qquad n = 1, 2, \ldots \tag{3.51}$$

Thus we have two parameters, κ_s and N_s, we can adjust. While κ_s determines the coarseness of the iteration, the number of iterations N_s determines the size of the smeared object. As we want to maximise the overlap of composite particles the resulting smeared quark source should approximately be of the nucleon size. A suitable measure of the RMS radius of the smeared source ${}^s s$ is

$$r^2 = \frac{\sum_{\vec{x}} (\vec{x} - \vec{x}_0)^2 |{}^s s(t_0;\vec{x},\vec{x}_0)|^2}{\sum_{\vec{x}} |{}^s s(t_0;\vec{x},\vec{x}_0)|^2}. \tag{3.52}$$

3.9 Setting the Scale

Before we turn our attention to the details of the lattice calculation for the nucleon distribution amplitudes, we have to discuss how the bare numbers obtained on a computer can be translated into physical units. On the computer our action does not involve any dimensionful parameters by construction. Besides the dimensionless coupling β it involves also the quark masses, however these appear always in the combination am, where a is the lattice spacing. The point is that the lattice spacing a is the regulator in our calculation and by performing simulations with fixed β we have in fact already chosen a certain a value, which fixes then also all other quantities. However, we do not know this value and have to determine it in physical units.

The lattice spacing a can be determined by comparing a physical quantity we know with numerical values we get from lattice calculation, like the mass on the lattice am, so that both agree with each other. This procedure of finding the physical units is called "setting the scale". Instead of using the masses to set the

scale we will use in our calculation the method introduced by R. Sommer [125, 126]. This method utilises the static quark potential $V(r)$, which is commonly, but not necessarily , parametrised as

$$V(r) = A + \frac{B}{r} + \sigma r \tag{3.53}$$

where σ is the "string tension". From QCD phenomenology one expects a value of $\sigma \approx 800\mathrm{MeV/fm}$. The parameter B is responsible for the strength of the Coulomb part of the potential and A is some irrelevant energy normalisation. The static potential is closely tied to a characteristic length scale r_0 which is defined by the equation

$$r_0^2 \frac{\partial}{\partial r} V(r)|_{r_0} = 1.65. \tag{3.54}$$

In lattice units we have then in the above parametrisation

$$\frac{r_0}{a} = \sqrt{\frac{1.65 + B}{a^2\sigma}}. \tag{3.55}$$

Calculating the static quark potential by Wilson loops on the lattice we can obtain the numbers B and $a^2\sigma$ by fitting $V(r)$ to the calculated potential. Using the physical value of r_0, we can then determine the lattice spacing in physical units. However, while r_0 has the advantage that on the lattice it can be determined with relatively high statistical accuracy, its experimental value is far less known. Recent results from different collaborations indicate that the value for r_0 is significantly smaller than the typically used value $r_0 = 0.5\,\mathrm{fm}$. In this work we use the value $r_0 = 0.467\,\mathrm{fm}$ [127, 128] and the present uncertainty of this empiric value is one of the systematic errors in our calculations.

3.10 Operator Choice on the Lattice for Distribution Amplitudes

We have already seen that the advantages of the lattice calculations compared to continuum calculations have to be paid for by problems which are not present in the continuum. But we also saw that it is possible to handle these problems. In this section we turn our attention to a further problem which arises on the lattice due to the reduction of the continous Lorentz symmetry to the hypercubic one.

The operators in QCD have to be renormalised. As the renormalisation matrix for an operator set is in general not diagonal, we expect mixing of different operators under renormalisation. However, due to the Lorentz symmetry in the continuum most of the mixings are not allowed. The lattice discretisation reduces

this symmetry strongly and leads to additional operator mixings which are not present in the continuum. Even worse, on the lattice we can also have mixing with lower dimensional operators due to $O(a)$ discretisation errors. A partial cure of this problem and an improved analysis can be achieved by using appropriate operator combinations. Thus a systematic analysis and careful choice of the used operators is mandatory as already partially outlined in [129]. As we are dealing with nucleon we have to find the relevant three quark operators. In [130] a complete classification with respect to the hypercubic spinorial $H(4)$ group of all three-quark operators without derivatives was obtained. Also for operators with one and two derivatives the classification of all leading twist operators relevant for our case has been worked out therein. This classification simplifies greatly our task to construct operators with good mixing properties relevant for the calculation of the distribution amplitudes.

	$d = 9/2$ (0 derivatives)	$d = 11/2$ (1 derivative)	$d = 13/2$ (2 derivatives)
$\tau_1^{\underline{4}}$	$\mathcal{B}^{(0)}_{1,i}$, $\mathcal{B}^{(0)}_{2,i}$, $\mathcal{B}^{(0)}_{3,i}$, $\mathcal{B}^{(0)}_{4,i}$, $\mathcal{B}^{(0)}_{5,i}$		$\mathcal{B}^{(2)}_{1,i}$, $\mathcal{B}^{(2)}_{2,i}$, $\mathcal{B}^{(2)}_{3,i}$
$\tau_2^{\underline{4}}$			$\mathcal{B}^{(2)}_{4,i}$, $\mathcal{B}^{(2)}_{5,i}$, $\mathcal{B}^{(2)}_{6,i}$
$\tau^{\underline{8}}$	$\mathcal{B}^{(0)}_{6,i}$	$\mathcal{B}^{(1)}_{1,i}$	$\mathcal{B}^{(2)}_{7,i}$, $\mathcal{B}^{(2)}_{8,i}$, $\mathcal{B}^{(2)}_{9,i}$
$\tau_1^{\underline{12}}$	$\mathcal{B}^{(0)}_{7,i}$, $\mathcal{B}^{(0)}_{8,i}$, $\mathcal{B}^{(0)}_{9,i}$	$\mathcal{B}^{(1)}_{2,i}$, $\mathcal{B}^{(1)}_{3,i}$, $\mathcal{B}^{(1)}_{4,i}$	$\mathcal{B}^{(2)}_{10,i}$, $\mathcal{B}^{(2)}_{11,i}$, $\mathcal{B}^{(2)}_{12,i}$, $\mathcal{B}^{(2)}_{13,i}$
$\tau_2^{\underline{12}}$		$\mathcal{B}^{(1)}_{5,i}$, $\mathcal{B}^{(1)}_{6,i}$, $\mathcal{B}^{(1)}_{7,i}$, $\mathcal{B}^{(1)}_{8,i}$	$\mathcal{B}^{(2)}_{14,i}$, $\mathcal{B}^{(2)}_{15,i}$, $\mathcal{B}^{(2)}_{16,i}$, $\mathcal{B}^{(2)}_{17,i}$, $\mathcal{B}^{(2)}_{18,i}$

Table 3.1: Overview of irreducibly transforming multiplets of three-quark operators $\mathcal{B}^{(d)}_{l,i}$ sorted by their mass dimension (number of derivatives d) taken from [130] with a notation adapted to our needs. Since for the classification it is not important on which quarks the derivatives act, only the sum $l + m + n$ is given as superscript. The subscript gives the numbering of the operators according to the convention in [130]. The first number corresponds to the lower index of [130] while the second number corresponds to the upper index in [130] numbering different operators within one multiplet (cf., Table 4.1 in [130]). In the first column we give also the representations where the superscript denotes the dimension.

Since operators belonging to different irreducible representations do not mix with each other we use operators which lie completely within one irreducible representation. In Table 3.1 we give an overview of the irreducible multiplets of op-

erators taken from Table 4.1 in [130], but with a modified notation adapted to our needs, e.g., the operator $B^{(2)}_{1,i}$ corresponds to $\mathcal{O}^{(i)}_{DD1}$ in [130]. The next-to-leading twist distribution amplitude operators (2.87) and (2.88) and the GUT related operators (2.108) and (2.109) lie completely within the $\tau_1^{\underline{4}}$ representation with mass dimension $9/2$. The operators for the leading twist distribution amplitudes belong to other multiplets. As operators without derivatives in the $\tau^{\underline{8}}$ representation do not have an overlap with the nucleon, the relevant operators with "good" mixing properties lie in $\tau_1^{\underline{12}}$ with mass dimension $9/2$, $\tau_2^{\underline{12}}$ with mass dimension $11/2$ and $\tau_2^{\underline{4}}$ with mass dimension $13/2$ for zero, one and two derivatives respectively.

By relating these irreducible operators to the local operators of distribution amplitude operators we were able to construct operators for distribution amplitude with best possible mixing properties on the lattice. In Appendix A.2 we summarise the obtained relations which can be used directly to construct the preferred set of the operators for different leading twist baryon distribution amplitudes. In the following we give some details on the operators as used by us.

Initially the irreducible operators in [130] have a general flavour content and are of the type

$$\Gamma^{\alpha\beta\gamma}_{\mu\nu} D^\mu D^\nu \epsilon^{abc} f^a_\alpha g^b_\beta h^c_\gamma. \tag{3.56}$$

where $\Gamma^{\alpha\beta\gamma}_{\mu\nu}$ is a tensor projecting the operator to a certain irreducible representation. It is not important for the construction of irreducibly transforming operators on which of the quarks the derivatives acts, as the possible combinations fall into the same irreducible representation. Therefore, at this stage we do not distinguish between the different positions of covariant derivatives.

To establish connection to the distribution amplitude operators $\mathcal{V}$, $\mathcal{A}$ and $\mathcal{T}$ we preferred a slightly generalized approach. We rewrite distribution amplitude operators from eqs. (2.58, 2.59 and 2.60) also as operators without definite flavour content, e.g.,

$$\begin{aligned}\mathcal{V}^{\rho\bar{l}\bar{m}\bar{n}}_\tau(0) = \epsilon^{abc}[i^l D^{\lambda_1} \dots D^{\lambda_l} f^a_\alpha(0)](C\gamma^\rho)_{\alpha\beta}[i^m D^{\mu_1} \dots D^{\mu_m} g^b_\beta(0)] \\ \times [i^n D^{\nu_1} \dots D^{\nu_n}(\gamma_5 h^c(0))]_\tau\end{aligned} \tag{3.57}$$

and similarly for $\mathcal{A}$ and $\mathcal{T}$. Since the distribution amplitude operators for other members of the baryon octet differ only by the flavor content the obtained relations can be used directly also for other octet baryons [47]. Furthermore these relations are applicable also to Δ, which is not in the octet. The nucleon distribution amplitudes are then restored by the identification

$$f \to u, \qquad g \to u, \qquad h \to d. \tag{3.58}$$

and subsequent isospin symmetrisation. Since we preferred a fixed flavor assignement for f, g, h the isospin $1/2$ operators are obtained in a different way compared

to [130]. For our purpose it is sufficient to combine appropriately different multiplets in the same representation to obtain an isospin $1/2$ operator[4].

3.11 Details of the Lattice Calculation

In this section we discuss the techniques used and the details of the lattice calculation in Euclidean space. We summarise the common properties in the first part of this section. Then, in the following parts we discuss the calculation of matrix elements relevant for leading and next-to-leading twist distribution amplitudes and the nucleon decay in GUTs.

3.11.1 Common Properties

To be as flexible as possible in our calculation we have adopted a two-stage approach in the evaluation of the correlators. In the first step we have calculated correlators of the form

$$C^{\bar{l}\bar{m}\bar{n}}_{\alpha\beta\gamma\tau} = \langle \epsilon^{abc} [D^{\lambda_1} \dots D^{\lambda_l} u]^a_\alpha [D^{\mu_1} \dots D^{\mu_m} u]^b_\beta [D^{\nu_1} \dots D^{\nu_n} d]^c_\gamma \bar{\mathcal{N}}_\tau \rangle, \qquad (3.59)$$

with $l + m + n \leq 2$. As interpolating operator for the nucleon we have used

$$\mathcal{N}_\tau = \epsilon^{abc} \left[u^{aT} C \gamma_5 d^b \right] u^c_\tau \qquad (3.60)$$

with the charge conjugation matrix C. Due to the presence of two *up*-quarks in the three-quark operator, $C^{\bar{m}\bar{l}\bar{n}}_{\alpha\beta\gamma\tau}$ can be reconstructed from $C^{\bar{l}\bar{m}\bar{n}}_{\alpha\beta\gamma\tau}$ by the appropriate interchange of Dirac indices. In this way we can halve the number of required general correlators, saving large amount of computer time.

In the second step, the general three-quark operator from (3.59) was used to calculate the matrix elements for the different quantities we discussed before. The general form of the correlation functions we compute at this stage is of the type

$$\langle \mathcal{O}_\tau(t, \vec{p}) \bar{\mathcal{N}}_{\tau'}(0, \vec{p}) \rangle = \sqrt{Z_N(\vec{p})} N_{\tau'}(\vec{p}) \exp\left(-E(\vec{p})t\right) \langle 0 | \mathcal{O}_\tau(t, \vec{p}) | p \rangle, \qquad (3.61)$$

which can be directly computed from the general correlation function in (3.59). The remaining matrix element on the right hand side is the quantity we want to determine.Thus, we have also to calculate the normalisation constant $Z_N(\vec{p})$, which can be extracted from the usual two-point nucleon correlator

$$C_N(\vec{p}) \equiv (\gamma_+)_{\tau'\tau} \langle \mathcal{N}_\tau(t, \vec{p}) \bar{\mathcal{N}}_{\tau'}(0, \vec{p}) \rangle = Z_N(\vec{p}) \frac{m + E(\vec{p})}{E(\vec{p})} \exp\left(-E(\vec{p})t\right) \qquad (3.62)$$

[4]Of course the results of both procedures are and must be equivalent.

with the positive parity projection $\gamma_+ = (1+\gamma_4)/2$. In the evaluation of the correlator in (3.59) the overlap of the nucleon interpolator with the nucleon state is improved by Jacobi smearing at the source while the sink is not smeared since we want to evaluate local matrix elements. Thus the nucleon correlator in (3.62) cannot be extracted from the general three-quark nucleon correlator (3.59) but must be computed separately with Jacobi smeared sink and source.

The normalisation constant $Z_N(\vec{p})$ could be removed by considering the ratio

$$\frac{\left((\gamma_+)_{\tau'\tau}\langle \mathcal{O}_\tau(t)\bar{\mathcal{N}}_{\tau'}(0)\rangle\right)^2}{(\gamma_+)_{\tau'\tau}\langle \mathcal{N}_\tau(t)\bar{\mathcal{N}}_{\tau'}(0)\rangle}. \tag{3.63}$$

However, as we will see later, the location of the effective mass plateaus is different for the two correlators, presumably due to the different smearings on the sink, spoiling this simple approach. Thus instead of calculating the ratio we perform a correlated fit to the two correlators in the range of the corresponding effective mass plateaus.

3.12 Moments of Distribution Amplitudes

3.12.1 Leading Twist

0th moment

Using the representation τ_1^{12} and the relations to the distribution amplitude operators given in Appendix A.2 we construct from the twelve irreducible three-quark operators three quadruplets of operators with isospin $1/2$ which can be used to calculate the normalisation constant f_N:

$$\mathcal{O}^{000}_{A,0} = \frac{4}{3}\begin{pmatrix} -\mathcal{B}^{000}_{8,6} + \mathcal{B}^{000}_{9,6} \\ \mathcal{B}^{000}_{8,1} - \mathcal{B}^{000}_{9,1} \\ -\mathcal{B}^{000}_{8,12} + \mathcal{B}^{000}_{9,12} \\ \mathcal{B}^{000}_{8,7} - \mathcal{B}^{000}_{9,7} \end{pmatrix}, \qquad \mathcal{O}^{000}_{B,0} = \frac{4}{3}\begin{pmatrix} -\mathcal{B}^{000}_{8,4} + \mathcal{B}^{000}_{9,4} \\ \mathcal{B}^{000}_{8,3} - \mathcal{B}^{000}_{9,3} \\ -\mathcal{B}^{000}_{8,10} + \mathcal{B}^{000}_{9,10} \\ \mathcal{B}^{000}_{8,9} - \mathcal{B}^{000}_{9,9} \end{pmatrix},$$
$$\mathcal{O}^{000}_{C,0} = \frac{4\sqrt{2}}{3}\begin{pmatrix} \mathcal{B}^{000}_{8,2} - \mathcal{B}^{000}_{9,2} \\ -\mathcal{B}^{000}_{8,5} + \mathcal{B}^{000}_{9,5} \\ \mathcal{B}^{000}_{8,8} - \mathcal{B}^{000}_{9,8} \\ -\mathcal{B}^{000}_{8,11} + \mathcal{B}^{000}_{9,11} \end{pmatrix}. \tag{3.64}$$

The three-quark operator $\mathcal{O}$ on the left hand side has also a Dirac index which we do not give explicitly here. The relations to the distribution amplitude operators

given in Appendix A.2 yield then

$$\langle 0|\mathcal{O}^{lmn}_{A,0}|p\rangle = f_N(ip_1\gamma_1 - ip_2\gamma_2)N(\vec{p}), \tag{3.65}$$

$$\langle 0|\mathcal{O}^{lmn}_{B,0}|p\rangle = f_N(ip_3\gamma_3 + E(\vec{p})\gamma_4)N(\vec{p}), \tag{3.66}$$

$$\langle 0|\mathcal{O}^{lmn}_{C,0}|p\rangle = f_N(ip_1\gamma_1 + ip_2\gamma_2 - ip_3\gamma_3 + E(\vec{p})\gamma_4)N(\vec{p}). \tag{3.67}$$

The operators $\mathcal{O}^{lmn}_{B,0}$ and $\mathcal{O}^{lmn}_{C,0}$ are most suitable for our calculation since the operator $\mathcal{O}^{lmn}_{A,0}$ would require non-zero spatial momenta in the 1 or 2 direction which would increase the statistical noise. Thus, in order to determine f_N we will evaluate finally only the following two correlators at $\vec{p} = \vec{0}$ on the lattice:

$$\begin{aligned} C^{000}_{B,0} \equiv &\langle \left(\gamma_4\mathcal{O}^{lmn}_{B,0}(t,\vec{p})\right)_\tau \left(\bar{\mathcal{N}}(0,\vec{p})\right)_{\tau'} (\gamma_+)_{\tau'\tau}\rangle = \\ &f_N\sqrt{Z_N(\vec{p})}\frac{E(\vec{p})\,(m_N + E(\vec{p})) + p_3^2}{E(\vec{p})}\exp\left(-E(\vec{p})t\right), \end{aligned} \tag{3.68}$$

$$\begin{aligned} C^{000}_{C,0} \equiv &\langle \left(\gamma_4\mathcal{O}^{lmn}_{C,0}(t,\vec{p})\right)_\tau \left(\bar{\mathcal{N}}(0,\vec{p})\right)_{\tau'} (\gamma_+)_{\tau'\tau}\rangle = \\ &f_N\sqrt{Z_N(\vec{p})}\frac{E(\vec{p})(m_N + E(\vec{p})) + p_1^2 + p_2^2 - p_3^2}{E(\vec{p})}\exp\left(-E(\vec{p})t\right). \end{aligned} \tag{3.69}$$

1st moment

We use irreducible operators with one derivative from Appendix A.2 to construct operators for the calculation of the first moments of the leading twist nucleon distribution amplitude,

$$\mathcal{O}^{lmn}_{A,1} = \frac{4\sqrt{2}}{3}\begin{pmatrix} \mathcal{B}^{lmn}_{6,1} - \mathcal{B}^{lnm}_{7,1} \\ -\mathcal{B}^{lmn}_{6,2} + \mathcal{B}^{lnm}_{7,2} \\ -\mathcal{B}^{lmn}_{6,7} + \mathcal{B}^{lnm}_{7,7} \\ \mathcal{B}^{lmn}_{6,8} - \mathcal{B}^{lnm}_{7,8} \end{pmatrix}, \quad \mathcal{O}^{lmn}_{B,1} = \frac{4\sqrt{2}}{3}\begin{pmatrix} -\mathcal{B}^{lmn}_{6,3} + \mathcal{B}^{lnm}_{7,3} \\ \mathcal{B}^{lmn}_{6,4} - \mathcal{B}^{lnm}_{7,4} \\ \mathcal{B}^{lmn}_{6,9} - \mathcal{B}^{lnm}_{7,9} \\ -\mathcal{B}^{lmn}_{6,10} + \mathcal{B}^{lnm}_{7,10} \end{pmatrix},$$

$$\mathcal{O}^{lmn}_{C,1} = \frac{4}{3}\begin{pmatrix} \mathcal{B}^{lmn}_{6,6} - \mathcal{B}^{lnm}_{7,6} \\ \mathcal{B}^{lmn}_{6,5} - \mathcal{B}^{lnm}_{7,5} \\ -\mathcal{B}^{lmn}_{6,12} + \mathcal{B}^{lnm}_{7,12} \\ -\mathcal{B}^{lmn}_{6,11} + \mathcal{B}^{lnm}_{7,11} \end{pmatrix}, \tag{3.70}$$

where $l + m + n = 1$ with nonnegative integers l, m, n. The matrix elements of these operators are then

$$\langle 0|\mathcal{O}^{lmn}_{A,1}|p\rangle = f_N\phi^{lmn}\left[(ip_1\gamma_1 - ip_2\gamma_2)(-ip_3\gamma_3 + E(\vec{p})\gamma_4) + 2p_1p_2\gamma_1\gamma_2\right]N(\vec{p}), \tag{3.71}$$

$$\langle 0|\mathcal{O}^{lmn}_{B,1}|p\rangle = f_N\phi^{lmn}\left[(ip_1\gamma_1 + ip_2\gamma_2)(ip_3\gamma_3 + E(\vec{p})\gamma_4) - 2ip_3E(\vec{p})\gamma_3\gamma_4\right]N(\vec{p}), \tag{3.72}$$

$$\langle 0|\mathcal{O}^{lmn}_{C,1}|p\rangle = f_N\phi^{lmn}(ip_1\gamma_1 - ip_2\gamma_2)(ip_3\gamma_3 + E(\vec{p})\gamma_4)N(\vec{p}), \tag{3.73}$$

where again a Dirac index is implied for the three-quark operators $\mathcal{O}$. Unlike the case of the 0th moment all operators require at least one non-zero component of the spatial momentum. Hence using all operators available in this case we evaluate the correlators

$$\begin{aligned} C^{lmn}_{A,1} \equiv &\langle \left(\gamma_4\gamma_1 \mathcal{O}^{lmn}_{A,1}(t,\vec{p})\right)_\tau \left(\bar{\mathcal{N}}(0,\vec{p})\right)_{\tau'} (\gamma_+)_{\tau'\tau} \rangle = \\ &f_N \phi^{lmn} \sqrt{Z_N(\vec{p})}\; ip_1 \frac{E(\vec{p})(m_N + E(\vec{p})) + 2p_2^2 - p_3^2}{E(\vec{p})} \exp\left(-E(\vec{p})t\right), \end{aligned} \tag{3.74}$$

$$\begin{aligned} C^{lmn}_{B,1} \equiv &\langle \left(\gamma_4\gamma_1 \mathcal{O}^{lmn}_{B,1}(t,\vec{p})\right)_\tau \left(\bar{\mathcal{N}}(0,\vec{p})\right)_{\tau'} (\gamma_+)_{\tau'\tau} \rangle = \\ &f_N \phi^{lmn} \sqrt{Z_N(\vec{p})}\; ip_1 \frac{E(\vec{p})(m_N + E(\vec{p})) + p_3^2}{E(\vec{p})} \exp\left(-E(\vec{p})t\right), \end{aligned} \tag{3.75}$$

$$\begin{aligned} C^{lmn}_{C,1} \equiv &\langle \left(\gamma_4\gamma_1 \mathcal{O}^{lmn}_{C,1}(t,\vec{p})\right)_\tau \left(\bar{\mathcal{N}}(0,\vec{p})\right)_{\tau'} (\gamma_+)_{\tau'\tau} \rangle = \\ &f_N \phi^{lmn} \sqrt{Z_N(\vec{p})}\; ip_1 \frac{E(\vec{p})(m_N + E(\vec{p})) + p_3^2}{E(\vec{p})} \exp\left(-E(\vec{p})t\right) \end{aligned} \tag{3.76}$$

to determine the first moments ϕ^{100}, ϕ^{010} and ϕ^{001}.

2nd moments

The calculation of the second moments requires the use of the four-dimensional irreducible representation τ_2^4 to avoid mixing with lower-dimensional operators. Unfortunately this decreases also the number of possible operators. Using the irreducible three-quark operators with two derivatives and the relations to the distribution amplitude operators from Appendix A.2 we construct

$$\mathcal{O}^{lmn}_2 := \frac{4}{3\sqrt{3}} \begin{pmatrix} \mathcal{B}^{lmn}_{5,4} - \mathcal{B}^{lnm}_{6,4} \\ \mathcal{B}^{lmn}_{5,3} - \mathcal{B}^{lnm}_{6,3} \\ \mathcal{B}^{lmn}_{5,2} - \mathcal{B}^{lnm}_{6,2} \\ \mathcal{B}^{lmn}_{5,1} - \mathcal{B}^{lnm}_{6,1} \end{pmatrix} \tag{3.77}$$

where now $l + m + n = 2$ with l, m, n nonnegative integers. The corresponding matrix element is given by

$$\begin{aligned} \langle 0|\mathcal{O}^{lmn}_2|p\rangle = f_N \phi^{lmn} \big[&-p_1 p_2 \gamma_1\gamma_2 \left(ip_3\gamma_3 + E(\vec{p})\gamma_4\right) \\ &-ip_3 E(\vec{p})\gamma_3\gamma_4 \left(ip_1\gamma_1 + ip_2\gamma_2\right)\big] N(\vec{p}) \end{aligned} \tag{3.78}$$

and the second moments are determined then from

$$\begin{aligned} C^{lmn}_2 \equiv &\langle \left(\gamma_2\gamma_3\gamma_4 \mathcal{O}^{lmn}_2(t,\vec{p})\right)_\tau \left(\bar{\mathcal{N}}(0,\vec{p})\right)_{\tau'} (\gamma_+)_{\tau'\tau} \rangle = \\ &f_N \phi^{lmn} \sqrt{Z_N(\vec{p})}\; p_2 p_3 \frac{E(\vec{p})(m_N + E(\vec{p})) + p_1^2}{E(\vec{p})} \exp\left(-E(\vec{p})t\right). \end{aligned}$$

with $p_2 = p_3 \neq 0$.

Next-to-leading twist distribution amplitudes.

For the higher twist distribution amplitudes we consider only the operators eqs. (2.87) and (2.88) without derivatives. These can be immediately expressed in terms of irreducible operators

$$\mathcal{L} = \sqrt{8} \begin{pmatrix} \mathcal{B}^{lmn}_{3,1} + \mathcal{B}^{lmn}_{4,1} \\ \mathcal{B}^{lmn}_{3,2} + \mathcal{B}^{lmn}_{4,2} \\ \mathcal{B}^{lmn}_{3,3} + \mathcal{B}^{lmn}_{4,3} \\ \mathcal{B}^{lmn}_{3,4} + \mathcal{B}^{lmn}_{4,4} \end{pmatrix} \qquad \mathcal{M} = \sqrt{96} \begin{pmatrix} \mathcal{B}^{lmn}_{2,1} \\ \mathcal{B}^{lmn}_{2,2} \\ \mathcal{B}^{lmn}_{2,3} \\ \mathcal{B}^{lmn}_{2,4} \end{pmatrix}. \tag{3.79}$$

The corresponding matrix elements have already been given in (2.89) and (2.90).

Proton decay matrix elements.

As for the next-to-leading twist constants the operators in (2.108) and (2.109) are irreducible and can be written immediately as

$$\mathcal{U} = - \begin{pmatrix} \sqrt{2}\, \mathcal{B}^{lmn}_{3,1} \\ \sqrt{2}\, \mathcal{B}^{lmn}_{3,2} \\ \sqrt{2/3}\, \left(\mathcal{B}^{lmn}_{1,3} - \mathcal{B}^{lmn}_{2,3} \right) \\ \sqrt{2/3}\, \left(\mathcal{B}^{lmn}_{1,4} - \mathcal{B}^{lmn}_{2,4} \right) \end{pmatrix}, \quad \mathcal{W} = \begin{pmatrix} \sqrt{2/3}\, \left(\mathcal{B}^{lmn}_{1,1} - \mathcal{B}^{lmn}_{2,1} \right) \\ \sqrt{2/3}\, \left(\mathcal{B}^{lmn}_{1,2} - \mathcal{B}^{lmn}_{2,2} \right) \\ \sqrt{2}\, \mathcal{B}^{lmn}_{3,3} \\ \sqrt{2}\, \mathcal{B}^{lmn}_{3,4} \end{pmatrix} \tag{3.80}$$

with the corresponding matrix elements already given in eqs. (2.110) and (2.111).

CHAPTER 4

Renormalisation

In this chapter we are going to discuss one of the essential steps in quantum field theory calculations, the renormalisation. In section 3.11 we have introduced the full set of operators we are going to use in our numerical calculations. However, the matrix elements calculated on the lattice are bare and have to be renormalised to get physical results. Therefore, in this chapter, we will sketch the general renormalisation procedure for our case to obtain renormalisation matrices to translate the bare lattice results to modified minimal substraction renormalisation scheme $\overline{MS}$, widely used in phenomenological calculations. As at the present this is a work in progress [131, 132] we can present here only some preliminary results for our special case. For the details of the renormalisation procedure and the general final numerical results we would like to refer the reader to the future work [131, 132]. Here we describe only the basic steps of this renormalisation procedure.

Our results are not directly comparable with experiment and must be combined with other phenomenological calculations in order to obtain quantities like the electromagnetic nucleon formfactors. Therefore we have to provide our final results also in the $\overline{MS}$ renormalisation scheme so that the perturbative and non-perturbative results can be combined. However, while on the lattice the regularisation is provided by the finite lattice spacing, the $\overline{MS}$ renormalisation scheme uses dimensional regularisation, where the four dimensions of space-time are reduced to $4 - \epsilon$ dimensions. Thus, due to this "incompatibility", as $\overline{MS}$ is only applicable in continuum, it is not possible to renormalise the lattice results using the $\overline{MS}$ renormalisation scheme.

This problem can be solved by an intermediate calculation step. One needs

a renormalisation procedure which is applicable on the lattice as well as in continuum. As our results are calculated nonperturbatively, we prefer to use also a nonperturbative renormalisation procedure. For two-quark operators such a nonperturbative scheme was proposed in [133] and is known as RI′-MOM renormalisation scheme. This scheme can be also applied to the case of three-quark operators but needs to be modified in some points. Thus the renormalisation procedure, as required here, will involve three main steps:

- Calculation[1] of lattice regularised amputated four-point functions $\Gamma_i^{\rm latt}$ numerically on the lattice.
- Calculation of the renormalisation matrices in the RI′-MOM scheme using $\Gamma_i^{\rm RI'} = Z_{ij}^{\rm RI'}\Gamma_j^{\rm latt}$.
- Scheme matching of the RI′-MOM renormalisation scheme to the continuum $\overline{MS}$ renormalisation scheme so that the results in the intermediate $RI-MOM$ scheme can be used in the continuum perturbation theory.

Let us now elaborate on these three main parts.

lattice calculation

The first step in the renormalisation procedure is the calculation of a four-point function with three quarks at different positions as sources and one three-quark sink. The calculation is greatly improved by performing it in momentum space [134]. Therefore, one imposes fixed momenta on incoming quarks . The resulting four point correlation function is then of the type

$$\begin{aligned} C(p_1,p_2,p_3)^{(i)}_{\alpha\beta\gamma} = \int \mathrm{d}x\,\mathrm{d}z_1\,\mathrm{d}z_2\,\mathrm{d}z_3\; e^{-i\sum_{i=1}^3 p_i x} e^{i\sum_{i=1}^3 p_i z_i} \\ \cdot\,\epsilon^{abc}\langle 0|\bar{u}^a_\alpha(z_1)\bar{u}^b_\beta(z_2)\bar{d}^c_\gamma(z_3)\mathcal{O}_i(x)|0\rangle \end{aligned} \tag{4.1}$$

with $q(z_i)$ being the quark sources at z_i and $\mathcal{O}_i$ the three-quark sink at x. The lattice regularised amputated "three-quark vertex" $\Gamma_i^{\rm latt}$ is then obtained from $C^{(i)}$ by multiplying the four-point function with the inverse propagator in momentum space

$$\Gamma_i^{\rm latt}(p_1,p_2,p_3)_{\alpha\beta\gamma} = D(p_1)_{\alpha\alpha'}D(p_2)_{\beta\beta'}D(p_3)_{\gamma\gamma'}C(p_1,p_2,p_3)^{(i)}_{\alpha'\beta'\gamma'} \tag{4.2}$$

[1] Although the correlators are based on the same operators as used in our calculation, the calculation procedure required here differs very strongly.

RI′-MOM scheme renormalisation

In the next step the lattice regularised bare operators are renormalised using the RI′-MOM scheme. In general a renormalised "three-quark vertex" is obtained from the bare one by the relation

$$\Gamma_i^{\mathrm{ren}} = Z_{ij}\Gamma_j \tag{4.3}$$

where Z_{ij} is the renormalisation matrix and in the case of non-vanishing off-diagonal elements therein we have operator mixing. In the RI′-MOM scheme one introduces a set of projectors P_k such that for the "three-quark vertex" at the tree-level Γ^{tree} the relation

$$P_k\Gamma_i^{\mathrm{tree}}\left(p_1,p_2,p_3\right) = \delta_{ki} \tag{4.4}$$

holds. Then the renormalisation condition in the RI′-MOM scheme can be formulated as

$$P_k\Gamma_i^{\mathrm{RI'}}(p_1,p_2,p_3;\mu)|_{\mu^2=\sum_i p_i^2/3} = \delta_{ki}. \tag{4.5}$$

Using the relation

$$\Gamma_i^{\mathrm{RI'}} = Z_{ij}^{\mathrm{RI'}}\Gamma_j^{\mathrm{latt}} \tag{4.6}$$

we can extract the renormalisation matrix in RI′-MOM renormalisation scheme at scale μ by

$$\left(Z^{\mathrm{RI'}}\right)_{ij}^{-1}(\mu) = P_j\Gamma_i^{\mathrm{latt}}(p_1,p_2,p_3)|_{\mu^2=\sum_i p_i^2/3}. \tag{4.7}$$

scheme Matching to $\overline{MS}$

The last task in this renormalisation procedure requires the determination of so-called scheme matching matrix $Z^{\overline{MS}\leftarrow\mathrm{RI'}}$ which relates the $\overline{MS}$ and the RI′-MOM renormalisation schemes

$$Z^{\overline{MS}\leftarrow\mathrm{RI'}} = Z^{\overline{MS}}\left(Z^{\mathrm{RI'}}\right)^{-1}. \tag{4.8}$$

Therefore $Z^{\overline{MS}}$ and $Z^{\mathrm{RI'}}$ are calculated in continuum perturbation theory by expanding in strong coupling constant and applying dimensional regularisation in both cases. The scheme matching matrix is then found by comparing the expansion coefficients. The final physical results are obtained by the evolution to e.g., $2\,\mathrm{GeV}$ and in principle should not depend on the scale at which the values were initially calculated. However, due to the truncation of the perturbative expansion as well as statistical and systematical errors on the lattice this cannot be exactly fullfiled. Therefore, a good estimate for the systematic uncertainty of the renormalisation matrices can be obtained from the variation of the initial scale $\mu^2 = \sum_i p_i^2/3$ on the lattice and comparing the different results then in $\overline{MS}$ scheme.

CHAPTER 5

Main Results

5.1 General Discussion

As already anticipated we can reduce the statistical noise by combining different momenta and/or different operators. However, the use of different momenta for the calculation of the general three-quark operator turned out to be too expensive. Hence the general correlators (3.59), and therefore also the correlators for distribution amplitude operators, were evaluated only at a minimal set of momenta. To extract the nucleon wave function normalisation constant f_N we have fitted the correlator

$$C_0^{000} = \frac{1}{2}(C_{B,0}^{000} + C_{C,0}^{000}) \tag{5.1}$$

where we have averaged over the two possible correlators at $\vec{p} = \vec{0}$. Similarly for the first moments we have used

$$C_1^{lmn} = \frac{1}{3}\left(C_{A,1}^{lmn} + C_{B,1}^{lmn} + C_{C,1}^{lmn}\right), \tag{5.2}$$

with $l + m + n = 1$ and $\vec{p} = (2\pi/L, 0, 0)$, where L is the spatial extent of our lattice. For the second moment we have only one correlator, hence no averaging is possible and we have evaluated it for $\vec{p} = (0, 2\pi/L, 2\pi/L)$.

To determine the normalisation constant $Z_N(\vec{p})$ we had also to evaluate the usual nucleon correlator. As the additional smearing on the sink introduces additional noise, in particular for $\vec{p} \neq \vec{0}$, we have improved our statistics by using different momenta in the nucleon correlator. For the $16^3 \times 32$ lattices we have

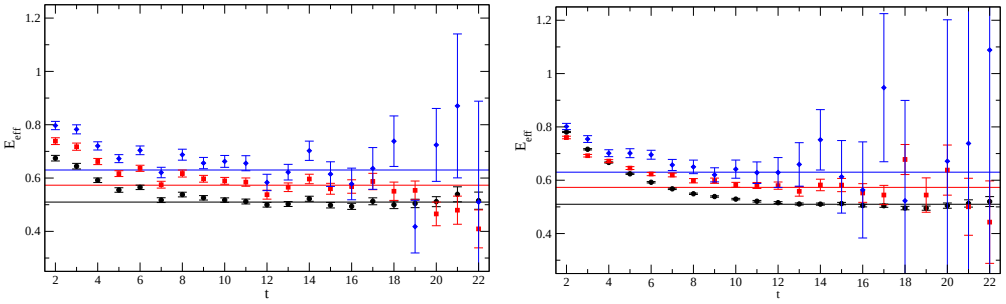

(a) (b)

Figure 5.1: Effective mass plots for the nucleon correlator (a) and the average of the distribution amplitude correlators (b) for different nucleon momenta at $\beta = 5.40$ and $\kappa = 0.13610$. The black dots were obtained at zero nucleon momentum, the red squares and blue diamonds correspond to $\vec{p}^2 = (2\pi/L)^2$ and $\vec{p}^2 = 2(2\pi/L)^2$ respectively. The lowest black straight line corresponds to the effective mass as obtained by the QCDSF collaboration. The middle red and the top blue line correspond to energies $E^2 = m^2 + \vec{p}^2$ with $\vec{p}^2 = (2\pi/L)^2$ and $\vec{p}^2 = 2(2\pi/L)^2$, respectively, obtained from QCDSF nucleon masses.

worked with

$$C_N^1 = \frac{1}{3}\left(C_N(2\pi/L,0,0) + C_N(0,2\pi/L,0) + C_N(0,0,2\pi/L)\right) \tag{5.3}$$

and

$$C_N^2 = \frac{1}{3}\left(C_N(0,2\pi/L,2\pi/L) + C_N(2\pi/L,0,2\pi/L) + C_N(2\pi/L,2\pi/L,0)\right), \tag{5.4}$$

while for the $24^3 \times 48$ lattices we have used a larger number of different momenta:

$$C_N^1 = \frac{1}{3}\left(C_N(2\pi/L,0,0) + C_N(0,2\pi/L,0) + C_N(0,0,2\pi/L)\right) \tag{5.5}$$

$$\begin{aligned} C_N^2 = \frac{1}{6}\big(&C_N(0,2\pi/L,2\pi/L) + C_N(0,-2\pi/L,2\pi/L) \\ &+ C_N(2\pi/L,0,2\pi/L) + C_N(2\pi/L,0,-2\pi/L) \\ &+ C_N(2\pi/L,2\pi/L,0) + C_N(2\pi/L,-2\pi/L,0)\big). \end{aligned} \tag{5.6}$$

As already mentioned, the location of the effective mass plateaus for the nucleon correlator and the distribution amplitude correlators (and also the "GUT correlators") is different as exemplified in Figure 5.1. Thus, instead of calculating the ratios of the correlators we perform a joint fit. As all correlators are evaluated on the same gauge configuration we should also take into account all possible

statistical correlations. We have employed two different fitting procedures with different possibilities for incorporating the correlations:

PC: The first possibility is to fit every moment of the distribution amplitude separately, e.g., for $f_N\phi^{100}$ we fit the correlators C_1^{100} and C_N^1 simultaneously and incorporate the cross-correlations of both correlators and those between different time slices. However since we want to extract ϕ^{100} and not $f_N\phi^{100}$ we should in principle also consider the cross-correlation with C^{000}. Due to the omission of such additional cross-correlations we call this procedure "Partially Correlated".

FC: For the second possibility we have estimated the full cross-correlation matrix and therefore call it here "Fully Correlated". In this case we take into account all cross-correlations fitting simultaneously the correlators for the zeroth, first and second moment as well as the nucleon correlator for the corresponding momentum.

Both methods have intrinsic disadvantages. In order to extract the moments we have to perform multi-parameter fits which involve nucleon mass, different normalisation constants and the wanted moments. The second disadvantage is the required knowledge of the smeared-smeared nucleon correlator for non-zero spatial momenta which introduces an additional source for statistical noise. This problem can be avoided if we consider the ratios of the nucleon distribution amplitude correlators, which are equal to ratios of moments:

$$l{+}m+n=1:$$
$$R^{lmn}=\frac{\phi^{lmn}}{S^1},\quad S^1=\phi^{100}+\phi^{010}+\phi^{001}, \tag{5.7}$$
$$l{+}m+n=2:$$
$$R^{lmn}=\frac{\phi^{lmn}}{S^2},\quad S^2=2(\phi^{011}+\phi^{101}+\phi^{110})+\phi^{200}+\phi^{020}+\phi^{002}. \tag{5.8}$$

The disadvantage of this approach is that we lose the information about the absolute normalisation of the moments and therefore only ratios can be extracted using this method. Thus, we need a criterion to determine the absolute normalisation of moments ϕ^{lmn} with $l+m+n\geq 1$. This can be achieved by using the constraint from (2.71), explicitly requiring e.g., for the first moments that

$$\sum_i^3 \phi_i^{\mathrm{lat}}=\frac{1}{\sum_{ij}^3 Z_{ij}R_j} \tag{5.9}$$

with

$$\phi_1^{\mathrm{lat}}:=\phi^{100},\quad \phi_2^{\mathrm{lat}}:=\phi^{020},\quad \phi_3^{\mathrm{lat}}:=\phi^{001},\quad R_i=\frac{\phi_i^{\mathrm{lat}}}{\sum_k^3\phi_k^{\mathrm{lat}}}, \tag{5.10}$$

β	κ	m_π[GeV]	volume	a[fm]	L[fm]
5.29	0.1340, 0.1350, 0.1359	1.411, 1.029, 0.587	$16^3 \times 32$	0.08	1.28
5.29	0.1355, 0.1359, 0.1362	0.800, 0.587, 0.383	$24^3 \times 48$	0.08	1.92
5.40	0.135, 1356, 0.1361, 0.13625, 13640	1.183, 0.856, 0.648, 0.559, 0.421	$24^3 \times 48$	0.07	1.68

Table 5.1: Overview of sets of lattice ensembles used in our computations.

where $\phi_i^{\rm lat}$ are the bare numbers on the lattice. In fact the "disadvantage" of this approach turned now effectively to an "advantage" as the constraint in (2.71) is fullfilled now exactly. As we are using explicitly one of many constraints we call this analysis method "partially constrained". The calculation of the ratios R^{lmn} also does not have the other disadvantages of the methods mentioned before as we have to fit only a constant term for R^{lmn}. Furthermore, the ratios exhibit a much better behaviour as the plateaus are less noisier and wider. However, this method is only applicable to higher moments. The normalisation constants f_N, α, β and λ_i must be determined using the methods mentioned before. The scetched "partially constrained" method can be extended further to the "fully constrained" by incorporating also the constraints for individual moments in eq. (2.71).

For our numerical results we have evaluated our correlators using the **QCDSF/ UKQCD/DIK** configurations generated with two flavours of clover fermions at two different β values summarised in Table 5.1. For $\beta = 5.29$ we have used two different lattice sizes $24^3 \times 48$ and $16^3 \times 32$ each at three different quark masses. For $\beta = 5.40$ we have evaluated the correlators at five different quark masses on $24^3 \times 48$ lattices. Additionally we have performed a partially quenched analysis where for the valence and see quarks one uses different κ values which correspond to different quark masses. Although the present data are fully consistent with the unquenched results we did not included these values in our final analysis as the theoretical status is uncertain and the values are still preliminary. However, in some of our plots we will show also these additional results to illustrate the agreement with the unquenched results.

To set the scale on the lattice we have used for the Sommer parameter the value $r_0 = 0.467\,\mathrm{fm}$. As far as it was possible we have also checked that the dependence of the final results on the fitting procedures (PC, FC) is only very mild and the deviations are consistent with the present statistical errors.

The lattice results are obtained at non-physical quark masses and we have to extrapolate them to the physical point. To our knowledge there are no calculations in chiral perturbation theory to guide our extrapolation. Therefore we rely on the behaviour of our data and extrapolate them linearly to the physical pion mass. To

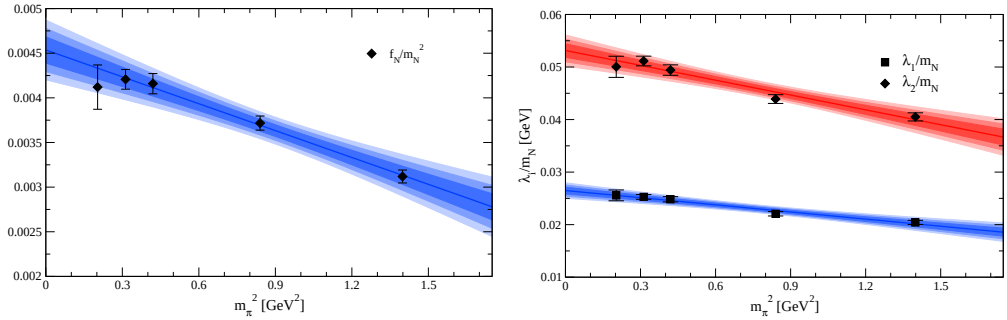

(a) (b)

Figure 5.2: Chiral extrapolation of f_N/m_N^2 (a) and λ_i/m_N (b) obtained from FC fitting procedure. The additional red point at $\approx 1.2\mathrm{GeV}^2$ denotes the partially quenched results which were not included in the fit. To demonstrate the associated uncertainties we show additionally for all fits the one, two and three sigma error bands.

estimate the uncertainty of such a chiral extrapolation we perform also a quadratic extrapolation of our data. These values are used to estimate the systematic uncertainty from the difference of the renormalised values from the quadratic and linear extrapolation procedure.

All operators used in our calculation require renormalisation. Although we have used operators with good mixing properties we still have to take into account the remaining operator mixings. The renormalisation matrices for the irreducible multiplets of three-quark operators were worked out in [132]. We have used them to translate our values into the $\overline{\mathrm{MS}}$ renormalisation scheme at $\mu = 2\,\mathrm{GeV}$. The corresponding raw lattice results and some additional bare asymmetries can be found in Appendix C. The systematic uncertainty of the renormalisation was estimated by variying the renormalisation scale μ^2 in the RI′-MOM scheme by a factor of two in the range $10\,\mathrm{GeV}^2$ to $40\,\mathrm{GeV}^2$ around the central value of $20\,\mathrm{GeV}^2$, which was used to obtain our renormalised results.

5.2 Unconstrained Analysis

5.2.1 Normalisation constants

First, we present in Table 5.2 on p. 77 the results for the different constants which are associated with operators without derivatives: the nucleon wave function normalisation constant f_N, the next-to-leading twist normalisation constants λ_1 and λ_2 and the GUT related constants α and β. It is particularly important to determine

β	5.40	5.29
$f_N/m_N^2 \cdot 10^3$	3.486(60)(56)(60)	3.290(62)(100)(72)
$-\lambda_1/m_N \cdot 10^3[\mathrm{GeV}]$	18.06(29)(86)(49)	18.33(32)(89)(57)
$-\lambda_1 \cdot 10^3[\mathrm{GeV}^2]$	22.15(42)(129)(60)	23.32(46)(60)(73)
$\lambda_2/m_N \cdot 10^3[\mathrm{GeV}]$	35.63(58)(176)(97)	36.48(65)(201)(113)
$\lambda_2 \cdot 10^3[\mathrm{GeV}^2]$	43.79(84)(267)(119)	46.72(93)(111)(144)
$-\alpha/m_N^2 \cdot 10^3[\mathrm{GeV}]$	11.43(26)(84)(18)	11.32(27)(27)(21)
$-\alpha \cdot 10^3[\mathrm{GeV}^3]$	15.16(49)(108)(22)	15.40(52)(30)(30)
$\beta/m_N^2 \cdot 10^3[\mathrm{GeV}]$	10.27(26)(35)(23)	10.37(29)(15)(28)
$\beta \cdot 10^3[\mathrm{GeV}^3]$	13.14(50)(350)(30)	14.20(57)(21)(38)
ϕ^{100}	0.3457(75)(89)(3)	0.3530(62)(132)(7)
ϕ^{010}	0.3124(81)(128)(4)	0.3176(62)(108)(2)
ϕ^{001}	0.3142(77)(100)(4)	0.3283(62)(68)(4)
ϕ^{011}	0.0823(73)(266)(51)	0.0835(61)(1)(50)
ϕ^{101}	0.1105(92)(254)(51)	0.1003(66)(178)(61)
ϕ^{110}	0.1035(67)(9)(11)	0.0962(54)(6)(7)
ϕ^{200}	0.1556(107)(705)(143)	0.1673(87)(219)(128)
ϕ^{020}	0.1300(98)(151)(112)	0.1308(80)(2)(89)
ϕ^{002}	0.1430(100)(48)(141)	0.1506(85)(39)(124)

Table 5.2: Chirally extrapolated lattice results from FC analysis for normalisation constants and ϕ^{lmn} at $\beta = 5.40$ and $\beta = 5.29$ in $\overline{\mathrm{MS}}$ renormalisation scheme at $\mu = 2\,\mathrm{GeV}$. The first error is the combined statistical error of the moments and renormalisation matrices mainly dominated by the statistical uncertainties of the moments. The second (third) errors are the systematic uncertainties due to the chiral extrapolation (renormalisation) estimated as explained in text.

the constant f_N to high accuracy so that the determination of higher moments of the leading-twist distribution amplitude will not be disturbed by its uncertainty.

For the GUT related constants we observe $\alpha + \beta \approx 0$ as in [135]. This is expected because of the relation

$$(\alpha + \beta)\, N(p) = -\langle 0|\epsilon^{abc}(u^{aT} C d^b)\gamma_5 u^c|p\rangle, \tag{5.11}$$

since the matrix element on the right hand side vanishes in the non-relativistic limit and is known to be small at small quark masses [136]. Furthermore we

β	5.40	5.29
$f_N/m_N^2 \cdot 10^3$	$3.672(78)(90)(63)$	$3.538(79)(283)(77)$
$-\lambda_1/m_N \cdot 10^3[\mathrm{GeV}]$	$18.75(36)(38)(51)$	$20.03(41(140)(62)$
$\lambda_2/m_N \cdot 10^3[\mathrm{GeV}]$	$36.85(76)(8)(100)$	$38.62(95)(285)(116)$
φ^{100}	$0.3871(313)(528)(4)$	$0.3903(204)(464)(12)$
φ^{010}	$0.3150(226)(290)(720)$	$0.3298(159)(118)(608)$
φ^{001}	$0.3155(272)(453)(2)$	$0.3277(190)(270)(5)$
φ^{011}	$0.0697(181)(128)(98)$	$0.0813(137)(104)(97)$
φ^{101}	$0.1074(112)(141)(56)$	$0.1160(105)(169)(57)$
φ^{110}	$0.1248(178)(88)(32)$	$0.1052(137)(100)(42)$
φ^{200}	$0.1915(252)(951)(151)$	$0.1742(186)(574)(134)$
φ^{020}	$0.1308(150)(109)(122)$	$0.1292(119)(81)(87)$
φ^{002}	$0.1390(235)(373)(149)$	$0.1280(194)(295)(121)$

Table 5.3: Chirally extrapolated PC results for different φ^{lmn} moments at $\beta = 5.40$ and $\beta = 5.20$ in $\overline{\mathrm{MS}}$ renormalisation scheme at $2\,\mathrm{GeV}$. The first error is the combined statistical error of the moments and renormalisation matrices mainly dominated by the statistical uncertainties of the moments. The second (third) errors are the systematic uncertainties due to the chiral extrapolation (renormalisation) estimated as explained in text.

confirm also the relative signs of f_N, λ_1 and λ_2 calculated in [50, 137]. Due to Fierz identities

$$\begin{aligned}
&\epsilon^{abc}\left[u^{aT}(0)C\gamma^{\mu}u^{b}(0)\right](\gamma_5\gamma_{\mu}d^{c}(0))_{\tau} \\
&\quad = 2\epsilon^{abc}\left(\left[u^{aT}(0)Cd^{b}(0)\right](\gamma_5 u^{c}(0))_{\tau} - \left[u^{aT}(0)C\gamma_5 d^{b}(0)\right]u^{c}(0)_{\tau}\right), \quad (5.12)\\
&\epsilon^{abc}\left[u^{aT}(0)C\sigma^{\mu\nu}u^{b}(0)\right](\gamma_5\sigma_{\mu\nu}d^{c}(0))_{\tau} \\
&\quad = 4\epsilon^{abc}\left(\left[u^{aT}(0)Cd^{b}(0)\right](\gamma_5 u^{c}(0))_{\tau} + \left[u^{aT}(0)C\gamma_5 d^{b}(0)\right]u^{c}(0)_{\tau}\right), \quad (5.13)
\end{aligned}$$

we have for the next-to-leading twist constants the relation

$$m_N(2\lambda_1+\lambda_2)N(p) = 8\langle 0|\epsilon^{abc}\left(u^{aT}Cd^{b}\right)\gamma_5 u^{c}|p\rangle, \quad (5.14)$$

therefore also observing $2\lambda_1 \approx -\lambda_2$.

As already mentioned, at present there are no results from chiral perturbation theory to guide our chiral extrapolation. Therefore, we have relied on the behaviour of our data as function of the quark mass. The nucleon wave function

normalisation constant f_N exhibited a clear non-linear behaviour. However, it turned out that the dimensionless ratio f_N/m_N^2 is much better suited for the linear extrapolation (cf., Figure 5.2(a)) and it has the additional advantage that it does not suffer from the uncertainty in setting the scale on the lattice. The chiral behaviour of λ_1 and λ_2 is less certain and we have performed two different chiral extrapolations for these quantities. We have extrapolated the constants λ_i and also the ratios λ_i/m_N linearly to physical quark masses. The ratios λ_i/m_N seems to be favoured by the linear fit, and we will use these values as our final results.

Very often one is interested in different combinations of moments presented in Table 5.3 on p. 78. These were determined using the PC fitting procedure. Therefore we had also to evaluate f_N using the PC fitting procedure. Due to the correlators of higher moments, in the FC fitting procedure the nucleon mass is slightly higher than for the zeroth moment correlators only. Therefore, the values for normalisation constant(s) obtained from FC fitting procedure are in general lower by $\approx 4\%$ indicating systematic uncertainties due to discretisation, the finite size of the lattice, contributions from excited states and the uncertainty to determine the position of the effective mass plateaus for higher moments.

5.2.2 Higher Moments

As expected, the non-zero spatial momenta make the results for the first moments (presented in the $\overline{\text{MS}}$ scheme in Table 5.2 on p. 77) noisier than for operators without derivatives. However, we can extrapolate the numbers linearly to the chiral limit (cf., 5.3) and the obtained results are consistent with sum rule calculations and phenomelogical estimates [47, 65, 50, 52]. Additionally we have checked the quality of our results by comparing them with the constraint from eq. (2.71) which is fullfilled very well within the errors (cf. Figure 5.4).

The renormalised results for the moments ϕ^{100}, ϕ^{010} and ϕ^{001} show clearly the deviation from the asymptotic case $\phi(x_i) = 120 x_1 x_2 x_3 f_N$ with $\phi^{100} = \phi^{010} = \phi^{001} = 1/3$. As the relative differences of these moments describe a deviation from the symmetric case, they are of particular interest in phenomenological applications. Thus, we have also evaluated additionally those combinations of moments in the chiral limit which were obtained from partially correlated values. The bare lattice values are given in Appendix C, while in Table 5.3 on p. 78 we present some combinations in the $\overline{\text{MS}}$ renormalisation scheme. The strongest asymmetry is the $\phi^{100} - \phi^{010}$ (see the raw lattice results in Appendix C). However, the large statistical errors reduce the reliability of the chiral extrapolation as seen in Figure 5.3(a) leading to large uncertainties for the final values. Therefore we will consider these interesting quntities using a better analysis method.

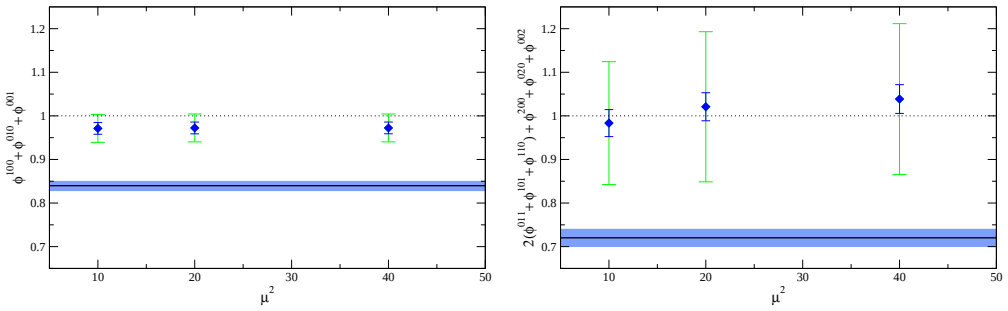

(a) (b)

Figure 5.4: The bare (solid black line with statistical error band) and renormalised (blue diamonds) sum of the first moments (a) and second moments (b) according to eq. (2.72) as obtained from FC analysis. The smaller errors for the renormalised values are purely statistical, while the larger are the sum of the statistical and systematical error due to chiral extrapolation. The three different points were obtained from three different renormalisation scales μ in the RI′-MOM scheme to estimate the systematic uncertainty due to the renormalisation as explained in text. The theoretical constraints that the sums should be exactly one are fulfilled very well in both cases.

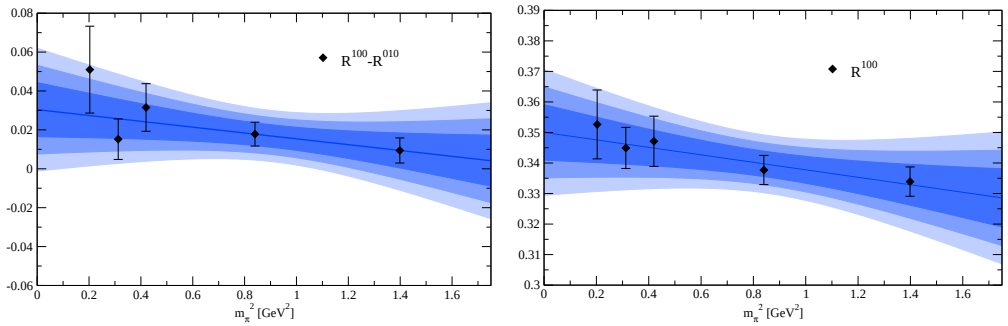

(a) (b)

Figure 5.3: Chiral extrapolation of $R^{100} - R^{010}$ asymmetries (a) from PC results and R^{100} ratio (b) from FC results. Additionally one, two and three sigma error bands are presented.

Although the calculation of the second moments requires spatial momenta with two non-zero components and the number of available operators is reduced to one, we could extract the different moments with reasonably small statistical errors. Thus, the chiral extrapolation of moments (cf., Figure 5.5) has a reasonable accuracy. However, as in the case of the first moments we give also the differ-

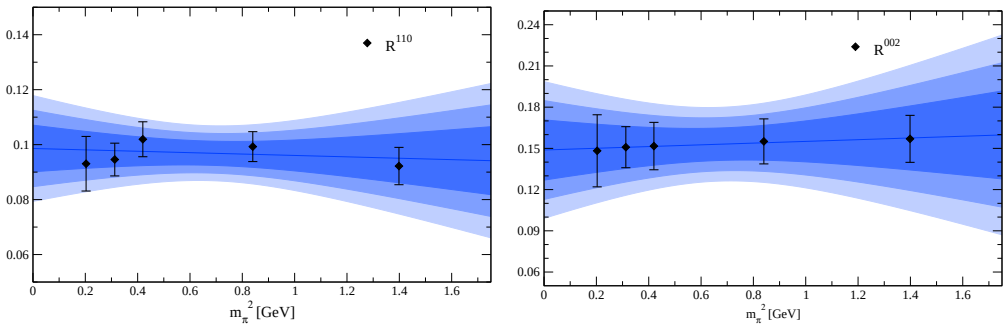

(a) (b)

Figure 5.5: FC results for R^{110} (a) and $R002$ (b) linearly extrapolated to the chiral limit with the corresponding one, two and three sigma error bands of the fits.

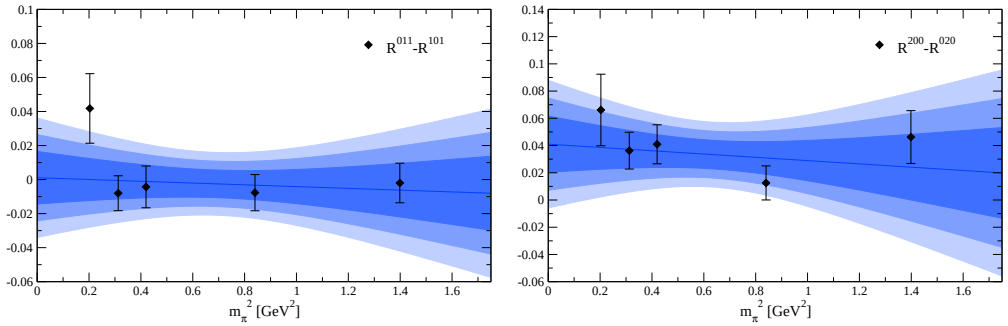

(a) (b)

Figure 5.6: PC results for $(R^{011} - R^{101})$ (a) and $(R^{200} - R^{020})$ (b) asymmetries linearly extrapolated to the chiral limit with the corresponding one, two and three sigma error bands of the fits.

ences of the second moments for raw results in Appendix C to illustrate the deviation from the symmetric asymptotic behaviour with $\phi^{200} = \phi^{020} = \phi^{002} = 1/7$ and $\phi^{011} = \phi^{101} = \phi^{110} = 2/21$. Although the chiral extrapolation gives some evidences for asymmetries the statistical errors of this analysis method do not allow us to estimate those with good quality.

5.3 Constrained Analysis of Higher Moments

5.3.1 Partially Constrained Analysis

In the last section we have seen that the unconstrained analysis of our data gives us consistent results. However, better estimates of moments and in particular of asymmetries are preferable. As already mentioned this can be achieved by overcoming the disadvantages of the previous analysis method by calculating the correlator ratios which are equivalent to the ratios of moments in eqs. (5.7) and (5.8)

$$l+m+n=1: \quad R^{lmn} = \frac{C_1^{lmn}}{C_{S,1}}, C_{S,1} = C_1^{100} + C_1^{010} + C_1^{001} \tag{5.15}$$

$$l+m+n=2: \quad R^{lmn} = \frac{C_2^{lmn}}{C_{S,2}},$$
$$C_{S,2} = 2(C_2^{011} + C_2^{101} + C_2^{110}) + C_2^{200} + C_2^{020} + C_2^{002}. \tag{5.16}$$

Fitting these ratios to a constant we can reach a much higher precision compared to the method before. In Figure 5.7 we present some of these ratios obtained on one of the ensembles with $\beta = 5.40$. It is obvious that these ratios are better behaved and the plateaus are more pronounced and start at earlier timeslices compared to the case of effective mass plateaus for the correlators in Figure 5.1. Thus, the extracted values for the ratios summarised in Table 5.4 on p. 85 are of higher quality compared to the unconstrained analysis. The main reasons for this improvement are that we do not have to determine the energy $E(\vec{p})$ and normalisation constant $Z_N(\vec{p})$ for non-zero spatial momenta as both drop out in the partially constrained analysis. This reduces also the statistical noise as the nucleon correlator with smeared source and sink is not involved anymore in data analysis. In principle one can calculate similar ratios for correlators involving

$$\varphi^{lmn} = V^{lmn} - A^{lmn}$$

instead of using

$$\phi^{lmn} = (V^{lmn} - A^{lmn} + 2T^{lnm})/3.$$

However this leads to a three times larger statistical error. Therefore the combination ϕ^{lmn} is much better adopted to lattice calculation as it reduces the statistical noise by combining the complete set of leading twist nucleon distribution amplitude operators. Furthermore, due to higher accuracy in the partially constrained analysis we see a deviation from linear behaviour for ϕ^{100} and ϕ^{010} while the chiral extrapolation for other moments is still described by linear fit very well. Therefore, considering φ^{lmn} instead of ϕ^{lmn} will propagate the resulting systematic uncertainty to all moments φ^{lmn} with $l+m+n=1$.

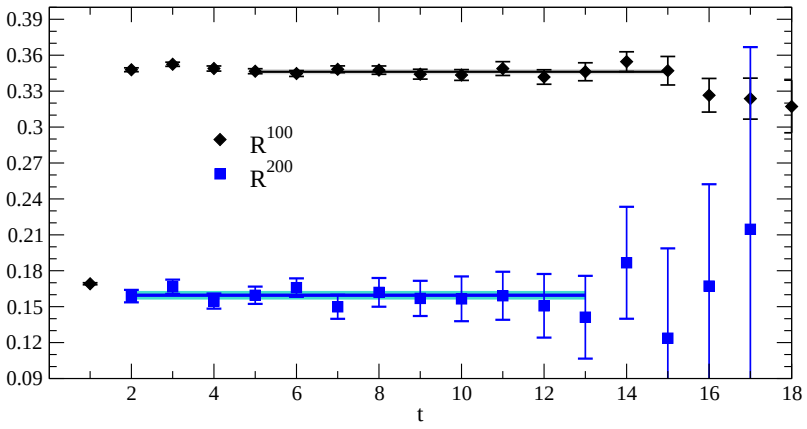

Figure 5.7: Plateaus of correlator ratios R^{100} (black diamonds) and R^{200} (blue squares) for $\beta = 5.40$ and $\kappa = 0.1361$ together with the corresponding fit values and the associated errorbands.

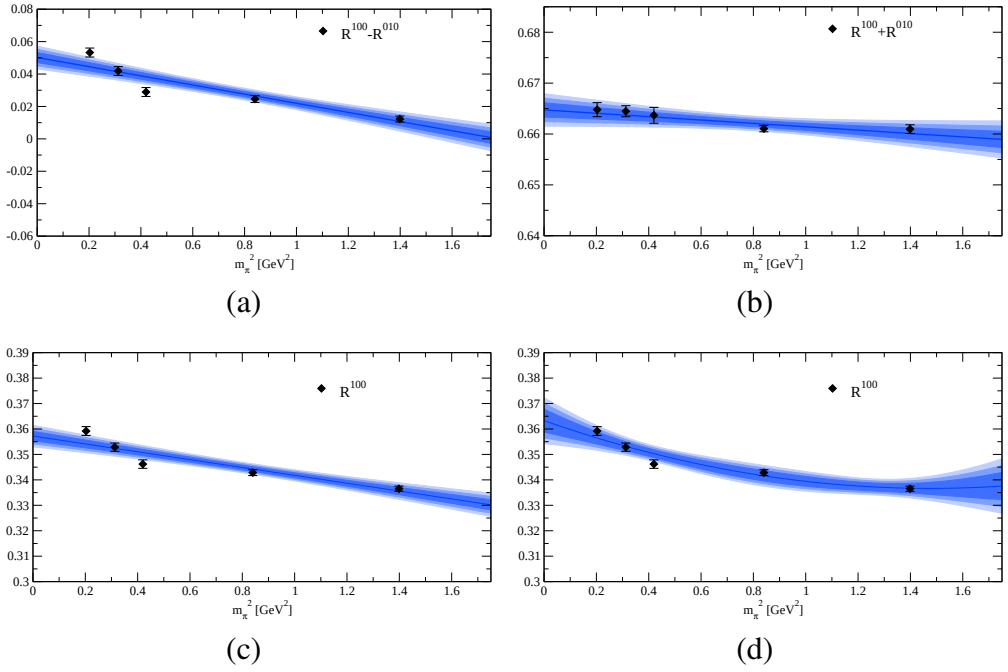

Figure 5.8: Linear chiral extrapolation of $R^{100} - R^{010}$ asymmetry (a) and the $R^{100} + R^{010}$ sum (b). The effect of different chiral extrapolation is demonstrated on the extreme case of R^{100} where in (c) a linear fit is applied and in (d) a quadratic one. All the plots contain also one, two and three sigma error bands of the corresponding fits.

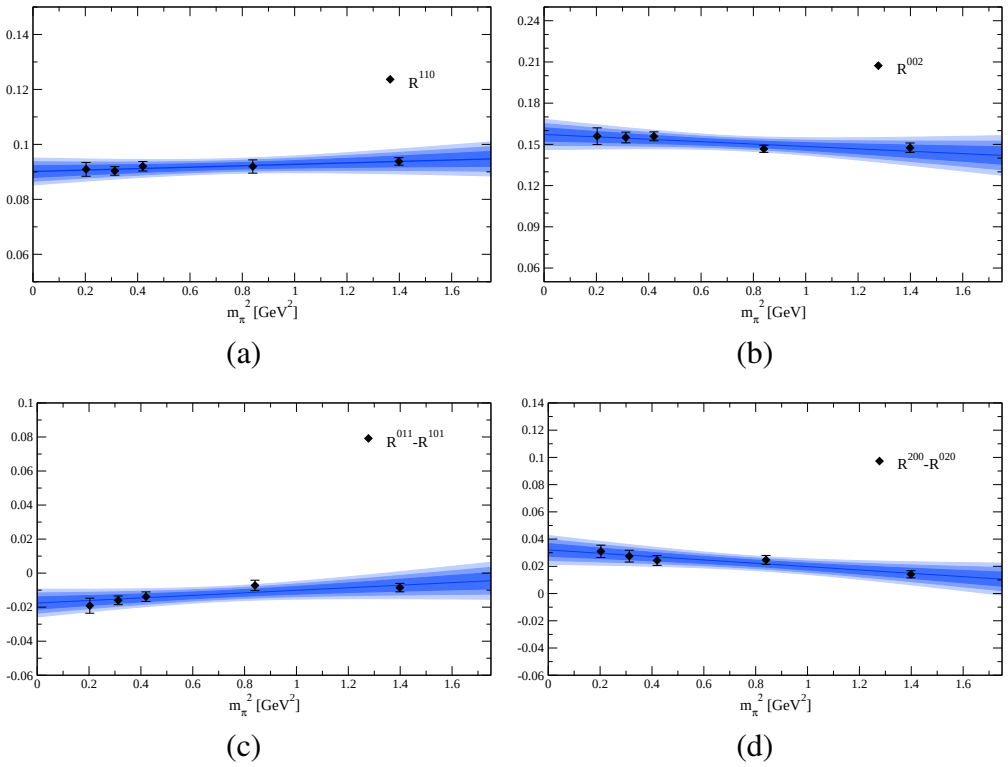

Figure 5.9: Linear chiral extrapolation of second moment ratios R^{110} (a) and R^{002} (b) and of $R^{011} - R^{101}$ (c) and $R^{200} - R^{020}$ (d) asymmetries as obtained from partially constrained analysis with one, two and three sigma error bands of the corresponding fits.

To illustrate the dependence of ϕ^{100} on the pion mass we present in Figs. 5.8(c) and 5.8(d) linear and quadratic chiral extrapolation of this quantity. As ϕ^{010} exhibits similar behaviour, but with inverted slope, the deviation from linear behaviour is emphasised for the $\phi^{100} - \phi^{010}$ asymmetry (Figure 5.8(a)). On the other hand this leads to linear behaviour of $\phi^{100} + \phi^{010}$ (Figure 5.8(b)). Thus, due to momentum conservation one expects also linear behaviour for ϕ^{001}, which is indeed observed in our data. In principle, smaller deviations from linear behaviour are also possible for all other moments. However, the present statistical accuracy does not allow us to resolve such deviations.

β	5.40	5.29
$f_N/m_N^2 \cdot 10^3$	3.573(69)(33)(61)	3.392(68)(178)(74)
$-\lambda_1/m_N \cdot 10^3[\mathrm{GeV}]$	18.35(33)(20)(50)	18.81(36)(123)(59)
$\lambda_2/m_N \cdot 10^3[\mathrm{GeV}]$	36.12(66)(40)(98)	37.29(74)(266)(116)
ϕ^{100}	0.3638(11)(68)(3)	0.3549(11)(61)(2)
ϕ^{010}	0.3023(10)(42)(5)	0.3100(10)(73)(1)
$\phi^{001\star}$	0.3339(9)(26)(2)	0.3351(9)(11)(2)
$\phi^{100} - \phi^{001}$	0.0300(23)(93)(1)	0.0199(23)(46)(4)
$\phi^{001} - \phi^{010}$	0.0313(17)(12)(7)	0.0251(16)(84)(2)
ϕ^{011}	0.0708(18)(82)(77)	0.0848(23)(97)(80)
ϕ^{101}	0.1119(17)(32)(14)	0.1119(23)(2)(28)
$\phi^{110\star}$	0.0920(16)(3)(45)	0.0938(21)(60)(37)
ϕ^{200}	0.1663(28)(7)(81)	0.1539(39)(215)(76)
$\phi^{020\star}$	0.1321(27)(37)(65)	0.1237(32)(45)(47)
ϕ^{002}	0.1521(32)(77)(86)	0.1416(37)(49)(76)
$\phi^{110} - \phi^{011}$	0.0210(27)(78)(32)	0.0074(33)(68)(44)
$\phi^{101} - \phi^{110}$	0.0204(21)(133)(50)	0.0171(29)(82)(56)
$\phi^{200} - \phi^{020}$	0.0323(34)(71)(56)	0.0336(44)(24)(79)
$\phi^{002} - \phi^{020}$	0.0194(24)(32)(42)	0.0171(36)(7)(56)

Table 5.4: The results for ϕ^{lmn} and the relevant asymmetries as obtained from chirally extrapolated ratios R^{lmn} in $\overline{\mathrm{MS}}$ renormalisation scheme at $2\,\mathrm{GeV}$. The values marked by a star were used in the analysis of the corresponding asymmetries to determine the overall normalisation. The first error is the combined statistical error of the moments and renormalisation matrices mainly dominated by the statistical uncertainties of the moments. The second (third) errors are the systematic uncertainties due to the chiral extrapolation (renormalisation) estimated as explained in text.

5.3.2 Fully Constrained Analysis

In the partially constrained analysis method described and applied in the last subsection we have incorporated only the normalisation condition from (2.72) in order to determine the absolute normalisation of the moments, while every ratio was fitted separately like in the partially correlated approach. However, by comparing the partially and fully correlated analysis methods we see that in the latter

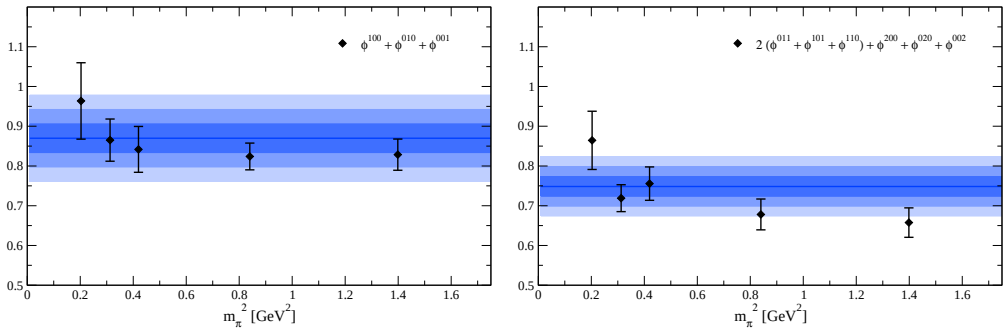

(a) (b)

Figure 5.10: Constant chiral extrapolation of the bare sum of first moments (a) and second moments (b) according to eq. (2.72) as obtained from PC analysis.

case the statistical errors are significantly reduced. Therefore one expects that a similar approach within the constrained analysis should also reduce the statistical errors. Note that in the partially constrained analysis we did not use the additional relation between the individual moments given in eq. (2.71) and the explicit use of these can help even further.

Due to these reasons we performed a similar analysis method as in the the fully correlated case in order to exploit the stronger relation (2.71) explicitly to improve the quality of our results even further. In the following we call this method "fully constrained". Such an approach is in particular useful for second moments as these are notably affected by statistical uncertainties. An additional advantage of this method is that the relations in eq. (2.71) are fulfilled exactly and we only fit a smaller, independent subset of moments, e.g., ϕ^{100}, ϕ^{001} ϕ^{011} , ϕ^{101} and ϕ^{110}. This set of moments does not require the calculation of second order derivatives on the lattice (e.g., for ϕ^{200}) which involve next-to-next neighbour terms. Therefore some of discretisation effects should be suppressed. This is expected as the derivative operator is more local for ϕ^{011} , ϕ^{101} and ϕ^{110}. For the same reasons we think that this method should be the first choice[1] if one calculates in the future the moments ϕ^{lmn} with $l + m + n = 3$ as one can again restrict oneself to the case $l, m, n \leq 2$.

The described analysis method requires the knowledge of the renormalisation matrices at a very early stage as the bare moments do not fulfil any of the relations in eq. (2.71) or eq. (2.71) as displayed in Figure. 5.10. However, the renormalisation matrices have relatively small statistical errors and therefore we do not expect a significant increase of the statistical error due to this additional uncertainty.

On the other hand also the bare ratios of the moments on the lattice sum up ex-

[1]However, we suggest that at the beginning the data should be analysed by the less advanced methods discussed before in order to check the consistency of data and analysis.

actly to one according to eq. (2.72). This implies that one of the ratios is hundred percent correlated to the remainder of the sum and must be omitted in the analyis. Thus in the case of first moments only two independent correlator ratios can be used, while in the case of the second moments we are left with five of six not completely independent correlator ratios. Taking into account all cross-correlation of these seven correlator ratios and fitting those to five independent moments leads to results which are fully consistent with the result from partially constrained analysis. While the resulting values and the errors for the first moments are almost unchanged, the errors for the three independent second moments are slightly increased, which is caused by the cross-correlations of the five correlaor ratios for the second moments. Since in our case we have calculated all moments φ^{lmn} with $l + m + n = 2$ from general correlators, this method does not have strong advantages compared to the "partially constrained" analysis. Thus as we are not forced to restrict ourselve to an inpendent subset of second moments we preferred the "partially constrained" approach so that we could test the reliability of our final results using the eq. (2.71) for individual moments.

5.3.3 Modelling the Nucleon Distribution Amplitude

Although our data do not allow to perform really controlled continuum extrapolation, the fact that $\beta = 5.29$ and $\beta = 5.40$ results are compatible with each other indicate that its effect is small. Thus we take the data from our finer lattice ($\beta = 5.40$) as our final numbers. From the results, presented in the last section, we can construct a model function for the nucleon distribution amplitude $\varphi(x_i, \mu)$ as described Section 2.5.4.

Using the values of ϕ^{100} and ϕ^{001} and the polynomial expansion up to conformal spin $N = 1$ we obtain the form of the nucleon distribution amplitude presented in Figure 5.11(b). Compared to the asymptotic case in Figure 5.11(a), the maximum is considerably shifted. In Figures. 5.11(c) and 5.11(d) we took also into account the second moments and the expansion is up to second conformal spin. As the central values for the moments ϕ^{lmn} with $l + m + n = 2$ do not exactly fullfill the relation in eq. (2.71) the model function is slightly dependent on the choice of ϕ^{lmn} to determine c_n. For the plot in Figure 5.11(c) we have used ϕ^{101}, ϕ^{200} and ϕ^{002} (set 1), while for the plot in Figure 5.11(c) we have incorporated ϕ^{101}, ϕ^{011} and ϕ^{110} (set 2). The effect of second moments is however in both cases the same, the maximum, respectively, the asymmetry is smeared out. While the model function from set 2 exhibits an obvious symmetry in x_1 and x_3, this feature is reduced in the case of set 1. Thus, the present systematic uncertainties allow slightly different model functions. However, the general pattern is preserved in Figures. 5.11(c) and 5.11(d). Let us emphasise at this point again, that the model presented here is not unique and in principle the distribution ampli-

tude can be completely different, as one can construct very different distribution amplitudes with the same set of moments.

To visualise the effect of the statistical error we present in Figure 5.12(a) also the uncertainty of $\varphi(x_i)/f_N$ at $x_3 = 0.5$ as function of x_1. However the deviations are reasonably small and consistent with the statistical errors. Therefore the general pattern in Figure 5.11(c) does not change. The effect of different subset choices is illustrated in Figure 5.12(b) where we plot the difference of $\varphi(x_i)/f_N$ for set 1 and set 2.

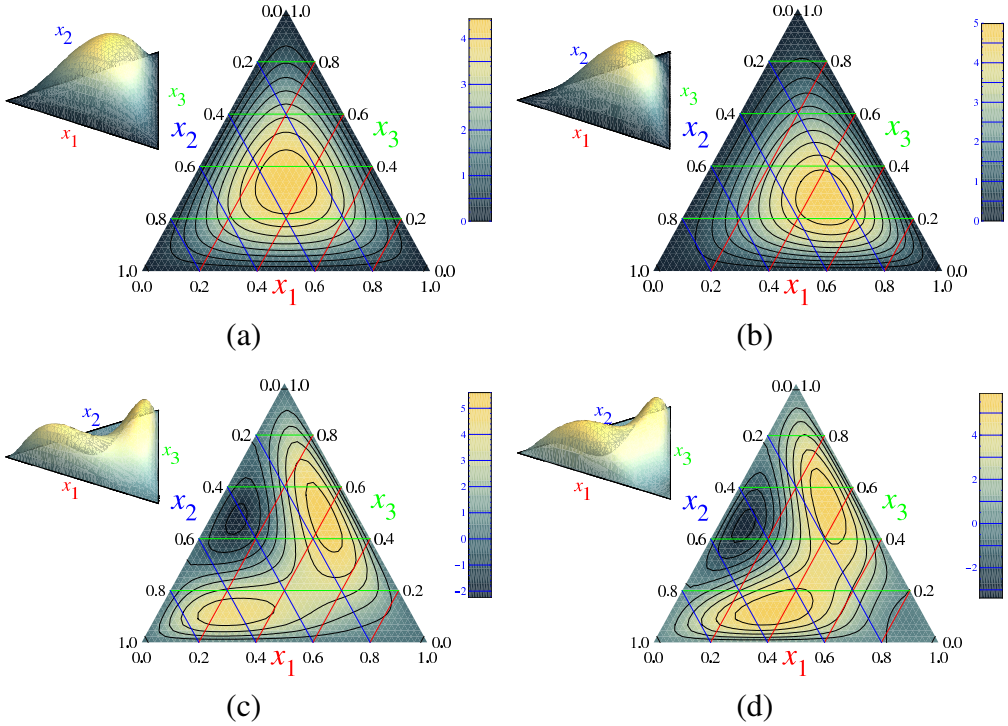

Figure 5.11: Barycentric density plot of the leading-twist distribution amplitude $\varphi(x_1, x_2, x_3)/f_N$ in the limit of $Q^2 \to \infty$ (a) and at $\mu = \mu_0 = 2\,\mathrm{GeV}$ (b-d) using expansion (2.73) as obtained from $\beta = 5.40$ moments presented in Table 5.4. The asymmetry caused by the first moments only $(N = 1)$ is illustrated in (b), while in (c-d) we took into account also the second moments $(N = 2)$. The slight difference of (c) and (d) plots is caused by the different choices of independent sets of momenta for $l + m + n = 2$.

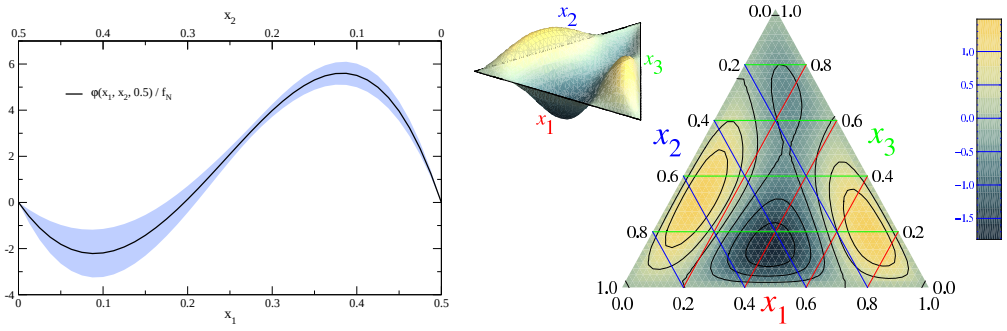

(a) (b)

Figure 5.12: Statistical uncertainty of the model function $\varphi(x_i)/f_N$ for x_1 at $x_3 = 0.5$ (a). Systematic uncertainty due to the choice of the independent subsets of ϕ^{lmn} with $l + m + n = 2$ (b) (for details see text).

5.4 Phenomenological Results

5.4.1 Comparison to Other Estimates

Let us now compare the obtained results with some estimates in the literature. Our results for ϕ^{lmn} imply that $\varphi^{100} \approx 0.4$, $\varphi^{010} \approx 0.3$ and $\varphi^{001} \approx 0.3$ at $1\,\mathrm{GeV}$. These moments can be interpreted as the fraction of momentum carried by the corresponding quarks [46, 47]. As in the QCD sum rule approach we find that the largest fraction of the proton longitudinal momentum is carried by one *up*-quark with spin aligned with the proton spin. However, this asymmetry is not as strong as found in the sum rule calculation. Our results for the first moments are close to phenomenological estimates [52, 138], cf. Table 5.5. On the other hand, our results for φ^{011}, φ^{101} and φ^{110} are similar to the sum rule values, while the asymmetries in the moments φ^{200}, φ^{020} and φ^{002} are clearly smaller. The phenomenological models BK and BLW which are based on experimental data and our lattice results are in good agreement with each other. It is worth to notice that the phenomenological models BLW and BK and as well as our lattice results show an approximate symmetry $\varphi^{lmn} \approx \varphi^{lnm}$.

5.4.2 Light Cone Sum Rule Results

After rescaling our results to $\mu = 1\,\mathrm{GeV}$ by eq. (2.84) and using the light cone sum rule approach discussed in Section 2.5.2 one can determine different nucleon form factors. The nucleon distribution amplitudes, more precisely their moments, provide the principal nonperturbative input to the light cone sum rules. Thus, it

	Asymptotic	QCD-SR	COZ	BK	BLW	Latt.
φ^{100}	$1/3 \approx 0.333$	$0.560(60)$	0.579	$8/21 \approx 0.38$	0.415	$0.3999(13)$
φ^{010}	$1/3 \approx 0.333$	$0.192(12)$	0.192	$13/42 \approx 0.31$	0.285	$0.2986(22)$
φ^{001}	$1/3 \approx 0.333$	$0.229(29)$	0.229	$13/42 \approx 0.31$	0.300	$0.3015(9)$
φ^{200}	$1/7 \approx 0.143$	$0.350(70)$	0.369	$5/28 \approx 0.18^\star$	$0.204^\star$	$0.1832(26)$
φ^{020}	$1/7 \approx 0.143$	$0.084(19)$	0.068	$1/8 \approx 0.13^\star$	$0.107^\star$	$0.1497(67)$
φ^{002}	$1/7 \approx 0.143$	$0.109(19)$	0.089	$1/8 \approx 0.13^\star$	$0.118^\star$	$0.1392(42)$
φ^{011}	$2/21 \approx 0.095$	$-0.030(30)$	0.027	$1/12 \approx 0.08^\star$	$0.075^\star$	$0.0473(55)$
φ^{101}	$2/21 \approx 0.095$	$0.102(12)$	0.113	$17/168 \approx 0.10^\star$	$0.107^\star$	$0.1151(21)$
φ^{110}	$2/21 \approx 0.095$	$0.090(10)$	0.097	$8/21 \approx 0.10^\star$	$0.104^\star$	$0.1016(34)$

Table 5.5: In the following table we compare different estimates for the moments of the leading twist nucleon distribution amplitude $\varphi(x_i)$ at $1\,\mathrm{GeV}$. We show the asymptotic values, the QCD sum rule estimates from [47], the COZ-model [47] based on QCD sum rule results, the BK-model [138], the BLW-model [52] and our lattice values with statitistical errors only. The BK and BLW model do not take into account contributions from next^2-to-leading conformal spin. Thus, the second moments denoted by * do not contain additional information and are fully determined by the first moments.

is essential to have these values with small statistical and systematical errors. At present the light cone sum rule calculations do not include α_s corrections. Thus, only the ratio of normalisation constants f_N and λ_1 and only the first moments were utilised in the calculation of the nucleon form factors and to present accuracy these do not depend on the higher moments. However, we plan to include these corrections in upcoming calculations to investigate the associated effects. Furthermore, the calculation of α_s corrections is work which is currently in progress and should provide us with even more accurate predictions. Unfortunately, at the moment we cannot provide from our lattice results information about first moments of the next-to-leading twist nucleon distribution amplitudes, denoted in the following as f_i^j, where i corresponds to the index of λ_i and j denotes on which quark the derivative acts on (for more details see [50]). For these moments we will use some other estimates from literature and combine them with our results if necessary.

In order to compare our results with other estimates we will use six different sets of moments obtained from

- QCD sum rule estimates (dotted red lines)
- Asymptotic form (dashed red lines)

- BLW model (solid red lines)
- Lattice results plus QCD sum rule estimates for f_i^d (dotted blue lines)
- Lattice results plus asymptotic values for f_i^d (dashed blue lines)
- Lattice results plus BLW estimates for f_i^d (solid blue lines)

	QCD-SR	Asymptotic	BLW	Lattice
$f_N[\mathrm{GeV}^2]$	$5.0 \cdot 10^{-3}$	$5.0 \cdot 10^{-3}(\star)$	$5.0 \cdot 10^{-3}(\star)$	$3.24 \cdot 10^{-3}$
$\lambda_1[\mathrm{GeV}^2]$	$-2.7 \cdot 10^{-2}$	$-2.7 \cdot 10^{-2}(\star)$	$-2.7 \cdot 10^{-2}(\star)$	$-2.01 \cdot 10^{-2}$
$\lambda_2[\mathrm{GeV}^2]$	$5.4 \cdot 10^{-2}$	$5.4 \cdot 10^{-2}(\star)$	$5.4 \cdot 10^{-2}(\star)$	$3.96 \cdot 10^{-2}$
$A_1^u \equiv 2A^{010}$	0.38	0.0	0.13	0.102
$V_1^d \equiv V^{001}$	0.23	$1/3$	0.30	0.301
f_1^d	0.40	0.30	0.33	–
f_1^u	0.07	0.10	0.09	–
f_2^d	0.22	$4/15$	0.25	–

Table 5.6: Parameter sets used in the LCSR calculations. The used QCD sum rule values (QCD-SR) are taken from [50, 64] while the BLW model values were introduced in [64]. The values denoted by $(\star)$ in phenomenological models were obtained from QCD-SR and therefore are equal to those.

The values for different models are summarised in Table 5.6. The numbers for the moments in the BLW model were obtained by comparing the light cone sum rule calculation with the experimental data and are not based on any systematic attempt to fit the data. The presented results show that the knwoledge of α_s corrections and a better understanding of higher twist corrections is necessary to describe the data wiht satisfactary precision.

Hence we believe that the radiative corrections to the light cone sum rules are of key importance. These will include order x^2 corrections to (2.51). Furthermore it would be interesting to include the higher moments of the distribution amplitudes in the calculation, particularly to investigate the dependence of the results on the choice of different independent subsets of second momenta. Thus we expect that all these improvements will allow to make good theoretical predictions in the experimentally attractive Q^2 region.

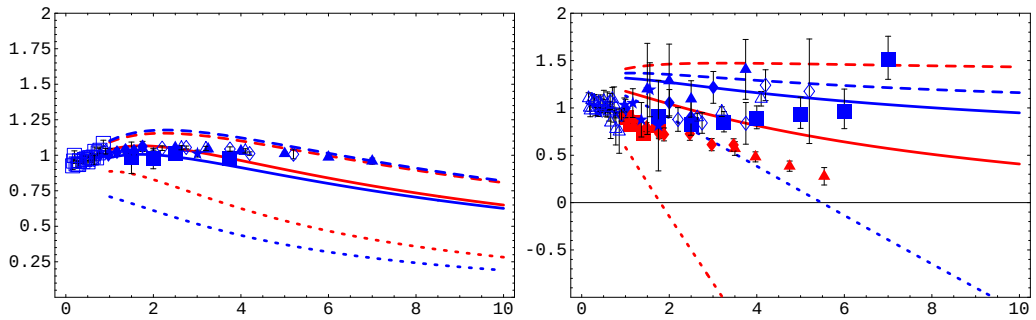

(a) (b)

Figure 5.13: Results for the electromagnetic form factors (left: $G_M/(\mu_p G_{Dipole})$ vs. Q^2; right: $\mu_p G_E/G_M$ vs. Q^2) of the proton, obtained from LCSR using different values for distribution amplitude moments as described in text on p. 90. The red data points in Figure (b) are JLAB data, while the blue ones are obtained via Rosenbluth separation.

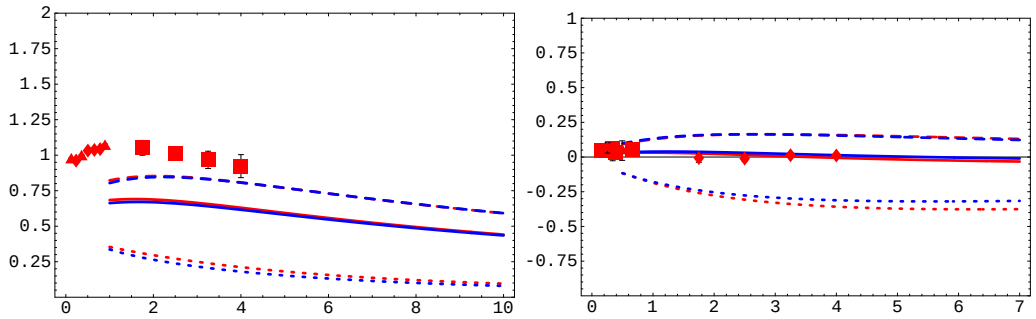

(a) (b)

Figure 5.14: LCSR results for the electromagnetic form factors of the neutron (left: $G_M/(\mu_n G_{Dipole})$ vs. Q^2; right: G_E vs. Q^2), obtained using different values for distribution amplitudes moments as described in text on p. 90.

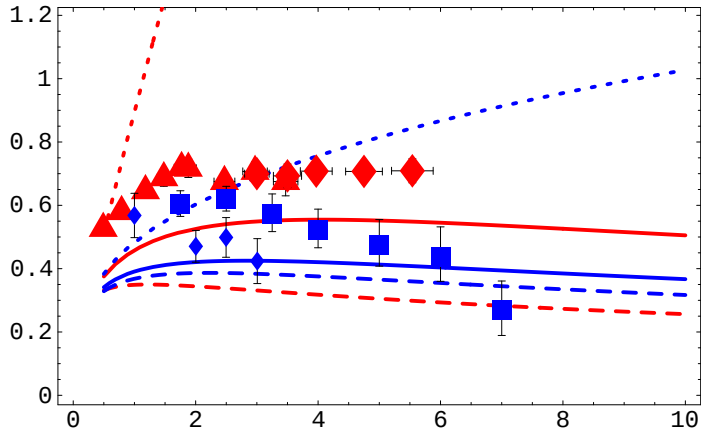

Figure 5.15: LCSR results for the ratio $\sqrt{Q^2}F_2^P/(1.79F_1^p)$ obtained using different values for distribution amplitudes moments as described in text on p. 90. *Red symbols:* experimental values obtained via Polarisation transfer. *Blue symbols:* experimental values obtained via Rosenbluth separation.

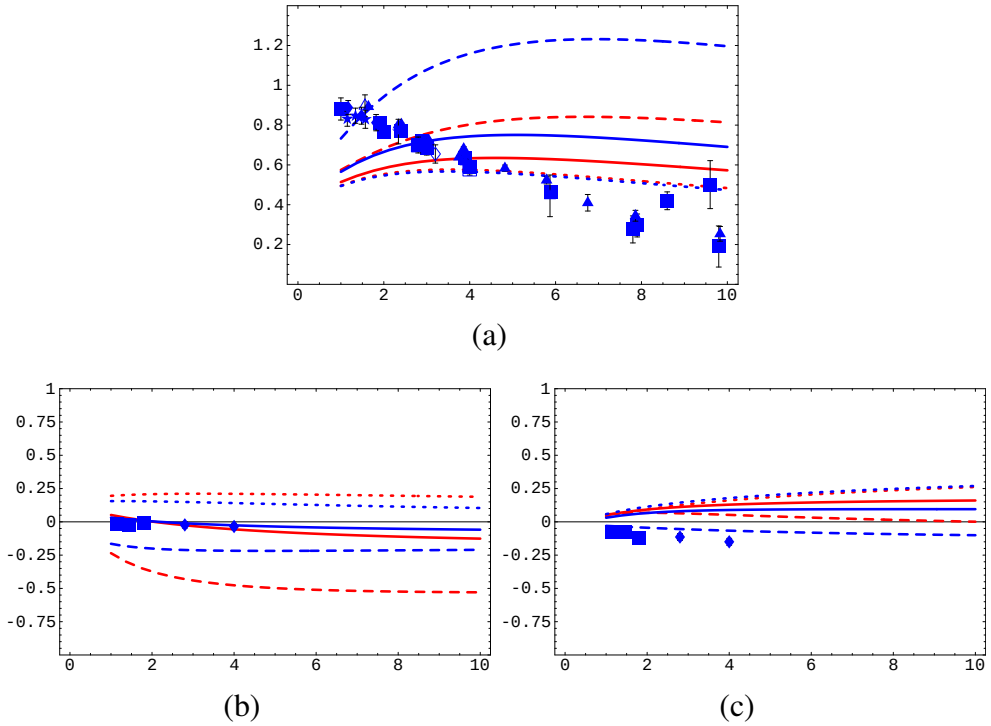

Figure 5.16: $\gamma^\star N \to \Delta$ transition form factors ($G_M^\star/(3G_{Dipole})$ vs. Q^2 (a), R_{EM} vs. Q^2 (b), R_{SM} vs. Q^2) obtained from LCSR calculation with different nonperturbative input parameters for the moments of nucleon distribution amplitudes as described in text on p. 90.

CHAPTER 6

Discussions and Outlook

Although quantum chromodynamics is based on a "simple" Lagrangian the very "complex" bound states such as nucleon are only poorly understood at our time. As discussed in the introductory part of this thesis the understanding of nucleonic properties will become a key factor in our understanding of the standard model as well as theories beyond it. Of course, a complete knowledge of the nucleon wave function would be highly desirable. However, at present it is not possible to access the full nucleon wave function due to the nonperturbative properties of the relevant strong interaction and the complexity of QCD. Thus, one considers quantities like structure functions or generalised parton distributions. The objects which come closest to the wave function are the distribution amplitudes. In this case one simplifies the problem by integrating out the transverse degrees of freedom in the wave function. Although the information content is thus reduced, the distribution amplitudes allow a more general study of the nucleon, as one can relate e.g., different nucleon formfactors to each other by means of the nucleon distribution amplitude.

The reduction of the complexity by the integration of transverse momenta is only one of three simplifications. Another one is the twist expansion of the relevant matrix elements justified by operator product expansion. Presently such calculations are usually limited to leading and next-to-leading twist. The nonlocal matrix elements which correspond to distribution amplitudes of different twist can be seen as generating functionals for a series of local operators. These local matrix elements are related to moments of the distribution amplitudes and can be directly accessed in Lattice QCD. Of course, the restriction to a small finite number of moments leads again to some loss of information and in principle one

would like to avoid this, preferring the full functional form of the nucleon distribution amplitude. On the other hand the physically relevant quantities are obtained from nucleon distribution amplitudes by convoluting them with a hard scattering kernel. The higher moments are suppressed in this case, and the lower moments contain exactly the important information needed.

Being nonperturbative objects, distribution amplitudes and the corresponding moments are difficult to calculate reliably in a model independent way. The QCD sum rule calculations which were used originally are known to overestimate strongly the asymmetries in the nucleon distribution amplitudes, leading to large systematic uncertainties in the obtained values. The exactly known results for the asymptotic case $Q^2 \to \infty$ are even less applicable to experimentally relevant calculations as the logarithmic evolution of the asymptotic distribution amplitude down to reasonable Q^2 values will not be meaningful.

In the case of distribution amplitudes the only systematic approach, except QCD sum rules, to calculate the corresponding moments is offered by lattice QCD. Of course one has to fight additional problems which are caused by discretisation and finite size effects. However, in this work many of the problems related to this have been significantly reduced leading to results of very good accuracy. Based on three-quark operators which transforms irreducibly under the spinorial hypercubic group $\overline{H}(4)$ obtained in [130] we have derived a full set of operators for leading twist distribution amplitudes with best mixing properties on the lattice. This was done such that the obtained operators can be used not only for the nucleon but also for other baryons simplifying greatly future work. These particular operators allowed us to suppress most of the unwanted operator mixings during the following renormalisation procedure. Even more important, by choosing the operators carefully it was possible to avoid mixing with lower dimensional operators completely. We suggest to use in future lattice calculations operator relations summarised in Appendix A.2, as these do not depend on the choice of the used lattice action and the described advantages do not have any side effects.

Using this optimal set of operators we have calculated the correlators from which we could extract the moments of the leading-twist distribution amplitudes up to order two and the normalisation constants λ_1 and λ_2 of next-to-leading twist distribution amplitudes as well as the couplings α and β relevant e.g., for the calculations of nucleon decay in grand unified theories. We were able to obtain this additional information because we have applied a two step approach. The general operators calculated in the first step could be used without great additional numerical effort to extract these theoretically interesting quantities. We plan to use these correlators also in future to extract further physically relevant numbers. Our results for normalisation constants suggested that $-2\lambda_1 \approx \lambda_2$ leading to the strong suspicion that these constants must be related to each other, what to our knowledge was not observed in the literature before. Indeed it turned out that in

the nonrelativistic limit the relation is exactly fulfilled.

Although the standard analysis of our data, called in this work "partially correlated", provided us with fully consistent results, we could improve the quality of our results by applying the "fully correlated" method. This method reduced the statistical errors so that also the asymmetries of the nucleon distribution amplitudes become visible. We could confirm the common belief that the asymmetries of the nucleon distribution amplitude are noticeably smaller than suggested by QCD sum rules. However, the results obtained from both analysis methods do not allow reliable quantitative predictions. Furthermore, by improving the quality of the values for higher moments by applying the "fully correlated" method, the results for the normalisation constants become worse as the correlators for higher moments introduced a small systematic shift of the nucleon mass on the lattice. Although the different results are still consistent to each other, this effect can be only reduced by higher statistics within this analysis approach.

Unsatisfied by this situation we have developed and applied a new analysis method, in this work called "partially constrained" (Subsection 5.3.1) as it is based on the theoretical constraints from momentum conservation. In this method the statistical properties of the relevant moment ratios are greatly improved and one can completely avoid the calculation of normalisation constants and energies for higher moments. Of course one has to use the renormalisation matrices obtained in [131] as input in a much earlier analysis stage for this method in order to determine the absolute values of moments and asymmetries. However, as the statistical uncertainties for the renormalisation matrices are small compared to other sources of statistical errors in this analysis, we could greatly improve the statistical quality of our results by the new approach. As an extension and a further improvement of this method we proposed a "fully constrained" analysis method described in Subsection 5.3.2, which improves the quality of results and at the same time reduce the required computer resources in future lattice calculations.

The accuracy of the constrained analysis allowed us to determine the asymmetries of the nucleon distribution amplitude with relatively small statistical uncertainty. This allowed also to resolve small but noticeable deviation from linear behaviour for ϕ^{100} and ϕ^{010} moments as function of the pion mass on the lattice. Thus, as long as we do not have any additional theoretical input from chiral perturbation theory, it could be interesting to investigate this aspect further numerically in order to reduce the systematic uncertainty due to chiral extrapolation. Of course also results from chiral perturbation theory are highly welcome for a quantitative understanding.

Finally, using our lattice results we have constructed a model function for the nucleon distribution amplitude guided by its renormalisation group properties. Of course this model function is not unique, but we can assume that the general pattern is similar also for the true one, as this model is a natural choice due to the

renormalisation group characteristics. Furthermore, by applying the light cone sum rule approach with our results as input, we have calculated some nucleon related form factors. To our knowledge these results are the first results obtained from first principle in a systematic, model independent way, and which are not based on any fits to experimental data.

As some of the calculated quantities are extremely sensitive to the exact values of the moments, we believe that with increased experimental and theoretical accuracy, which should be within the reach in near future, it will be possible to improve the constraints for the nucleon distribution amplitude even further.

APPENDIX A

Definitions and Relations

A.1 Weyl representation

In Euclidean spacetime the Dirac matrices in Weyl representation have the form

$$\gamma_1 = \begin{pmatrix} 0 & 0 & 0 & i \\ 0 & 0 & i & 0 \\ 0 & -i & 0 & 0 \\ -i & 0 & 0 & 0 \end{pmatrix} \qquad \gamma_2 = \begin{pmatrix} 0 & 0 & 0 & 1 \\ 0 & 0 & -1 & 0 \\ 0 & -1 & 0 & 0 \\ 1 & 0 & 0 & 0 \end{pmatrix}$$

$$\gamma_3 = \begin{pmatrix} 0 & 0 & i & 0 \\ 0 & 0 & 0 & -i \\ -i & 0 & 0 & 0 \\ 0 & i & 0 & 0 \end{pmatrix} \qquad \gamma_4 = \begin{pmatrix} 0 & 0 & 1 & 0 \\ 0 & 0 & 0 & 1 \\ 1 & 0 & 0 & 0 \\ 0 & 1 & 0 & 0 \end{pmatrix}. \tag{A.1}$$

Furthermore we use in our calculations the following conventions

$$\gamma_5 = \gamma_1\gamma_2\gamma_3\gamma_4 = \begin{pmatrix} -1 & 0 & 0 & 0 \\ 0 & -1 & 0 & 0 \\ 0 & 0 & 1 & 0 \\ 0 & 0 & 0 & 1 \end{pmatrix}, \qquad \sigma_{\mu\nu} \equiv \frac{i}{2}\left[\gamma_\mu, \gamma_\nu\right]. \tag{A.2}$$

A.2 Operators Relations for Leading Twist Distribution Amplitudes on the Lattice

In the following we summarise the multiplets of irreducibly transforming nucleon distribution amplitude operators in Euclidean space-time obtained from irreducible three-quark operators [130]. To be as general as possible in these relations we have rewritten the distribution amplitude operators in the form

$$\begin{aligned}\mathcal{V}_\tau^{\rho\bar{l}\bar{m}\bar{n}}(0) &= \epsilon^{abc}[i^l D_{\lambda_1}\dots D_{\lambda_l} f_\alpha^a(0)](C\gamma_\rho)_{\alpha\beta}[i^m D_{\mu_1}\dots D_{\mu_m} g_\beta^b(0)] \\ &\quad\times [i^n D_{\nu_1}\dots D_{\nu_n}(\gamma_5 h^c(0))]_\tau, \qquad \text{(A.3)}\\ \mathcal{A}_\tau^{\rho\bar{l}\bar{m}\bar{n}}(0) &= \epsilon^{abc}[i^l D_{\lambda_1}\dots D_{\lambda_l} f_\alpha^a(0)](C\gamma_\rho\gamma_5)_{\alpha\beta}[i^m D_{\mu_1}\dots D_{\mu_m} g_\beta^b(0)] \\ &\quad\times [i^n D^{\nu_1}\dots D^{\nu_n}(h^c(0))]_\tau, \qquad \text{(A.4)}\\ \mathcal{T}_\tau^{\rho\bar{l}\bar{m}\bar{n}}(0) &= \epsilon^{abc}[i^l D_{\lambda_1}\dots D_{\lambda_l} f_\alpha^a(0)](C\sigma_{\xi\rho}\gamma_5)_{\alpha\beta}[i^m D_{\mu_1}\dots D_{\mu_m} g_\beta^b(0)] \\ &\quad\times [i^n D_{\nu_1}\dots D_{\nu_n}(\gamma_\xi\gamma_5 h^c(0))]_\tau. \qquad \text{(A.5)}\\ & \qquad \text{(A.6)}\end{aligned}$$

In the following the total symmetrisation in Lorentz indices denoted by the curly brackets, e.g.,

$$\mathcal{V}^{\{23\}} = \frac{1}{2!}\left(\mathcal{V}^{23} + \mathcal{V}^{32}\right)$$

reflects the leading twist projection, thus there is no need to distinguish between the Lorentz indices connected to derivatives and the uncontracted index of the γ matrix. In the formulas below we do not note explicitly on which quark the derivatives act. In all cases it is implied that on left- and right-hand side the position of the derivatives is the same. The relations for the nucleon distribution amplitudes, as used by us, are easily obtained from the following relations by the identification

$$f \to u, \qquad g \to u, \qquad h \to d. \qquad \text{(A.7)}$$

0th moment $(l+m+n=0)$

$$\left(\mathcal{B}_{9,6}^{lmn}, -\mathcal{B}_{9,1}^{lmn}, -\mathcal{B}_{9,12}^{lmn}, \mathcal{B}_{9,7}^{lmn}\right) = \frac{1}{4}\left(\gamma_3\gamma_4\left[\gamma_2\mathcal{T}^1 + \gamma_1\mathcal{T}^2\right]\right) \qquad \text{(A.8)}$$

$$\left(\mathcal{B}_{9,4}^{lmn}, -\mathcal{B}_{9,3}^{lmn}, -\mathcal{B}_{9,10}^{lmn}, \mathcal{B}_{9,9}^{lmn}\right) = \frac{1}{4}\left(\gamma_1\gamma_2\left[\gamma_4\mathcal{T}^3 + \gamma_3\mathcal{T}^4\right]\right) \qquad \text{(A.9)}$$

$$\begin{aligned}\left(\mathcal{B}_{9,2}^{lmn}, -\mathcal{B}_{9,5}^{lmn}, -\mathcal{B}_{9,8}^{lmn}, \mathcal{B}_{9,11}^{lmn}\right) =& \frac{1}{4}\left(\gamma_1\gamma_2\left[\gamma_4\mathcal{T}^3 - \gamma_3\mathcal{T}^4\right]\right. \\ &\left.+\gamma_3\gamma_4\left[\gamma_1\mathcal{T}^2 - \gamma_2\mathcal{T}^1\right]\right) \qquad \text{(A.10)}\end{aligned}$$

The $\mathcal{B}_{7,i}^{lmn}$ ($\mathcal{B}_{8,i}^{lmn}$) operators from the symmetry class $-++$ $(+-+)$ are obtained from the above by replacing $\mathcal{T}$ on the right hand side by $\mathcal{V}+\mathcal{A}$ $(\mathcal{V}-\mathcal{A})$.

1st moments $(l+m+n=1)$

$$\begin{aligned}\left(\mathcal{B}^{lmn}_{7,1},-\mathcal{B}^{lmn}_{7,2},\mathcal{B}^{lmn}_{7,7},-\mathcal{B}^{lmn}_{7,8}\right) =&2\left(2\gamma_4\gamma_3\mathcal{T}^{\{12\}}+\gamma_4\gamma_2\mathcal{T}^{\{13\}}+\gamma_2\gamma_3\mathcal{T}^{\{14\}}\right.\\ &\left.+\gamma_4\gamma_1\mathcal{T}^{\{23\}}+\gamma_1\gamma_3\mathcal{T}^{\{24\}}\right) \qquad \text{(A.11)}\\ \left(\mathcal{B}^{lmn}_{7,3},-\mathcal{B}^{lmn}_{7,4},\mathcal{B}^{lmn}_{7,9},-\mathcal{B}^{lmn}_{7,10}\right) =&2\left(2\gamma_1\gamma_2\mathcal{T}^{\{34\}}+\gamma_4\gamma_2\mathcal{T}^{\{13\}}+\gamma_3\gamma_2\mathcal{T}^{\{14\}}\right.\\ &\left.+\gamma_1\gamma_4\mathcal{T}^{\{23\}}+\gamma_1\gamma_3\mathcal{T}^{\{24\}}\right) \qquad \text{(A.12)}\\ \left(\mathcal{B}^{lmn}_{7,6},\mathcal{B}^{lmn}_{7,5},\mathcal{B}^{lmn}_{7,12},\mathcal{B}^{lmn}_{7,11}\right) =&2\left(\gamma_2\gamma_4\mathcal{T}^{\{13\}}+\gamma_2\gamma_3\mathcal{T}^{\{14\}}+\gamma_1\gamma_4\mathcal{T}^{\{23\}}\right.\\ &\left.+\gamma_1\gamma_3\mathcal{T}^{\{24\}}\right) \qquad \text{(A.13)}\end{aligned}$$

The $\mathcal{B}^{lmn}_{5,i}$ ($\mathcal{B}^{lmn}_{6,i}$) operators from the symmetry class $D--++$ $(D+-+)$ are obtained from the above by replacing $\mathcal{T}$ on the right hand side by $\mathcal{V}+\mathcal{A}$ $(\mathcal{V}-\mathcal{A})$.

2nd moments $(l+m+n=2)$

$$\begin{aligned}\left(-\mathcal{B}^{lmn}_{6,4},-\mathcal{B}^{lmn}_{6,3},\mathcal{B}^{lmn}_{6,2},\mathcal{B}^{lmn}_{6,1}\right) =&\frac{\sqrt{3}}{4}\left(\gamma_4\mathcal{T}^{\{123\}}+\gamma_3\mathcal{T}^{\{124\}}+\gamma_2\mathcal{T}^{\{134\}}\right.\\ &\left.+\gamma_1\mathcal{T}^{\{234\}}\right) \qquad \text{(A.14)}\end{aligned}$$

The $\mathcal{B}^{lmn}_{4,i}$ ($\mathcal{B}^{lmn}_{5,i}$) operators from the symmetry class $DD--+$ $(DD+-+)$ are obtained from the above by replacing $\mathcal{T}$ on the right hand side by $\mathcal{V}+\mathcal{A}$ $(\mathcal{V}-\mathcal{A})$.

APPENDIX B

Lattice Setup

We have used gauge configurations obtained from rational hybrid Monte Carlo simulations. Independent configuration were obtained every 40 trajectories. To increase the number of usable configurations we used multiple source technique, so that we were able to incorporate every fifth configuration. The parameters of our lattices are given in Table B.1, while the smearing parameters are summarised in Table B.2. For results in physical units the scale is set using the Sommer parameter with $r_0 = 0.467\,\mathrm{fm}$.

β	r_0/a	$a\,[\mathrm{fm}]$	$L\,[\mathrm{fm}]$	κ_{sea}	$N^3 \times T$	am_π	$m_\pi L$
5.29	6.201(25)	0.075	1.2	0.13400	$16^3 \times 32$	0.5767(11)	9.2
			1.2	0.13500	$16^3 \times 32$	0.42057(92)	6.7
			1.8	0.13550	$24^3 \times 48$	0.32696(64)	7.8
			1.8	0.13590	$24^3 \times 48$	0.23997(47)	5.8
			1.8	0.13620	$24^3 \times 48$	0.15644(92)	3.8
5.40	6.946(44)	0.067	1.6	0.13500	$24^3 \times 48$	0.40301(43)	9.7
			1.6	0.13560	$24^3 \times 48$	0.31232(67)	7.5
			1.6	0.13610	$24^3 \times 48$	0.22081(72)	5.3
			1.6	0.13625	$24^3 \times 48$	0.19053(47)	4.6
			1.6	0.13640	$24^3 \times 48$	0.15353(41)	3.7

Table B.1:

β	κ_{sea}	N_{smear}	κ_{smear}
5.29	0.13400	60	0.21
	0.13500	60	0.21
	0.13550	60	0.21
	0.13590	60	0.21
	0.13620	60	0.21
5.40	0.13500	65	0.21
	0.13560	65	0.21
	0.13610	75	0.21
	0.13625	75	0.21
	0.13625	75	0.21

Table B.2: Summary of the smearing parameters used in the evaluation of our correlators.

APPENDIX C

Raw Lattice Results

	all		24	
	#	χ^2/d.o.f	#	χ^2/d.o.f
$f_N/m_N^2 \cdot 10^3$	4.088(77)	6.563	4.53(14)	0.555
$-\lambda_1/m_N \cdot 10^3[\mathrm{GeV}]$	27.02(47)	19.31	30.79(78)	6.209
$-\lambda_1 \cdot 10^3[\mathrm{GeV}^2]$	34.37(66)	18.46	36.55(93)	3.484
$\lambda_2/m_N \cdot 10^3[\mathrm{GeV}]$	54.67(95)	19.98	62.9(16)	4.928
$\lambda_2 \cdot 10^3[\mathrm{GeV}^2]$	70.0(14)	18.31	74.8(19)	2.388
$-\alpha/m_N^2 \cdot 10^3[\mathrm{GeV}]$	14.64(39)	8.399	17.02(79)	3.012
$-\alpha \cdot 10^3[\mathrm{GeV}^3]$	19.91(76)	15.69	22.9(10)	2.877
$\beta/m_N^2 \cdot 10^3[\mathrm{GeV}]$	14.98(42)	8.191	17.42(83)	0.339
$\beta \cdot 10^3[\mathrm{GeV}^3]$	20.52(83)	14.08	23.2(11)	0.053
ϕ^{100}	0.2987(49)	1.125	0.315(10)	0.033
ϕ^{010}	0.2746(48)	0.768	0.263(11)	0.765
ϕ^{001}	0.2840(48)	1.566	0.271(11)	2.555
ϕ^{011}	0.0647(37)	0.276	0.0633(87)	0.711
ϕ^{101}	0.0606(39)	0.821	0.067(12)	0.744
ϕ^{110}	0.0651(32)	0.712	0.0592(79)	0.445
ϕ^{200}	0.1149(54)	2.367	0.146(14)	0.597
ϕ^{020}	0.0922(50)	0.717	0.096(12)	1.908
ϕ^{002}	0.1067(54)	0.944	0.108(13)	2.729

Table C.1: Linear extrapolations of FC results to the chiral limit at $\beta = 5.29$ using the $16^3 \times 32$ and $24^3 \times 48$ lattices (all) and the $24^3 \times 48$ lattices only (24). The χ^2/d.o.f refers to the linear chiral extrapolation.

	#	χ^2/d.o.f
$f_N/m_N^2 \cdot 10^3$	4.287(74)	0.658
$-\lambda_1/m_N \cdot 10^3[\mathrm{GeV}]$	26.40(42)	1.060
$-\lambda_1 \cdot 10^3[\mathrm{GeV}^2]$	32.38(60)	1.901
$\lambda_2/m_N \cdot 10^3[\mathrm{GeV}]$	52.96(85)	1.498
$\lambda_2 \cdot 10^3[\mathrm{GeV}^2]$	65.1(12)	2.716
$-\alpha/m_N^2 \cdot 10^3[\mathrm{GeV}]$	14.76(37)	1.359
$-\alpha \cdot 10^3[\mathrm{GeV}^3]$	19.66(70)	1.161
$\beta/m_N^2 \cdot 10^3[\mathrm{GeV}]$	14.73(38)	0.952
$\beta \cdot 10^3[\mathrm{GeV}^3]$	18.83(72)	5.351
ϕ^{100}	0.2939(59)	1.384
ϕ^{010}	0.2719(62)	0.335
ϕ^{001}	0.2740(60)	0.972
ϕ^{011}	0.0646(44)	1.831
ϕ^{101}	0.0688(55)	1.057
ϕ^{110}	0.0707(39)	0.610
ϕ^{200}	0.1126(68)	5.534
ϕ^{020}	0.0949(61)	0.288
ϕ^{002}	0.1060(64)	0.114

Table C.2: Linear extrapolations of FC results to the chiral limit at $\beta = 5.40$. The χ^2/d.o.f refers to the linear chiral extrapolation.

	all		24	
	#	χ^2/d.o.f	#	χ^2/d.o.f
$f_N/m_N^2 \cdot 10^3$	4.396(99)	2.417	4.67(19)	1.208
$V^{100} = V^{010}$	0.308(13)	0.416	0.298(35)	0.027
$A^{100} = -A^{010}$	0.0133(40)	2.495	0.046(13)	0.038
$T^{100} = T^{010}$	0.307(12)	0.425	0.297(25)	0.263
φ^{100}	0.324(16)	0.352	0.360(49)	0.001
$\varphi^{010} = \phi^{010} = T^{001}$	0.286(12)	1.636	0.248(26)	0.550
$\varphi^{001} = V^{001}$	0.289(15)	1.892	0.229(37)	1.532
$\phi^{100} - \phi^{010}$	0.0194(49)	2.230	0.054(15)	0.056
$\phi^{100} - \phi^{001}$	0.0076(39)	2.017	0.036(14)	1.011
$\phi^{001} - \phi^{010}$	0.0114(41)	0.679	0.016(13)	1.719
$V^{011} = V^{101}$	0.0698(56)	0.197	0.072(17)	0.228
$A^{011} = -A^{101}$	−0.0006(49)	0.038	0.000(15)	0.004
$T^{011} = T^{101}$	0.0689(44)	0.395	0.068(12)	0.035
φ^{011}	0.0709(85)	0.068	0.076(27)	0.061
$\varphi^{101} = \phi^{101} = T^{110}$	0.0699(62)	0.428	0.071(18)	0.135
$\varphi^{110} = V^{110}$	0.0637(79)	0.149	0.064(24)	0.101
$\phi^{101} - \phi^{011}$	0.0012(62)	0.068	0.006(19)	0.023
$\phi^{011} - \phi^{110}$	0.0025(45)	0.048	0.004(15)	0.096
$\phi^{101} - \phi^{110}$	−0.0001(47)	0.155	0.005(17)	0.383
$V^{200} = V^{020}$	0.1059(78)	0.557	0.129(22)	0.015
$A^{020} = -A^{200}$	0.0132(59)	0.698	0.036(18)	0.131
$T^{200} = T^{020}$	0.1108(79)	0.576	0.119(19)	1.336
φ^{200}	0.117(12)	0.739	0.165(37)	0.006
$\varphi^{020} = \phi^{020} = T^{002}$	0.0913(73)	0.261	0.097(19)	0.590
$\varphi^{002} = V^{002}$	0.096(12)	0.724	0.066(35)	1.320
$\phi^{200} - \phi^{020}$	0.0206(68)	0.406	0.039(21)	0.001
$\phi^{200} - \phi^{002}$	0.0060(61)	0.847	0.032(20)	0.601
$\phi^{002} - \phi^{020}$	0.0114(55)	0.291	0.005(19)	0.757

Table C.3: Linear extrapolations of PC results to the chiral limit for different momenta combinations at $\beta = 5.29$ using the $16^3 \times 32$ and $24^3 \times 48$ lattices (all) and the $24^3 \times 48$ lattices only (24). The χ^2/d.o.f refers to the linear chiral extrapolation.

	#	χ^2/d.o.f
$f_N/m_N^2 \cdot 10^3$	4.517(96)	0.342
$V^{100} = V^{010}$	0.298(19)	0.966
$A^{100} = -A^{010}$	0.0196(64)	0.960
$T^{100} = T^{010}$	0.300(16)	0.483
φ^{100}	0.323(24)	0.777
$\varphi^{010} = \phi^{010} = T^{001}$	0.276(17)	0.446
$\varphi^{001} = V^{001}$	0.280(21)	0.399
$\phi^{100} - \phi^{010}$	0.0258(77)	0.928
$\phi^{100} - \phi^{001}$	0.0129(66)	1.291
$\phi^{001} - \phi^{010}$	0.0144(66)	2.118
$V^{011} = V^{101}$	0.0676(69)	0.260
$A^{011} = -A^{101}$	0.0022(60)	1.063
$T^{011} = T^{101}$	0.0707(54)	0.580
φ^{011}	0.064(11)	0.533
$\varphi^{101} = \phi^{101} = T^{110}$	0.0673(67)	0.504
$\varphi^{110} = V^{110}$	0.077(10)	0.049
$\phi^{101} - \phi^{011}$	0.0005(73)	1.711
$\phi^{011} - \phi^{110}$	−0.0042(62)	0.246
$\phi^{101} - \phi^{110}$	−0.0036(62)	0.627
$V^{200} = V^{020}$	0.115(10)	2.034
$A^{020} = -A^{200}$	0.0195(81)	1.812
$T^{200} = T^{020}$	0.1203(89)	1.450
φ^{200}	0.134(16)	2.305
$\varphi^{020} = \phi^{020} = T^{002}$	0.0963(93)	0.646
$\varphi^{002} = V^{002}$	0.106(15)	0.279
$\phi^{200} - \phi^{020}$	0.0300(97)	1.864
$\phi^{200} - \phi^{002}$	0.0092(83)	1.380
$\phi^{002} - \phi^{020}$	0.0215(80)	0.438

Table C.4: Linear extrapolations of PC results to the chiral limit for different momenta combinations at $\beta = 5.40$. The χ^2/d.o.f refers to the linear chiral extrapolation.

	#	χ^2/d.o.f
$f_N/m_N^2 \cdot 10^3$	4.395(85)	0.267
$-\lambda_1/m_N \cdot 10^3$[GeV]	26.8204(48)	0.184
$\lambda_2/m_N \cdot 10^3$[GeV]	53.69(96)	0.403
$\alpha/m_N^2 \cdot 10^3$[GeV]	15.09(42)	0.414
$\beta/m_N^2 \cdot 10^3$[GeV]	14.96(44)	1.174
$f_N/(\lambda_1 m_N)$[GeV$^-$1]	0.1683(14)	0.592
ϕ^{100}	0.3358(11)	6.115
$\phi^{010} = \varphi^{010}$	0.2891(9)	6.960
$\phi^{001}(\star)$	0.3155(9)	1.312
$\phi^{100} - \phi^{010}$	0.0468(19)	7.732
$\phi^{100} - \phi^{001}$	0.0206(18)	3.300
$\phi^{001} - \phi^{010}$	0.0263(14)	2.526
ϕ^{011}	0.0932(19)	1.544
ϕ^{101}	0.1124(18)	0.287
$\phi^{110}(\star)$	0.1034(16)	0.135
ϕ^{200}	0.1924(30)	0.338
$\phi^{020} = \varphi^{020}(\star)$	0.1539(28)	0.265
ϕ^{002}	0.1801(36)	0.856
$\phi^{101} - \phi^{011}$	0.0200(27)	0.900
$\phi^{110} - \phi^{011}$	0.0100(25)	0.775
$\phi^{101} - \phi^{110}$	0.0094(20)	0.257
$\phi^{200} - \phi^{020}$	0.0364(35)	0.514
$\phi^{200} - \phi^{002}$	0.0115(39)	0.810
$\phi^{002} - \phi^{020}$	0.0255(24)	0.597

Table C.5: Linear extrapolations of ϕ^{lmn} and asymmetries to the chiral limit as obtained from the partially constrained analysis at $\beta = 5.40$. The χ^2/d.o.f refers to the linear chiral extrapolation. The values denoted by the $\star$ were used to determine the absolute normalisation of the associated asymmetries.

	#	χ^2/d.o.f
φ^{100}	0.3563(29)	4.301
$\varphi^{001}(\star)$	0.2949(26)	2.511
$\varphi^{100} - \varphi^{010}$	0.0666(34)	6.115
$\varphi^{100} - \varphi^{001}$	0.0616(54)	3.300
$\varphi^{010} - \varphi^{001}$	0.0056(26)	1.312
φ^{011}	0.0833(40)	1.259
$\varphi^{110}(\star)$	0.1135(38)	0.345
φ^{200}	0.2042(63)	0.564
φ^{002}	0.1692(68)	1.064
$\varphi^{101} - \varphi^{011}$	0.0302(47)	1.074
$\varphi^{110} - \varphi^{011}$	0.0301(74)	0.775
$\varphi^{110} - \varphi^{101}$	0.0006(37)	0.425
$\varphi^{200} - \varphi^{020}$	0.0491(70)	0.505
$\varphi^{200} - \varphi^{002}$	0.0345(117)	0.810
$\varphi^{002} - \varphi^{020}$	0.0157(56)	1.335

Table C.6: Linear extrapolations of φ^{lmn} and asymmetries to the chiral limit as obtained from the partially constrained analysis at $\beta = 5.40$. The χ^2/d.o.f refers to the linear chiral extrapolation. The values denoted by the $\star$ were used to determine the absolute normalisation of the associated asymmetries.

	#	χ^2/d.o.f
$f_N/m_N^2 \cdot 10^3$	4.215(85)	1.878
$-\lambda_1/m_N \cdot 10^3$[GeV]	27.71(52)	10.57
$\lambda_2/m_N \cdot 10^3$[GeV]	55.89(11)	10.54
$\alpha/m_N^2 \cdot 10^3$[GeV]	15.10(44)	4.253
$\beta/m_N^2 \cdot 10^3$[GeV]	15.41(45)	2.514
$f_N/(\lambda_1 m_N)$[GeV$^-$1]	0.1555(11)	15.49
ϕ^{100}	0.3286(12)	7.559
$\phi^{010} = \varphi^{010}$	0.2943(9)	8.530
$\phi^{001}(\star)$	0.3164(9)	1.112
$\phi^{100} - \phi^{010}$	0.0350(20)	9.960
$\phi^{100} - \phi^{001}$	0.0126(19)	3.996
$\phi^{001} - \phi^{010}$	0.0225(14)	3.315
ϕ^{011}	0.1113(26)	3.593
ϕ^{101}	0.1148(26)	0.370
$\phi^{110}(\star)$	0.1085(22)	1.716
ϕ^{200}	0.1820(44)	4.176
$\phi^{020} = \varphi^{020}(\star)$	0.1489(35)	0.363
ϕ^{002}	0.1728(42)	1.677
$\phi^{101} - \phi^{011}$	0.0042(39)	2.489
$\phi^{110} - \phi^{011}$	0.0042(34)	0.636
$\phi^{101} - \phi^{110}$	0.0053(29)	1.159
$\phi^{200} - \phi^{020}$	0.0367(48)	1.515
$\phi^{200} - \phi^{002}$	0.0076(59)	1.763
$\phi^{002} - \phi^{020}$	0.0230(39)	1.010

Table C.7: Linear extrapolations of ϕ^{lmn} and asymmetries to the chiral limit as obtained from the partially constrained analysis at $\beta = 5.29$. The χ^2/d.o.f refers to the linear chiral extrapolation. The values denoted by the $\star$ were used to determine the absolute normalisation of the associated asymmetries.

	#	χ^2/d.o.f
φ^{100}	$0.3410(30)$	5.363
$\varphi^{001}(\star)$	$0.3037(26)$	2.682
$\varphi^{100} - \varphi^{010}$	$0.0472(36)$	7.560
$\varphi^{100} - \varphi^{001}$	$0.0373(55)$	3.996
$\varphi^{010} - \varphi^{001}$	$0.0106(26)$	1.112
φ^{011}	$0.1164(56)$	1.797
$\varphi^{110}(\star)$	$0.1048(50)$	0.236
φ^{200}	$0.1881(93)$	3.071
φ^{002}	$0.1640(96)$	0.819
$\varphi^{101} - \varphi^{011}$	$0.0001(66)$	1.921
$\varphi^{110} - \varphi^{011}$	$0.0125(101)$	0.636
$\varphi^{110} - \varphi^{101}$	$0.0094(50)$	0.069
$\varphi^{200} - \varphi^{020}$	$0.0442(99)$	1.939
$\varphi^{200} - \varphi^{002}$	$0.0227(178)$	1.763
$\varphi^{002} - \varphi^{020}$	$0.0148(91)$	1.006

Table C.8: Linear extrapolations of φ^{lmn} and asymmetries to the chiral limit as obtained from the partially constrained analysis at $\beta = 5.29$. The χ^2/d.o.f refers to the linear chiral extrapolation. The values denoted by the $\star$ were used to determine the absolute normalisation of the associated asymmetries.

Acknowledgements

I wish to thank Andreas Schäfer for supervising my PhD thesis, the possibility to work on different interesting topics and sharing his experience and knowledge with me, which helped solving different problems during this work. I am indebted also to Meinulf Göckeler for many profitable and illuminating discussions we had on Lattice QCD. I would like also to appreciate the fruitful cooperation with Thomas Kaltenbrunner. Furthermore I am thankful to my colleagues of the QCDSF collaboration for sharing their insights into physics and starting help with various technical problem, in particular I would like to mention Dirk Pleiter, James Zanotti and Philipp Hägler. I appreciate also the possibility to benefit from the experience and the thoughts of Alexander Lenz, Alexander Manashov and Vladimir M. Braun on many different topics at the end of this work.

My special thanks goes to my dear friends and colleagues Michael Hartung, Christian Hagen, Dieter Hierl, Stefan Solbrig and Thilo Maurer for very vivid discussions on many different and extremely interesting physical problems, which started below the Planck scale and stopped only beyond any reasonable cosmological scale. Of course, these discussion were made only possible by the good coffee prepared by the Saeco coffee machine, which bravely produced to this minute exactly 40892 coffees.

This work surely benefited a lot from already existing gauge configurations generated and provided within QCDSF, UKQCD and DIK collaborations. Not to forget the large amount of computer time on APEmille in Zeuthen to compute the general two-point functions. I also acknowledge at this point the financial support of BMBF.

I am thankful also for support from near and far by my friends, Anreas Pfund, Claudia and Thomas Röhrl, Simon Kulla, Andreas Heckel and Carmen Niesner. Finally I want to thank my parents and my sister for making all this possible.

Bibliography

[1] A. Fäßler and F. Simkovic, "Double beta decay," *J. Phys.* **G24** (1998) 2139–2178, arXiv:hep-ph/9901215.

[2] F. Wilczek, "The universe is a strange place," *Nucl. Phys. Proc. Suppl.* **134** (2004) 3–12, arXiv:astro-ph/0401347.

[3] W. Buchmüller and C. Lüdeling, "Field theory and standard model," arXiv:hep-ph/0609174.

[4] F. Wilczek, "Anticipating a New Golden Age," arXiv:0708.4236 [hep-ph].

[5] M. E. Peskin and D. V. Schroeder, "An Introduction to quantum field theory,". Reading, USA: Addison-Wesley (1995) 842 p.

[6] **Particle Data Group** Collaboration, W. M. Yao *et al.*, "Review of particle physics," *J. Phys.* **G33** (2006) 1–1232.

[7] L. D. Faddeev and V. N. Popov, "Feynman diagrams for the Yang-Mills field," *Phys. Lett.* **B25** (1967) 29–30.

[8] C. Becchi, A. Rouet, and R. Stora, "Renormalization of Gauge Theories," *Annals Phys.* **98** (1976) 287–321.

[9] I. V. Tyutin, "Gauge invariance in field theory ans statistical physics in operator formalism,". LEBEDEV-75-39.

[10] M. Z. Iofa and I. V. Tyutin, "Gauge Invariance of Spontaneously Broken Nonabelian Theories in the Bogolyubov-Parasiuk-HEPP-Zimmerman Method," *Teor. Mat. Fiz.* **27** (1976) 38–47.

[11] M. Gell-Mann, "A Schematic Model of Baryons and Mesons," *Phys. Lett.* **8** (1964) 214–215.

[12] G. Zweig, "An SU(3) model for strong interaction symmetry and its breaking,". CERN-TH-401 (unpublished).

[13] G. Zweig, "An SU(3) model for strong interaction symmetry and its breaking. 2,". CERN-TH-412 (unpublished).

[14] J. Joyce, *Finnegan's Wake*. Viking Press, New York, 1939.

[15] O. W. Greenberg, "Spin and Unitary Spin Independence in a Paraquark Model of Baryons and Mesons," *Phys. Rev. Lett.* **13** (1964) 598–602.

[16] M. Y. Han and Y. Nambu, "Three-triplet model with double SU(3) symmetry," *Phys. Rev.* **139** (1965) B1006–B1010.

[17] J. D. Bjorken and E. A. Paschos, "Inelastic Electron Proton and gamma Proton Scattering, and the Structure of the Nucleon," *Phys. Rev.* **185** (1969) 1975–1982.

[18] H. Fritzsch and M. Gell-Mann, "Current algebra: Quarks and what else?," *eConf* **C720906V2** (1972) 135–165, arXiv:hep-ph/0208010.

[19] H. Fritzsch, M. Gell-Mann, and H. Leutwyler, "Advantages of the Color Octet Gluon Picture," *Phys. Lett.* **B47** (1973) 365–368.

[20] D. J. Gross and F. Wilczek, "Ultraviolet behavior of non-Abelian gauge theories," *Phys. Rev. Lett.* **30** (1973) 1343–1346.

[21] H. D. Politzer, "Reliable perturbative results for strong interactions?," *Phys. Rev. Lett.* **30** (1973) 1346–1349.

[22] G. S. Bali *et al.*, "String breaking," *Nucl. Phys. Proc. Suppl.* **153** (2006) 9–16, arXiv:hep-lat/0512018.

[23] E. T. Tomboulis, "Confinement for all values of the coupling in four-dimensional SU(2) gauge theory," arXiv:0707.2179 [hep-th].

[24] E. T. Tomboulis and A. Velytsky, "Improved actions and lattice coarsening effects in MCRG studies in SU(2) LGT," *PoS LATTICE* **2007** (2007) 381, arXiv:0709.3077 [hep-lat].

[25] F. Wilczek, "Four big questions with pretty good answers," arXiv:hep-ph/0201222.

[26] S. Chandrasekharan and U. J. Wiese, "An introduction to chiral symmetry on the lattice," *Prog. Part. Nucl. Phys.* **53** (2004) 373–418, arXiv:hep-lat/0405024.

[27] R. C. Walker *et al.*, "Measurements of the proton elastic form-factors for $1 \leq Q^2 \leq 3\,(\mathrm{GeV}/c)^2$ at SLAC," *Phys. Rev.* **D49** (1994) 5671–5689.

[28] W. Bartel *et al.*, "Measurement of proton and neutron electromagnetic form- factors at squared four momentum transfers up to $3\,(\mathrm{GeV}/c)^2$," *Nucl. Phys.* **B58** (1973) 429–475.

[29] **Jefferson Lab Hall A** Collaboration, M. K. Jones *et al.*, "G_{Ep}/G_{Mp} ratio by polarization transfer in $\vec{e}p \to e\vec{p}$," *Phys. Rev. Lett.* **84** (2000) 1398–1402, arXiv:nucl-ex/9910005.

[30] O. Gayou *et al.*, "Measurements of the elastic electromagnetic form factor ratio $\mu_p G_{Ep}/G_{Mp}$ via polarization transfer," *Phys. Rev.* **C64** (2001) 038202.

[31] K. G. Wilson, "Nonlagrangian models of current algebra," *Phys. Rev.* **179** (1969) 1499–1512.

[32] W. Zimmermann, "Normal products and the short distance expansion in the perturbation theory of renormalizable interactions," *Ann. Phys.* **77** (1973) 570–601.

[33] B. Schroer, J. A. Swieca, and A. H. Volkel, "Global Operator Expansions in Conformally Invariant Relativistic Quantum Field Theory," *Phys. Rev.* **D11** (1975) 1509.

[34] M. Lüscher, "Operator Product Expansions on the Vacuum in Conformal Quantum Field Theory in Two Space-Time Dimensions," *Commun. Math. Phys.* **50** (1976) 23.

[35] G. Mack, "Convergence of Operator Product Expansions on the Vacuum in Conformal Invariant Quantum Field Theory," *Commun. Math. Phys.* **53** (1977) 155.

[36] H. Bostelmann, "Operator product expansions as a consequence of phase space properties," *J. Math. Phys.* **46** (2005) 082304, arXiv:math-ph/0502004.

[37] H. Bostelmann, "Phase space properties and the short distance structure in quantum field theory," *J. Math. Phys.* **46** (2005) 052301, arXiv:math-ph/0409070.

[38] K. Fredenhagen and J. Hertel, "Local Algebras of Observables and Point-like localazed Fields," *Commun. Math. Phys.* **80** (1981) 555.

[39] K. Fredenhagen and M. Jorss, "Conformal Haag-Kastler nets, point - like localized fields and the existence of operator product expansions," *Commun. Math. Phys.* **176** (1996) 541–554.

[40] S. Hollands, "The operator product expansion for perturbative quantum field theory in curved spacetime," *Commun. Math. Phys.* **273** (2007) 1–36, arXiv:gr-qc/0605072.

[41] V. L. Chernyak and A. R. Zhitnitsky, "Asymptotic Behavior of Hadron Form-Factors in Quark Model. (In Russian)," *JETP Lett.* **25** (1977) 510.

[42] V. L. Chernyak and A. R. Zhitnitsky, "Asymptotic Behavior of Exclusive Processes in QCD," *Phys. Rept.* **112** (1984) 173.

[43] A. V. Efremov and A. V. Radyushkin, "Factorization and Asymptotical Behavior of Pion Form- Factor in QCD," *Phys. Lett.* **B94** (1980) 245–250.

[44] G. P. Lepage and S. J. Brodsky, "Exclusive Processes in Quantum Chromodynamics: The Form- Factors of Baryons at Large Momentum Transfer," *Phys. Rev. Lett.* **43** (1979) 545–549.

[45] G. P. Lepage and S. J. Brodsky, "Exclusive Processes in Perturbative Quantum Chromodynamics," *Phys. Rev.* **D22** (1980) 2157.

[46] V. L. Chernyak and I. R. Zhitnitsky, "Nucleon Wave Function and Nucleon Form-Factors in QCD," *Nucl. Phys.* **B246** (1984) 52–74.

[47] V. L. Chernyak, A. A. Ogloblin, and I. R. Zhitnitsky, "The wave functions of the octet baryons," *Z. Phys.* **C42** (1989) 569.

[48] G. P. Lepage and S. J. Brodsky, "Exclusive Processes in Quantum Chromodynamics: Evolution Equations for Hadronic Wave Functions and the Form-Factors of Mesons," *Phys. Lett.* **B87** (1979) 359–365.

[49] V. M. Braun, A. Lenz, N. Mahnke, and E. Stein, "Light-cone sum rules for the nucleon form factors," *Phys. Rev.* **D65** (2002) 074011, arXiv:hep-ph/0112085.

[50] V. Braun, R. J. Fries, N. Mahnke, and E. Stein, "Higher twist distribution amplitudes of the nucleon in QCD," *Nucl. Phys.* **B589** (2000) 381–409, arXiv:hep-ph/0007279.

[51] M.-Q. Huang and D.-W. Wang, "Light-cone QCD sum rules for the semileptonic decay $\Lambda_b \to p l \bar{\nu}$," *Phys. Rev.* **D69** (2004) 094003, arXiv:hep-ph/0401094.

[52] V. M. Braun, A. Lenz, and M. Wittmann, "Nucleon form factors in QCD," *Phys. Rev.* **D73** (2006) 094019, arXiv:hep-ph/0604050.

[53] **Jefferson Lab Hall A** Collaboration, O. Gayou *et al.*, "Measurement of G_{Ep}/G_{Mp} in $\vec{e}p \to e\vec{p}$ to $Q^2 = 5.6\,\mathrm{GeV}^2$," *Phys. Rev. Lett.* **88** (2002) 092301, arXiv:nucl-ex/0111010.

[54] V. Punjabi *et al.*, "Proton elastic form factor ratios to $Q^2 = 3.5$ GeV^2 by polarization transfer," *Phys. Rev.* **C71** (2005) 055202, arXiv:nucl-ex/0501018.

[55] C. F. Perdrisat, V. Punjabi, and M. Vanderhaeghen, "Nucleon electromagnetic form factors," *Prog. Part. Nucl. Phys.* **59** (2007) 694–764, arXiv:hep-ph/0612014.

[56] **QCDSF** Collaboration, M. Göckeler *et al.*, "A lattice study of the spin structure of the Lambda hyperon," *Phys. Lett.* **B545** (2002) 112–118, arXiv:hep-lat/0208017.

[57] **QCDSF** Collaboration, M. Göckeler, R. Horsley, D. Pleiter, P. E. L. Rakow, and G. Schierholz, "A lattice determination of moments of unpolarised nucleon structure functions using improved Wilson fermions," *Phys. Rev.* **D71** (2005) 114511, arXiv:hep-ph/0410187.

[58] K. Orginos, T. Blum, and S. Ohta, "Nucleon structure functions with domain wall fermions," *Phys. Rev.* **D73** (2006) 094503, arXiv:hep-lat/0505024.

[59] **LHPC** Collaboration, P. Hägler *et al.*, "Moments of nucleon generalized parton distributions in lattice QCD," *Phys. Rev.* **D68** (2003) 034505, arXiv:hep-lat/0304018.

[60] **LHPC** Collaboration, P. Hägler *et al.*, "Nucleon Generalized Parton Distributions from Full Lattice QCD," arXiv:0705.4295 [hep-lat].

[61] **UKQCD** Collaboration, P. A. Boyle *et al.*, "A lattice computation of the first moment of the kaon's distribution amplitude," *Phys. Lett.* **B641** (2006) 67–74, arXiv:hep-lat/0607018.

[62] M. Göckeler *et al.*, "Lattice Operators for Moments of the Structure Functions and their Transformation under the Hypercubic Group," *Phys. Rev.* **D54** (1996) 5705–5714, arXiv:hep-lat/9602029.

[63] V. L. Chernyak, A. R. Zhitnitsky, and V. G. Serbo, "Asymptotic hadronic form-factors in quantum chromodynamics," *JETP Lett.* **26** (1977) 594–597.

[64] A. Lenz, M. Wittmann, and E. Stein, "Improved light-cone sum rules for the electromagnetic form factors of the nucleon," *Phys. Lett.* **B581** (2004) 199–206, arXiv:hep-ph/0311082.

[65] I. D. King and C. T. Sachrajda, "Nucleon Wave Functions and QCD Sum Rules," *Nucl. Phys.* **B279** (1987) 785.

[66] V. L. Chernyak, A. A. Ogloblin, and I. R. Zhitnitsky, "Calculations of exclusive processes involving baryons," *Z. Phys.* **C42** (1989) 583.

[67] S. J. Brodsky, G. P. Lepage, and S. A. A. Zaidi, "Weak and electromagnetic form factors of baryons ar large momentum transfer," *Phys. Rev.* **D23** (1981) 1152.

[68] I. I. Balitsky and V. M. Braun, "Evolution Equations for QCD String Operators," *Nucl. Phys.* **B311** (1989) 541–584.

[69] M. Diehl, T. Feldmann, R. Jakob, and P. Kroll, "Linking parton distributions to form factors and Compton scattering," *Eur. Phys. J.* **C8** (1999) 409–434, arXiv:hep-ph/9811253.

[70] A. B. Henriques, B. H. Kellett, and R. G. Moorhouse, "General Three Spinor Wave Functions and the Relativistic Quark Model," *Ann. Phys.* **93** (1975) 125.

[71] V. M. Braun, S. E. Derkachov, G. P. Korchemsky, and A. N. Manashov, "Baryon distribution amplitudes in QCD," *Nucl. Phys.* **B553** (1999) 355–426, arXiv:hep-ph/9902375.

[72] N. G. Stefanis, "The physics of exclusive reactions in QCD: Theory and phenomenology," *Eur. Phys. J. direct* **C7** (1999) 1, arXiv:hep-ph/9911375.

[73] G. Mack and A. Salam, "Finite component field representations of the conformal group," *Ann. Phys.* **53** (1969) 174–202.

[74] V. M. Braun and I. E. Filyanov, "Conformal Invariance and Pion Wave Functions of Nonleading Twist," *Z. Phys.* **C48** (1990) 239–248.

[75] P. Ball, "Theoretical update of pseudoscalar meson distribution amplitudes of higher twist: The nonsinglet case," *JHEP* **01** (1999) 010, arXiv:hep-ph/9812375.

[76] S. J. Brodsky, Y. Frishman, G. P. Lepage, and C. T. Sachrajda, "Hadronic Wave Functions at Short Distances and the Operator Product Expansion," *Phys. Lett.* **B91** (1980) 239.

[77] A. P. Bukhvostov, G. V. Frolov, L. N. Lipatov, and E. A. Kuraev, "Evolution Equations for Quasi-Partonic Operators," *Nucl. Phys.* **B258** (1985) 601–646.

[78] B. L. Ioffe, "Calculation of Baryon Masses in Quantum Chromodynamics," *Nucl. Phys.* **B188** (1981) 317–341.

[79] Y. Chung, H. G. Dosch, M. Kremer, and D. Schall, "Baryon Sum Rules and Chiral Symmetry Breaking," *Nucl. Phys.* **B197** (1982) 55.

[80] M. Salmhofer and E. Seiler, "Proof of chiral symmetry breaking in lattice gauge theory," *Lett. Math. Phys.* **21** (1991) 13–22.

[81] M. Salmhofer and E. Seiler, "Proof of chiral symmetry breaking in strongly coupled lattice gauge theory," *Commun. Math. Phys.* **139** (1991) 395–432.

[82] J. Gasser and H. Leutwyler, "Chiral Perturbation Theory to One Loop," *Ann. Phys.* **158** (1984) 142.

[83] T. Becher and H. Leutwyler, "Baryon chiral perturbation theory in manifestly Lorentz invariant form," *Eur. Phys. J.* **C9** (1999) 643–671, arXiv:hep-ph/9901384.

[84] A. D. Sakharov, "Violation of CP Invariance, c Asymmetry, and Baryon Asymmetry of the Universe," *Pisma Zh. Eksp. Teor. Fiz.* **5** (1967) 32–35.

[85] G. 't Hooft, "Symmetry breaking through Bell-Jackiw anomalies," *Phys. Rev. Lett.* **37** (1976) 8–11.

[86] V. A. Kuzmin, V. A. Rubakov, and M. E. Shaposhnikov, "On the Anomalous Electroweak Baryon Number Nonconservation in the Early Universe," *Phys. Lett.* **B155** (1985) 36.

[87] A. Bueno *et al.*, "Nucleon decay searches with large liquid argon TPC detectors at shallow depths: Atmospheric neutrinos and cosmogenic backgrounds," *JHEP* **04** (2007) 041, arXiv:hep-ph/0701101.

[88] **Super-Kamiokande** Collaboration, K. Kobayashi *et al.*, "Search for nucleon decay via modes favored by supersymmetric grand unification models in Super- Kamiokande-I," *Phys. Rev.* **D72** (2005) 052007, arXiv:hep-ex/0502026.

[89] **Soudan 2** Collaboration, J. Chung, T. Fields, and M. Goodman, "Search for nucleon decay and n anti-n oscillation in Soudan 2,". Prepared for 27th International Cosmic Ray Conference (ICRC 2001), Hamburg, Germany, 7-15 Aug 2001.

[90] J. B. Dent and T. W. Kephart, "Proton Decay Constraints on Low Scale AdS/CFT Unification," *Phys. Rev.* **D76** (2007) 085021, arXiv:0704.1451 [hep-ph].

[91] Y. Tomozawa, "Proton Decay Rate," *Phys. Rev. Lett.* **46** (1981) 463.

[92] M. B. Wise, R. Blankenbecler, and L. F. Abbott, "Three-body decays of the proton," *Phys. Rev.* **D23** (1981) 1591.

[93] M. Claudson, M. B. Wise, and L. J. Hall, "Chiral Lagrangian for deep mine physics," *Nucl. Phys.* **B195** (1982) 297.

[94] V. S. Berezinsky, B. L. Ioffe, and Y. I. Kogan, "The calculation of matrix element for proton decay," *Phys. Lett.* **B105** (1981) 33.

[95] S. J. Brodsky, J. R. Ellis, J. S. Hagelin, and C. T. Sachrajda, "Baryon wave functions and nucleon decay," *Nucl. Phys.* **B238** (1984) 561.

[96] K. G. Wilson, "Confinement of Quarks," *Phys. Rev.* **D10** (1974) 2445–2459.

[97] R. Horsley, *The Hadronic Structure of Matter - a lattice approach*. PhD thesis, Institut für Physik, Humboldt-Universität zu Berlin, Germany, 1999.

[98] I. Montvay and G. Munster, "Quantum fields on a lattice,". Cambridge, UK: Univ. Pr. (1994) 491 p. (Cambridge monographs on mathematical physics).

[99] J. E. Mandula, G. Zweig, and J. Govaerts, "Representations of the Rotation Reflection Group of the Four-Dimensional Cubic Lattice," *Nucl. Phys.* **B228** (1983) 91.

[100] J. E. Mandula and E. Shpiz, "Doubled valued Representations of the Four-Dimensional Cubic Lattice Rotation Group," *Nucl. Phys.* **B232** (1984) 180.

[101] H. B. Nielsen and M. Ninomiya, "Absence of Neutrinos on a Lattice. 1. Proof by Homotopy Theory," *Nucl. Phys.* **B185** (1981) 20.

[102] D. Friedan, "A Proof of the Nielsen-Ninomiya Theorem," *Commun. Math. Phys.* **85** (1982) 481–490.

[103] R. Narayanan and H. Neuberger, "Chiral fermions on the lattice," *Phys. Rev. Lett.* **71** (1993) 3251–3254, arXiv:hep-lat/9308011.

[104] R. Narayanan and H. Neuberger, "A Construction of lattice chiral gauge theories," *Nucl. Phys.* **B443** (1995) 305–385, arXiv:hep-th/9411108.

[105] D. B. Kaplan, "A Method for simulating chiral fermions on the lattice," *Phys. Lett.* **B288** (1992) 342–347, arXiv:hep-lat/9206013.

[106] Y. Shamir, "Chiral fermions from lattice boundaries," *Nucl. Phys.* **B406** (1993) 90–106, arXiv:hep-lat/9303005.

[107] K. Symanzik, "Continuum Limit and Improved Action in Lattice Theories. 1. Principles and ϕ^4 Theory," *Nucl. Phys.* **B226** (1983) 187.

[108] M. Lüscher, "Advanced lattice QCD," arXiv:hep-lat/9802029.

[109] R. Sommer, "Non-perturbative renormalization of QCD," arXiv:hep-ph/9711243.

[110] B. Sheikholeslami and R. Wohlert, "Improved Continuum Limit Lattice Action for QCD with Wilson Fermions," *Nucl. Phys.* **B259** (1985) 572.

[111] **ALPHA** Collaboration, K. Jansen and R. Sommer, "$O(\alpha)$ improvement of lattice QCD with two flavors of Wilson quarks," *Nucl. Phys.* **B530** (1998) 185–203, arXiv:hep-lat/9803017.

[112] M. Creutz, "Overrelaxation and Monte Carlo Simulation," *Phys. Rev.* **D36** (1987) 515.

[113] S. Duane, A. D. Kennedy, B. J. Pendleton, and D. Roweth, "Hybrid Monte Carlo," *Phys. Lett.* **B195** (1987) 216–222.

[114] M. R. Hestenes and E. Stiefel, "Methods of conjugate gradients for solving linear systems," *Journal of Research of the National Bureau of Standards* **49 (6)** (1952) 409–436.

[115] Y. Oyanagi, "An incomplete ldu decomposition of lattice fermions and its application to conjugate residual methods," *Comput. Phys. Commun.* **42** (1986) 333–343.

[116] H. A. van der Vorst, "Bi-cgstab: A fast and smoothly converging variant of bi-cg for the solution of nonsymmetric linear systems," *SIAM J. Sci. and Stat. Comput.* **13** (1992) 631–644.

[117] **Bern-Graz-Regensburg** Collaboration, D. Brömmel *et al.*, "Low lying nucleons from chirally improved fermions," *Nucl. Phys. Proc. Suppl.* **129** (2004) 251–253, arXiv:hep-lat/0309036.

[118] C. Alexandrou, S. Gusken, F. Jegerlehner, K. Schilling, and R. Sommer, "The Static approximation of heavy - light quark systems: A Systematic lattice study," *Nucl. Phys.* **B414** (1994) 815–855, arXiv:hep-lat/9211042.

[119] C. Michael, "Adjoint Sources in Lattice Gauge Theory," *Nucl. Phys.* **B259** (1985) 58.

[120] M. Lüscher and U. Wolff, "How To Calculate The Elastic Scattering Matrix In Two-Dimensional Quantum Field Theories By Numerical Simulation," *Nucl. Phys.* **B339** (1990) 222–252.

[121] T. Burch, C. Gattringer, L. Y. Glozman, C. Hagen, and C. B. Lang, "Variational method for lattice spectroscopy with ghosts," *Phys. Rev.* **D73** (2006) 017502, arXiv:hep-lat/0511054.

[122] **UKQCD** Collaboration, C. R. Allton *et al.*, "Gauge invariant smearing and matrix correlators using Wilson fermions at $\beta = 6.2$," *Phys. Rev.* **D47** (1993) 5128–5137, arXiv:hep-lat/9303009.

[123] C. Best *et al.*, "Pion and rho structure functions from lattice QCD," *Phys. Rev.* **D56** (1997) 2743–2754, arXiv:hep-lat/9703014.

[124] D. Daniel, R. Gupta, G. W. Kilcup, A. Patel, and S. R. Sharpe, "Phenomenology with Wilson fermions using smeared sources," *Phys. Rev.* **D46** (1992) 3130–3145, arXiv:hep-lat/9204011.

[125] R. Sommer, "A New way to set the energy scale in lattice gauge theories and its applications to the static force and alpha-s in SU(2) Yang-Mills theory," *Nucl. Phys.* **B411** (1994) 839–854, arXiv:hep-lat/9310022.

[126] **ALPHA** Collaboration, M. Guagnelli, R. Sommer, and H. Wittig, "Precision computation of a low-energy reference scale in quenched lattice QCD," *Nucl. Phys.* **B535** (1998) 389–402, arXiv:hep-lat/9806005.

[127] A. Ali Khan *et al.*, "Axial coupling constant of the nucleon for two flavours of dynamical quarks in finite and infinite volume," *Phys. Rev.* **D74** (2006) 094508, arXiv:hep-lat/0603028.

[128] **QCDSF** Collaboration, M. Göckeler *et al.*, "Probing the chiral limit with clover fermions II: The baryon sector," *PoS* **LAT2007** (2007) 129, arXiv:0712.0010 [hep-lat].

[129] **QCDSF** Collaboration, M. Göckeler *et al.*, "Moments of nucleon distribution amplitudes from irreducible three-quark operators," *PoS* **LAT2007** (2007) 147, arXiv:0710.2489 [hep-lat].

[130] T. Kaltenbrunner, M. Gockeler, and A. Schafer, "Irreducible Multiplets of Three-Quark Operators on the Lattice: Controlling Mixing under Renormalization," *Eur. Phys. J.* **C55** (2008) 387–401, arXiv:0801.3932 [hep-lat].

[131] T. Kaltenbrunner. PhD thesis, University of Regensburg, 2008. (in preparation).

[132] T. Kaltenbrunner, M. Göckeler, and A. Schäfer, "Non-Perturbatie Renormalization of Three-Quark Operators,". (in preparation).

[133] G. Martinelli, C. Pittori, C. T. Sachrajda, M. Testa, and A. Vladikas, "A General method for nonperturbative renormalization of lattice operators," *Nucl. Phys.* **B445** (1995) 81–108, arXiv:hep-lat/9411010.

[134] M. Göckeler *et al.*, "Lattice renormalization of quark operators," *Nucl. Phys. Proc. Suppl.* **63** (1998) 868–870, arXiv:hep-lat/9710052.

[135] Y. Aoki, C. Dawson, J. Noaki, and A. Soni, "Proton decay matrix elements with domain-wall fermions," *Phys. Rev.* **D75** (2007) 014507, arXiv:hep-lat/0607002.

[136] S. Sasaki, T. Blum, and S. Ohta, "A lattice study of the nucleon excited states with domain wall fermions," *Phys. Rev.* **D65** (2002) 074503, arXiv:hep-lat/0102010.

[137] A. V. Kolesnichenko, "Second moments of quark and gluon distribution functions in a proton calculated making use of the QCD sume rules. (in Russian)," *Yad. Fiz.* **39** (1984) 1527–1544.

[138] J. Bolz and P. Kroll, "Modelling the nucleon wave function from soft and hard processes," *Z. Phys.* **A356** (1996) 327, arXiv:hep-ph/9603289.